Enhanced Multicarrier Techniques for Professional Ad-Hoc and Cell-Based Communications

(EMPhAtiC)

Document Number D6.1
Cooperative communications and synchronization

Contractual date of delivery to the CEC:	31/08/2013
Actual date of delivery to the CEC:	31/08/2013
Project Number and Acronym:	318362 EMPhAtiC
Editor:	Martin Haardt (ITU)
Authors:	Yao Cheng (ITU), Peng Li (ITU), Martin Haardt (ITU), Slobodan Nedic (UNS), Sladjana Josilo (UNS), Stefan Tomic (UNS), Yahia Medjahdi (CNAM), Rostom Zakaria (CNAM), Mylene Pischella (CNAM), Didier Le Ruyet (CNAM), Eleftherios Kofidis (CTI), Christos Mavrokefalidis (CTI)
Participants:	ITU, UNS, CNAM, CTI
Workpackage:	WP6
Security:	Public(PU)
Nature:	Report
Version:	1.0
Total Number of Pages:	65

Abstract:

This report summarizes the investigations on the feasibility and the performance of filter bank-based multicarrier (FB-MC) in cooperative communications. In such a scenario with some loss of synchronization, it is known that orthogonal frequency division multiplexing with the cyclic prefix insertion (CP-OFDM) in general fails to provide a satisfactory performance. To investigate the advantages of FB-MC when used in cooperative communications, comparative performance evaluations of FB-MC and CP-OFDM are carried out in delay- and frequency-synchronized as well as unsynchronized scenarios. Moreover, to provide solutions to the channel estimation issue in cooperative communications using FB-MC an optimal training design is investigated. In addition, a preliminary study of using widely linear processing in the context of FB-MC is presented. To provide some insights into the design of distributed beamforming techniques as a future task, we point out challenges and possible research directions.

Keywords:

Document Revision History

Version	Date	Author	Summary of main changes
0.1	31.05.2013	Yao Cheng (ITU), Peng Li (ITU), Martin Haardt (ITU), Slobodan Nedic (UNS), Sladjana Josilo (UNS), Stefan Tomic (UNS), Didier Le Ruyet (CNAM), Eleftherios Kofidis (CTI)	Initial structure of the document
0.2	17.07.2013	Yao Cheng (ITU), Peng Li (ITU), Martin Haardt (ITU), Yahia Medjahdi (CNAM), Rostom Zakaria (CNAM), Mylene Pischella (CNAM), Didier Le Ruyet (CNAM), Eleftherios Kofidis (CTI), Christos Mavrokefalidis (CTI), Slobodan Nedic (UNS), Sladjana Josilo (UNS), Stefan Tomic (UNS)	Initial draft of the document
0.3	08.08.2013	Yao Cheng (ITU), Peng Li (ITU), Martin Haardt (ITU), Eleftherios Kofidis (CTI), Christos Mavrokefalidis (CTI)	Updating Chapter 3; Updating Chapter 2.1 and 2.2; Minor changes in Chapter 4
0.4	21.08.2013	Yao Cheng (ITU) Peng Li (ITU), Martin Haardt (ITU), Slobodan Nedic (UNS), Sladjana Josilo (UNS), Stefan Tomic (UNS)	Updating Chapter 2.3
1.0	31.08.2013	Yao Cheng (ITU), Peng Li (ITU), Martin Haardt (ITU), Yahia Medjahdi (CNAM), Rostom Zakaria (CNAM), Mylene Pischella (CNAM), Didier Le Ruyet (CNAM), Eleftherios Kofidis (CTI), Christos Mavrokefalidis (CTI), Slobodan Nedic (UNS), Sladjana Josilo (UNS), Stefan Tomic (UNS)	Minor changes in Chapter 2.3

Table of Contents

1. Introduction

This document addresses filter bank-based multi-carrier (FB-MC) in the context of cooperative communications. The major focus is on the performance evaluation of FB-MC in scenarios where perfect time and frequency synchronization is not guaranteed, channel estimation issue in cooperative networks with FB-MC, and the investigation of applying widely linear processing in the context of FB-MC.

First, a comparison of filter bank-based multi-carrier with OQAM subcarrier modulation (FBMC/OQAM) and orthogonal frequency division multiplexing with the cyclic prefix insertion (CP-OFDM) is presented in an uplink scenario in the presence of symbol timing offset or carrier frequency offset. The nodes are equipped with multiple antennas, and different frequency selective channel models are considered in the simulations. The greater robustness of FBMC/OQAM against the lack of synchronization in the time and the frequency domain compared to CP-OFDM is shown via extensive numerical results. Moreover, the CP-OFDM-based and FB-MC-based techniques are compared in distributed cooperative multiple-input multiple output (MIMO) configuration with inherent time and frequency asynchronism between the constituent signals. The analysis of the robustness is conducted in the scenario that the independent single-input single-out (SISO) signal acting as co-channel interference to the others. A system model with two dislocated transmitters and two dislocated receivers whose mutual communications are mediated by a relay is used. The performances of the circular (CIR) and non-circular (NCIR) receivers are compared. An overview of the widely linear filtering (WLF) framework as inherently doubling the signal-antenna spatial degree of freedom is conducted and the optimal receivers for second order (SO) circular/non-circular noise are considered. Furthermore, CP-OFDM-based and FB-MC-based techniques are considered in a synchronous multicarrier based relay network. Multi-taps equalization of asynchronous relay transmission techniques are reviewed. Cooperative MIMO relays for asynchronous multi-user transmissions are also considered. Asynchronous interference due to co-channel interference is analyzed in detail. Simulation and analytically results further conclude that CP-OFDM performances are subjected to sever degradation resulting from the loss of the orthogonality and a novel multi-taps subchannel equalizer is able to counteract the detrimental effect of timing asynchronism on the FB-MC performance. In addition, training design for the channel estimation in cooperative communications using FB-MC is analyzed. Both full (i.e., with pilots at all the subcarriers) and sparse (i.e., with isolated pilot subcarriers surrounded by nulls) preambles are considered. The problem of optimally designing the preambles is investigated for Least-Squares (LS) channel estimation. The optimality is in the sense of the minimum Mean Square Error (MSE) estimation subject to transmit energy constraints. Last but not the least, we investigate the application of widely linear processing in the context of FB-MC. A two-step receiver is proposed for point-to-point MIMO FBMC/OQAM systems where both linear processing and widely linear processing are combined. It is also discussed how widely linear processing can be incorporated into a cooperative MIMO network. Developing widely linear distribute beamforming techniques is then an interesting topic as future work.

The remainder of the document is organized as follows. Chapter 2 presents a thorough comparison of CP-OFDM and FBMC/OQAM in cooperative communications taking into account time and frequency misalignments. Channel estimation and training design in a cooperative network with FB-MC are investigated in Chapter 3. Chapter 4 focuses on the application of widely linear processing in MIMO FBMC/OQAM systems.

2. Performance comparison of FBMC/OQAM with CP-OFDM in cooperative MIMO systems

2.1 Comparison of FBMC/OQAM and CP-OFDM in a delay-unsynchronized scenario

2.1.1 Scenario description and data model

A cooperative wireless network with two or more transmitters is considered. We assume an uplink multiple access scenario for a multi-carrier interference network, where a number of U users transmit their signals to a single access point (AP) at their assigned subcarriers simultaneously. The AP is equipped with Q receiving antennas, and the i-th user node has P_i transmitting antennas, $i = 1, 2, \ldots, U$. As illustrated by Fig. 2-1, the transmitted signals from each user suffer from frequency selective fading, characteristics of multipath channels. We employ QAM and OQAM signals for CP-OFDM and FBMC transmission respectively.

The subcarriers of the two users are allocated in a block-wise fashion as illustrated in Fig. 2-2, where the user 1 occupies the subcarriers with indices $k = 0, 1, \ldots, M_u^1 - 1$, and user 2 occupies the subcarriers with indices $k = M_u^1 + G, \ldots, M_u^1 + M_u^2 + G - 1$, where M_u^i denotes the number of used subcarriers of the i-th user. A number of G subcarriers with zero power are assigned between the blocks of the subcarriers of users as guard band. In case of U users, the system can be similarly defined except that multiple guard bands are employed between two adjacent subcarrier blocks. In Fig. 2-3, an interleaved subcarriers allocation scheme is considered, the subcarriers for each user are assigned alternately where no guard band is placed between them.

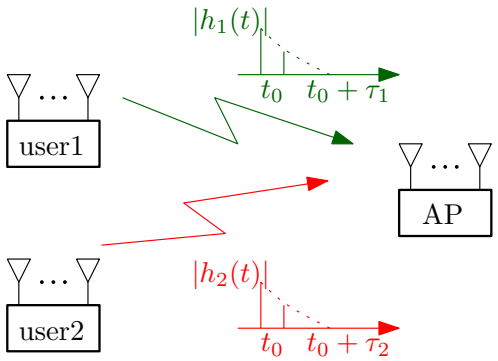

Figure 2-1: A number of 2 users transmit their signals at their assigned subcarriers simultaneously. The signals transmitted from the two users suffer from independent multipath fading $h_1(t)$ and $h_2(t)$ and channel maximum delays τ_1, τ_2, respectively.

In the following subsections the multipath system model is given where the timing offsets are taken into account. The difference between an FBMC-based system and a CP-OFDM-based system is also pointed out and reflected in the introduction of the data model.

2.1.1.1 Frequency-selective fading channel model

In order to describe a frequency-selective fading channel, a power delay profile for multipath channels is usually required for modeling a frequency-selective fading channel. The delay profile provides a distribution of the averaged power for the signal received over individual path at

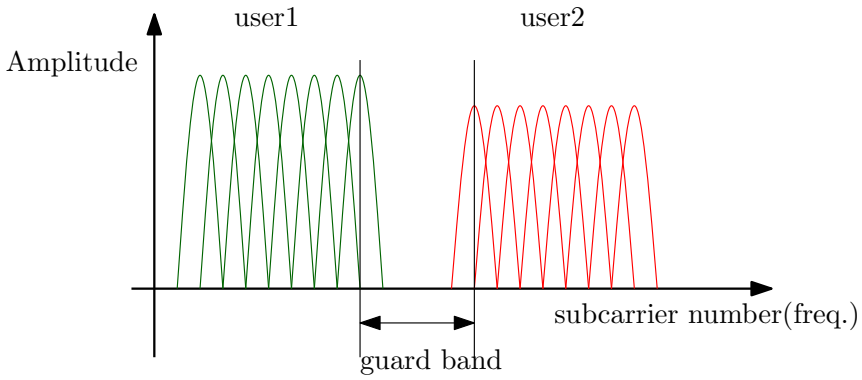

Figure 2-2: 2 users transmit their signals at their assigned subcarriers simultaneously.

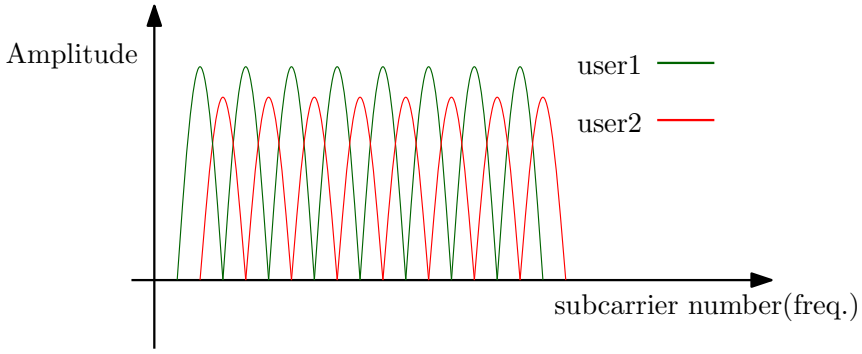

Figure 2-3: 2 users transmit their signals at their assigned subcarriers simultaneously.

the receiver. The power profile is measured by the relative power of each path related to the earliest arrival path. In this section, a simple tapped delay line (TDL) model is adopted for implementing the frequency selective channel. This channel model employs a summation of a number of frequency flat fading components which are independent of each other. Besides the simplified TDL multipath channel model, another commonly used set of empirical channel models is considered in ITU recommendation M.1225. Because the ITU-R specified channel model is more practical compared with the simple TDL model, we incorporate this channel model in our simulations to demonstrate the benefit of using FBMC/OQAM in multicarrier communications.

2.1.1.2 Delay synchronization offset

In the uplink scenario, the users may transmit their signals with different subcarriers allocated by an AP subband scheduler. Although the subcarriers are allocated orthogonally, adjacent channel interference may occur due to the loss of orthogonality as the signals from different users do not arrive at the AP simultaneously. Fig. 2-4 shows a timing misalignment between user 1 and user 2. It is difficult to recover the transmitted symbols when interference occurs between the users, which results in a significant performance degradation.

In order to process the M multicarriers, a multicarrier symbol-timing synchronization is required to detect the signal. However, in an uplink multiple access system, the exact symbol-timing is not usually sufficiently warranted and the performance may heavily degrade. In the presence of symbol timing offset, the received signal at the q-th receiving antenna of the AP,

where $q = 1, 2, \ldots, Q$, can be expressed as

$$r_q(t) = \sum_{i=1}^{U} \sum_{p=1}^{P_i} h_{pq}^{(i)}(t) * s_p^{(i)}(t - \Delta t_i) + n_q(t), \tag{2.1}$$

where $*$ denotes the convolution operation, and $h_{pq}^{(i)}(t)$ means the frequency selective channel impulse response on the link between the p-th transmitting antenna of the i-th user and the q-th receiving antenna of the AP. At each user node, full multiplexing is considered, i.e., the number of data streams transmitted by the i-th user equals the number of transmitting antennas P_i. The multi-carrier signal transmitted at the p-th antenna of the i-th user is denoted by $s_p^{(i)}(t)$, and it is obtained by either a CP-OFDM/QAM modulator or an FMBC/OQAM modulator. Moreover, we use Δt_i to denote the symbol timing offset of the i-th user. The noise term $n_q(t)$ is modeled as a circular symmetric complex Gaussian process with zero mean, and the noise power spectral density is denoted by N_0.

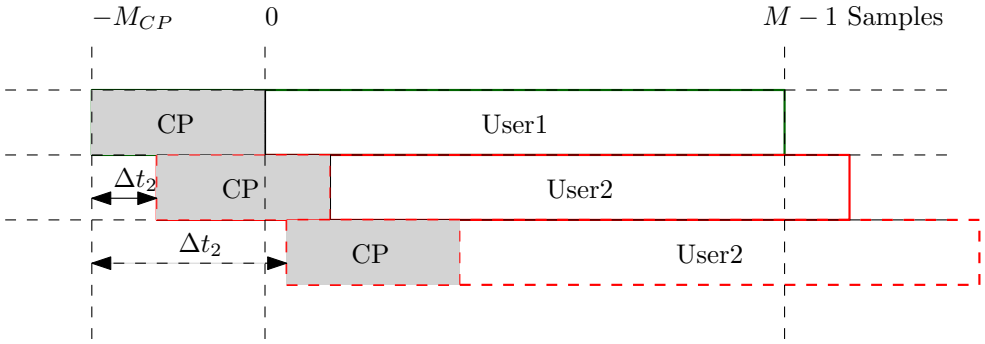

Figure 2-4: Timing mismatch of 2 users' symbol received at the AP in an uplink multicarrier system. The user 1 is perfectly synchronized but user 2 suffers from a time mismatch Δt_2, its performance degrades heavily due to ISI when $\Delta t_2 >$ length of CP.

2.1.1.3 Review of CP-OFDM and FBMC/OQAM

In a conventional CP-OFDM system, a simple rectangular OFDM window is applied in the time domain before the iFFT processing, this operation results in a sinc shaped frequency response with the first side-lobe 13 dB lower than the main-lobe. Thanks to the orthogonality provided by the iFFT operation, no interference is picked up among adjacent subcarriers if perfect synchronization is achieved. The basic CP-OFDM modulator is given as below

$$s(t) = \sum_{k=0}^{M} S(k) e^{j2\pi f_k t} \tag{2.2}$$

where $S(k)$ denotes the QAM signal assigned to subcarrier k, and term f_k represents its carrier frequency. Each subcarrier component of a CP-OFDM symbol with the effective duration of T_{sym} can be considered as a narrowband signal within a rectangular window of length T_{sym}. The sinc function obtained in the frequency domain occupies the bandwidth of $2/T_{\text{sym}}$. Out-of-band power is produced by the power spectrum of a set of many frequency separated sinc functions. Significant interference will be picked up by two adjacent broadband channels if the signals are not perfectly synchronized. A guard band in the frequency domain is inserted between the

channels to reduce the effect of channel interference at the price of a further loss of spectrum efficiency.

In order to warrant the OFDM performance, the guard intervals (such as CP) between two consecutive OFDM symbols are introduced, dealing with the ISI and ICI effects over the multipath channel. In conventional OFDM transmission schemes, bandwidth loss incurs due to the introduction of the guard interval.

The conventional OFDM subcarriers have poor side lobes caused by the introduction of the rectangular window. In order to avoid these inter-subcarrier interference, a window that roles-off gently may be applied to significantly suppress the side lobes. These windows are called root-raised-cosine pulse shaping filters defined by a factor α. However, this method further wastes bandwidth efficiency by a factor of α [1]. It is also worth to mention that even for $\alpha = 1$, (halved spectrum efficiency), the side lobes adjacent to the main lobe still remain.

In case of FBMC/OQAM systems, the OQAM symbols are used and the transmitter builds the signal as

$$\begin{aligned} s(t) = \sum_{k=0}^{M/2-1} \sum_{n} \Big(\Re\{S_n(2k)\} g(t-nT) + j\Im\{S_n(2k)\} g(t-nT-\frac{T}{2}) \Big) e^{j2\pi(2k)f_{2k}t} + \\ \Big(\Re\{S_n(2k+1)\} g(t-nT-\frac{T}{2}) + j\Im\{S_n(2k+1)\} g(t-nT) \Big) e^{j2\pi(2k+1)f_{2k+1}t} \end{aligned} \tag{2.3}$$

where n is the tap index of the pulse shaping filter $g(t)$, and time T is the symbol duration. The items $\Re\{S(k)\}$ and $\Im\{S(k)\}$ denote the real and imaginary parts of the QAM complex-valued symbols, respectively. The in-phase and quadrature components of the QAM signal have a time offset of half a symbol period. In order to achieve ISI free transmission, instead of using IFFT and FFT at CP-OFDM transmitter and receiver, a set of spectrally well contained synthesis and analysis filter banks is considered in the FBMC/OQAM transmission systems. One of the common approaches is to use modulated uniform polyphase filter banks based on prototype filter design, and the system spectral characteristics are determined by the prototype filter. The orthogonality can be maintained by designing pulse shapes different from a rectangular window. By introducing FBMC/OQAM, the side lobes of multicarrier components can be significantly reduced [2].

2.1.2 Simulation results

In this section, we present numerical results with respect to the comparison between CP-OFDM and FBMC/OQAM in an uplink scenario where symbol timing offset is present. The multi-carrier scheme-related parameters are set according to those for LTE 5 MHz transmissions. The sub-carrier spacing is 15 kHz, and the FFT size is 512. Here the CP length for CP-OFDM is set to $T/8$, where T denotes the symbol duration. In the case of FBMC/OQAM, the PHYDYAS prototype filter [2] is used, and the overlapping factor is chose as $K = 4$.

The ITU recommendation specifies outdoor-to-indoor pedestrian and vehicular test environments. Since the delay spread can vary significantly, the recommendation specifies two different delay spreads for each test environment: low delay spread (A) and medium delay spread (B). In each test environment, a multipath tap delay profile is specified in Table 2-1 for indoor to outdoor pedestrian and Table. 2-2 for vehicular test environments.

First, we consider a 2-user scenario where the two users and the base station are each equipped with two antennas. A block-wise sub-carrier allocation scheme as illustrated in Fig. 2-2 is adopted. An MMSE receiver in the frequency domain is employed, i.e., the equalization is performed on each sub-carrier. Assuming perfect synchronization in the time domain and

Table 2-1: ITU Channel Model for Pedestrian Test Environment

Tap	Relative delay (ns)	Average power (dB)	Relative delay (ns)	Average power (dB)	Doppler spectrum
	Channel A	Channel A	Channel B	Channel B	
1	0	0	0	0	Classic
2	110	-9.7	200	-0.9	Classic
3	190	-19.2	800	-4.9	Classic
4	410	-22.8	1200	-8	Classic
5	-	-	2300	-7.8	Classic
6	-	-	3700	-23.9	Classic

Table 2-2: ITU Channel Model for Vehicular Test Environment

Tap	Relative delay (ns)	Average power (dB)	Relative delay (ns)	Average power (dB)	Doppler spectrum
	Channel A	Channel A	Channel B	Channel B	
1	0	0	0	-2.5	Classic
2	310	-1	300	0	Classic
3	710	-9	8900	-12.8	Classic
4	1090	-10	12900	-10	Classic
5	1730	-15	17100	-25.2	Classic
6	2510	-20	20000	-16	Classic

in the frequency domain and flat Rayleigh fading channel, we present the bit error rate (BER) performances of CP-OFDM and FBMC/OQAM in Fig. 2-5. It can be observed that when

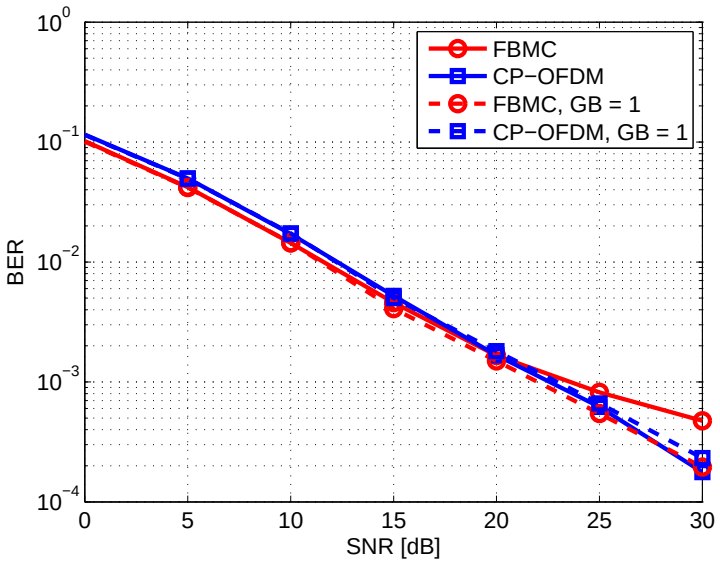

Figure 2-5: Comparison between FBMC/OQAM and CP-OFDM for a 2-user uplink scenario considering perfect synchronization in the time domain and in the frequency domain (GB - guard band in the number of sub-carriers)

no guard band is employed, the performance of FBMC/OQAM becomes worse than that of CP-OFDM in high SNR regime. The reason is that without a guard band the last sub-carrier of the first user is interfered by the transmission of its adjacent sub-carrier which belongs to the second user and experiences a different channel, while in the MMSE receiver the channel is treated as the same for the desired symbol on each subcarrier and the intrinsic interference. It also applies to the detection of the signal on the first sub-carrier of the second user. This fact results in the performance degradation of FBMC/OQAM. On the other hand, when employing one sub-carrier as guard band, the aforementioned problem is solved, and the transmissions of the two users are well separated. The corresponding results shown in Fig. 2-5 comply with this argument.

We now continue to examine an unsynchronized scenario where the symbol timing offset with respect to each user is assumed to be in the range of $(T/8, T/4)$. The ITU Pedestrian-A channel model is used in the simulations. Other parameters and settings are the same as introduced in previous text. Fig. 2-6 shows the BER performances of CP-OFDM and FBMC/OQAM in the presence of symbol timing offsets. The impacts of different sizes of the guard band on CP-OFDM and FBMC/OQAM are illustrated, respectively. Note that the SNR here represents E_{b}/N_0. It can be seen that when there is no guard band, FBMC/OQAM significantly outper-

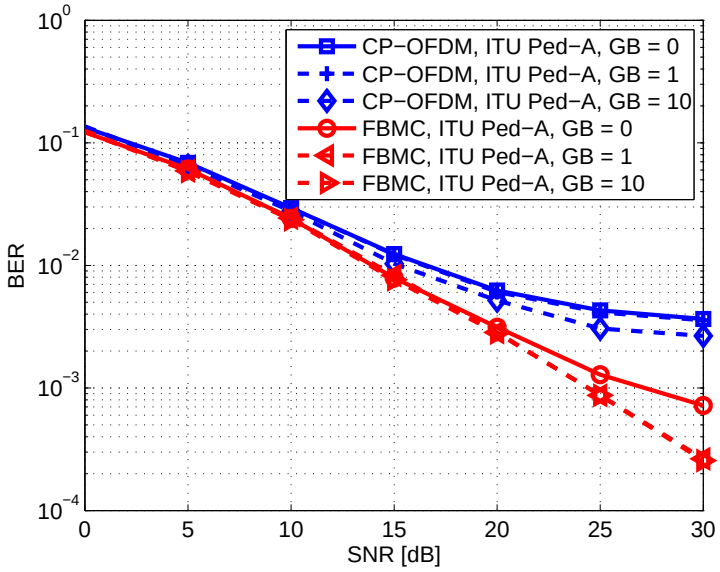

Figure 2-6: Comparison between FBMC/OQAM and CP-OFDM for a 2-user uplink scenario in the presence of symbol timing offset in the range of $(T/8, T/4)$ (GB - guard band in the number of sub-carriers)

forms CP-OFDM. With a single sub-carrier as the guard band, a performance improvement is observed in the case of FBMC/OQAM, while for CP-OFDM the gain compared to the zero-guard-band case is negligible. As the size of the guard band is increased to 10 sub-carriers, we can only see a very slight improvement for CP-OFDM, and it still suffers from an error floor. On the other hand, it can be observed that for FBMC/OQAM when one sub-carrier is used as the guard band, the performance is as good as that in the case of 10 sub-carriers. These results comply with the theory that as FBMC/OQAM systems are endowed with an agile spectrum, guard bands with very small sizes suffice to isolate groups of sub-carriers for different users or services.

We further show results for a 4-user scenario in Fig. 2-7. The other simulation parameters are

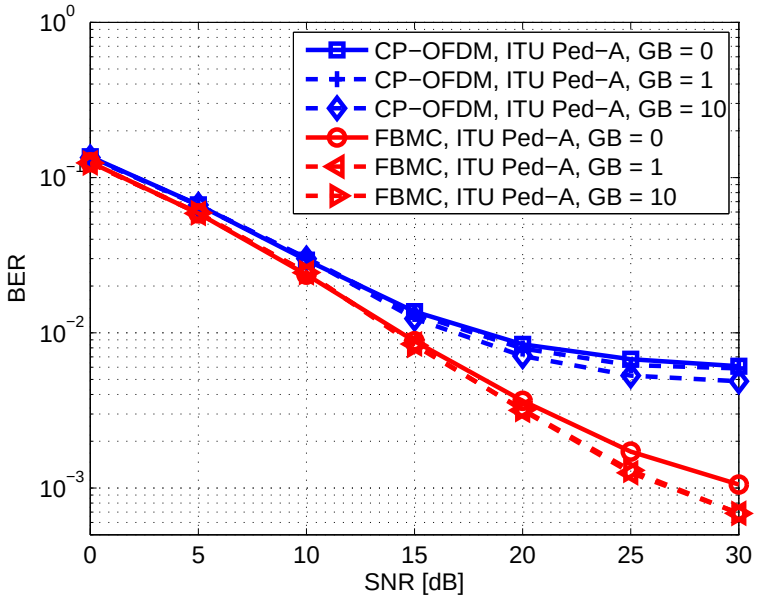

Figure 2-7: Comparison between FBMC/OQAM and CP-OFDM for a 4-user uplink scenario in the presence of symbol timing offsets in the range of $(T/8, T/4)$ (GB - guard band in the number of sub-carriers)

same as described in the first experiment. Similar observations can be made that FBMC/OQAM is more robust against symbol timing offset compared to CP-OFDM. Moreover, the size of guard band required to separated different groups of sub-carriers is substantially smaller than that for CP-OFDM.

2.2 Comparison of FBMC/OQAM and CP-OFDM in a frequency-unsynchronized scenario

2.2.1 Scenario description and data model

A cooperative wireless network with two or more transmitters is considered (referring to the scenario that is introduced in detail in the previous section). The data model is given where the frequency offsets are taken into account. The difference between an FBMC-based system and a CP-OFDM-based system is also pointed out and reflected in the introduction of the data model.

2.2.1.1 Frequency synchronization offset

The OFDM/FBMC systems carry the information data on frequency orthogonal subcarriers for parallel transmission to combat the distortion effect caused by inter-symbol-interference in the multi-path fading channel. The advantage of the OFDM technique relies on the assumption that the orthogonality is always maintained. However for practical implementations, the orthogonality is not guaranteed due to the synchronization error, in this case, its performance might be heavily degraded.

In general there are two types of frequency distortions associated with the multicarrier signal [3]. These synchronization errors may be due to the phase noise of oscillators at both the

transmitter and the receiver, the Doppler frequency shift of the carrier frequency as well as the velocity of the transmitter/receiver. In this report we define the normalized carrier frequency offset (CFO) as a ratio of the frequency mismatch to the subcarrier spacing. Thereby, the received signal at the q-th receiving antenna of the AP, where $q = 1, 2, \ldots, Q$, in the presence of carrier frequency offsets is written as

$$r_q(t) = \sum_{i=1}^{U} e^{j\frac{2\pi\eta_i t}{T}} \sum_{p=1}^{P_i} h_{pq}^{(i)}(t) * s_p^{(i)}(t) + n_q(t), \tag{2.4}$$

where T denotes the symbol duration, and η_i is the normalized carrier frequency offset of the i-th user. Here perfect synchronization in the time domain is assumed.

2.2.1.2 CFO estimation with training symbols

By using training symbols, the CFO can be estimated in multicarrier based transmission systems. Since the CFO can be large, we may need an algorithm which is able to cope with a frequency offset with a wider range. This can be realized by using training symbols that are repetitive with some shorter period.

Let us assume two identical training symbols $x(n)$ and $x'(n)$ are transmitted consecutively, by ignoring the channel response and noise, we obtain the received signal $r(n)$ and $r'(n)$ with frequency domain transformation

$$r'(n) = r(n)e^{j2\pi\eta} \overset{FFT}{\rightarrow} Y'(k) = Y(k)e^{j2\pi\eta} \tag{2.5}$$

The CFO can be estimated by using a maximum likelihood estimator as [4, 5]

$$\hat{\eta} = \frac{1}{2\pi}\tan^{-1}\left\{\frac{\sum_{k=0}^{N-1}\Im[Y'(k)Y^*(k)]}{\sum_{k=0}^{N-1}\Re[Y'(k)Y^*(k)]}\right\} \tag{2.6}$$

The range of CFO estimated by above equation is $\eta = |1/2|$, the range can be extended by using multiple repetitive patterns in the time-domain. It is obvious to see that by increasing repetitive patterns, the spectrum efficiency decreases. These CFO estimation techniques reduce the actual CFO caused by phase noise, Doppler frequency shift and physical limitation of oscillators, however, a perfect CFO estimation is still unavailable and the residual frequency offsets remains as $\eta_{\text{residual}} = |\hat{\eta} - \eta|$.

2.2.2 Simulation results

In this section, we compare CP-OFDM with FBMC/OQAM in an uplink scenario where CFO is present by means of numerical simulations. The multi-carrier scheme-related parameters are set according to those for LTE 5 MHz transmissions. The sub-carrier spacing is 15 kHz, and the FFT size is 512. Here the CP length for CP-OFDM is set to $T/8$. In the case of FBMC/OQAM, the PHYDYAS prototype filter [2] is used, and the overlapping factor is chose as $K = 4$.

In the first example, we consider a 2-user scenario where the two users and the base station are each equipped with two antennas. A block-wise sub-carrier allocation scheme as illustrated in Fig. 2-2 is adopted. The ITU Vehicular-A channel model is used in the simulations. Moreover, an MMSE receiver in the frequency domain is employed. The users are assumed to be perfectly synchronized in the time domain. Fig. 2-8 shows the BER performances of CP-OFDM and FBMC/OQAM in the presence of CFO. Note that the SNR here represents E_{b}/N_0. As the maximum possible value of residual CFO is increased to 0.15, we

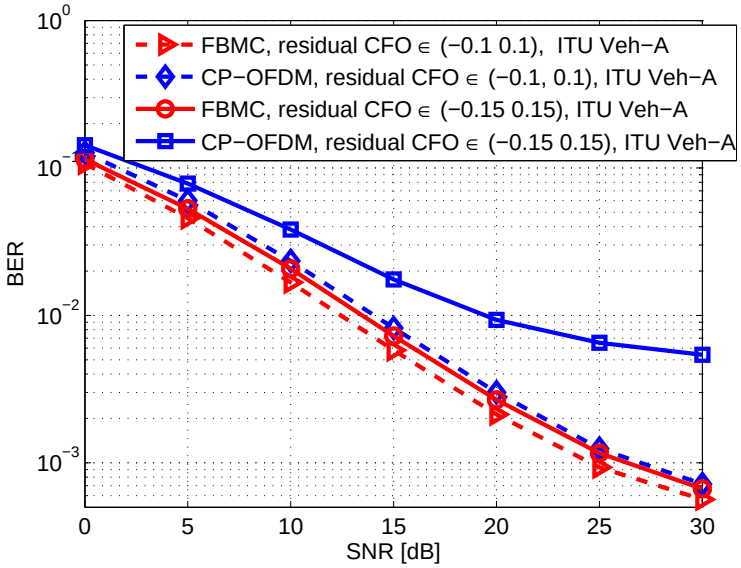

Figure 2-8: Comparison between FBMC/OQAM and CP-OFDM for a 2-user uplink scenario in the presence of carrier frequency offset

observe a significant performance degradation for CP-OFDM due to inter-carrier interference. By comparison, FBMC/OQAM shows a greater robustness against frequency misalignment, as the performance loss is much smaller compared to that of CP-OFDM when the residual CFO increases. Meanwhile, FBMC/OQAM outperforms CP-OFDM in both cases.

Second, a 4-user scenario is investigated. The other simulation parameters are the same as in the first example. The corresponding results are illustrated in Fig. 2-9. Similarly, it can be

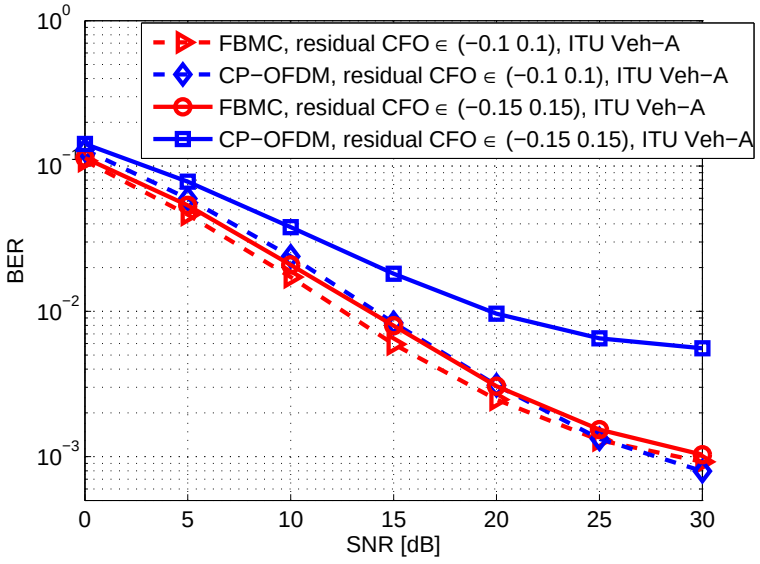

Figure 2-9: Comparison between FBMC/OQAM and CP-OFDM for a 4-user uplink scenario in the presence of carrier frequency offset

seen that CP-OFDM is more sensitive to CFO compared to FBMC/OQAM. When the residual CFO is increased, the gap of performances between FBMC/OQAM and CP-OFDM is larger. It

should be noted that in addition to the frequency misalignment, another factor that affects the performance of FBMC/OQAM is the multi-path channel considered in this example. The reason is that there is no insertion of any CP in the case of FBMC/OQAM. Thereby, it suffers from inter symbol interference, and an MMSE receiver in the frequency domain (a one-tap equalizer) which is normally used in OFDM systems does not suffice to provide a satisfactory performance. When a multi-tap equalizer [6] is used for FBMC/OQAM, a performance improvement can be expected.

2.3 Investigation of the expected benefits that FBMC/OQAM provides in terms of the relaxation of the required synchronization compared to CP-OFDM

In order to arrive at some relevant results regarding the comparative evaluation of the CP-OFDM and FBMC formats as applied in distributed cooperative MIMO configurations with inherent time and frequency asynchronism between the constituent SISO signals, we thought that it would be appropriate and insightful enough if the analysis is conducted in terms of robustness of one SISO signal in presence of another independent SISO signal acting as co-channel interference. On one hand, a justification for this approach can be found in the fact that the SDM and STBC configurations are essentially a system of co-channel interfering signals. On the other hand, in particular for distributed MIMO configurations, the co-channel interference can be expected to be, due to an essentially ad-hoc networking mechanism, of much more importance than in conventional, co-located MIMO systems and conventional networking, with various means of co-channel interference control.

In all this, we go out from the fact that the staggered QAM (multi-carrier) modulation formats exhibit improper second order (SO) statistics, and can bring significant advantages in increasing the cell/network throughput in interference limited scenarios, as has been extensively demonstrated during last decade in 2G+ wireless system enhancements, through application of the Widely Linear Filtering (WLF) concept [7] [8]. The basis here was the single-carrier Gaussian-shaped Minimum Shift Keying (GMSK) signal, which has the same staggering structure as the OFDM/OQAM and TLO formats studied in the EMPhAtiC project. Based on that, there have been some recent attempts to exploit such effect in the LTE networks, as well. To do so, in the CP-OFDM only in-phase component is used, while the quadrature QAM component is zeroed. Although in this way the nominal link-level throughput is halved, on the cell, i.e. network-level the performance have been shown to significantly exceed the one with conventional OFDM configuration [9].

In order to keep the CP-OFDM and the FBMC formats on equal footing, in comparative evaluation from the point of view of robustness against lack of time- and/or frequency synchronism, primarily the BPSK modulation will be used, and results provided in terms of the minimum mean-square error (MSE). The QPSK will also be conducted here, mostly for illustration of vulnerability of two-dimensional constellations in the CP-OFDM, and a more detailed comparative evaluation will be conducted at some later stage, after the staggered CP-OFDM format might sufficiently be elaborated within the WP2 activities.

Concentrating on the flat-fading channel model, it has been shown that while for BPSK the one-tap equalization is sufficient, for M-QAM the involvement of time-domain degree(s) of freedom is necessary in addition to the quasi-spatial one (complex-conjugated version of a signal can be considered as an virtually spatial signal component). The WLF-based per-subchannel equalizer [10] [11] turns out to be identical to a heuristically derived structure [12] where the adaptation

of the $T/2$ taped FIR filter complex coefficient is performed by using the received complex signal samples as its inputs (no explicit utilization of its complex-conjugated version) and the quasi-complex (purely real or purely imaginary) errors. Since the combination of the two complex signal versions contributes to even larger spread of input signal covariance matrix, and thus contributes to slowing-down of the convergence process [13].

2.3.1 Scenario considered

The communications scenario used in this evaluation is a subset of a more complete configuration with two dislocated transmitters and two dislocated receivers, whose mutual communications are mediated by a relay. As indicated in Fig. 2-10, we keep only two transmitters, whereas the second source (S2) acts as co-channel interferer to S1, which is transmitting its data to destination D1. Due to the sources generally different distance to the destination node D1, there is the Line-of-Sight physical propagation delay difference, along with the relative drift of their clocks at the receiver terminal. Basically (not considering the phase jitter) it is a linear function of the transmit terminals symbols clocks, which are derived for their individual high frequency clocks, in Fig. 2-10 is denoted by Δf, tacitly representing the respective carrier frequency offsets. This additional time-variant symbol delays, i.e. clock drifts are not taken into account in this evaluation. Also, time-variant physical delay difference is not accounted for, and they are emulated by setting a range of physical delays that span one whole data (BPSK) symbol duration. Also, only a range of fixed carrier frequency offsets, without accounting for the terminals phase jitter components is used. The receiver's clock is deemed ideal, as well as are is its synchronization to the transmitters symbol and carrier frequencies, including the very initial detection of the useful signal and its alignment for the subsequent equalizer adaptation. Both the useful and interfering signals are considered to be of the same form (kindred), either CP-OFDM or OFDM/OQAM.

2.3.2 Overview of the WLF framework as inherently doubling the single-antenna spatial degree of freedom

As discussed in the above introductory part, in the following is presented distinction between the traditional Strictly Linear Filtering (SLF), and the recently actualized Widely Linear Filtering (WLF) framework, as very insightfully had been exposed in [14]. They reflect the differences in the Second Order (SO) statistics, that is respectively the Circular (CIR) and the Non-circular (NCIR) ones. The difference is the dependence of auto-correlation on the signal's phase-shift in the latter case.

Optimal receiver for a SO circular total noise

The complex envelope of a BPSK useful signal is given by

$$s(t) = \mu_s \sum_n a_n v(t - nT - t_s)$$

where $a_n = \pm 1$ are independent identically distributed random variables corresponding to the transmitted symbols, T is the symbol duration, $t_s,\ (0 = t_s = T)$ is the time origin of the useful signal, $v(t)$ is a raised-cosine pulse shape filter, and μ_s is a real-valued parameter that controls the instantaneous power $s(t)$.
Assuming an optimal sampling time for the useful signal $t_s = 0$ and noting $\boldsymbol{x}(t) = [x_1(t)\ x_2(t)]^T$ the vector of complex amplitudes of the signals at the output of the two receiving antennas, the

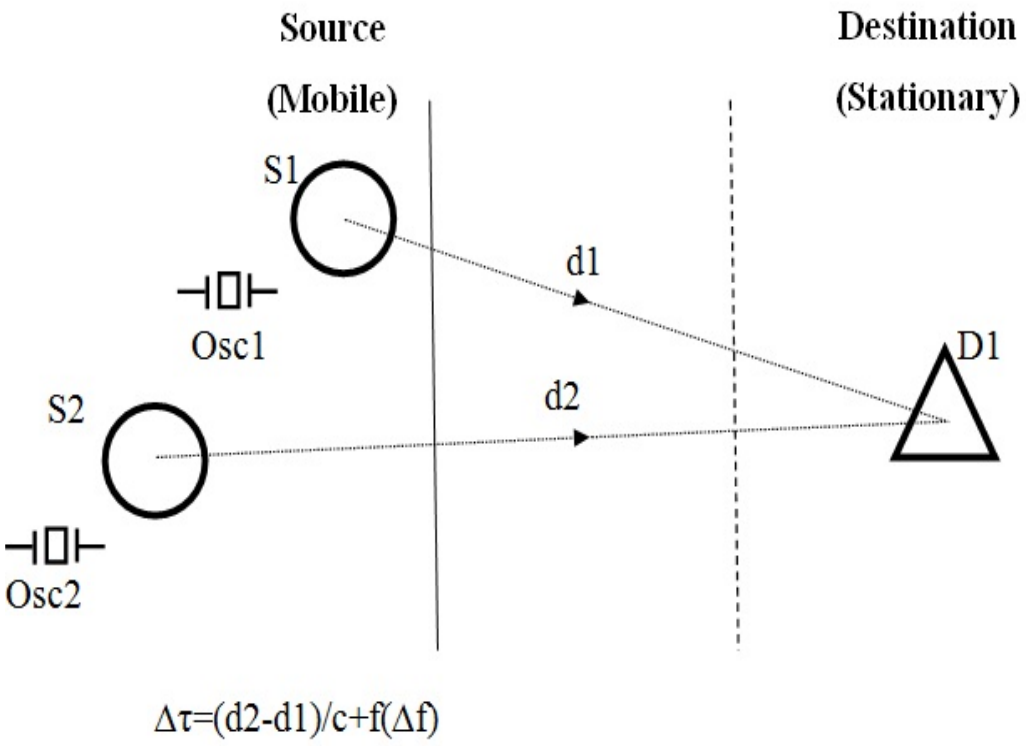

Figure 2-10: Block-diagram of the co-channel interference scenario.

sampled observations vector $\boldsymbol{x}_v(kT) = \boldsymbol{x}(t) \otimes v(-t)^* |_{t=kT}$, obtained after a matched filtering operation to the pulse shape filter $v(t)$ and a decimation operation at the symbol rate is given by

$$\boldsymbol{x}_v(kT) \approx s_v(kT)\boldsymbol{h}_s + \boldsymbol{b}_{Tv}(kT) = \mu_s r(0) a_k \boldsymbol{h}_s + \boldsymbol{b}_{Tv}(kT)$$

where $s_v(kT) = s(t) \otimes v(-t) * |_{t=kT}$, $r(t) = v(t) \otimes v(-t)^*$ is a Nyquist filter, $\otimes$ is the convolution operation, $\boldsymbol{h}_\mathrm{s}$ is the channel impulse response vector of the useful signal and $\boldsymbol{b}_{Tv}(kT)$, assumed stationary and statistically independent of the useful symbols, is the sampled total noise vector at the output of the filter $v(-t)^*$.
The optimal receiver for an SO circular total noise is depicted in Fig. 2-11. The output of the filter is given as

$$z(kT) = \boldsymbol{w}_s^H \boldsymbol{x}_v(kT),$$

where $\boldsymbol{x}_v(kT)$ is input vector of complex amplitudes and $\boldsymbol{w}_s$ is spatial matched filter (SMF) defined by

$$\boldsymbol{w}_s = \boldsymbol{R}^{-1}\boldsymbol{h}_s,$$

where $\boldsymbol{R} = E[\boldsymbol{b}_{Tv}(kT)\, \boldsymbol{b}_{Tv}(kT)^H]$ is the correlation matrix of the total noise vector $\boldsymbol{b}_{Tv}(kT)$. Assuming uncorrelated sampled vectors $\boldsymbol{b}_{Tv}(kT)$, the classical maximum likelihood estimation (MLE)[1] receiver, called CIR-MLE receiver, generates the sequence of symbols $a_k(1 \le k \ge K)$. The symbol +1 (respectively, -1) is decided when $z(kT) = 2\mathrm{Re}[\boldsymbol{w}_s^\mathrm{H}\boldsymbol{x}_v(kT)] > 0$ (respectively, <0).

[1]It is indicated in [14] that there exists direct proportionality connection between the ML and the minimum mean square error (MMSE) derived receivers, and it is defined by the following expression $\boldsymbol{w}_{mse} = \boldsymbol{R}_x^{-1}\boldsymbol{r}_{xa} = [\pi_s^{1/2}/(1 \pm \pi_s \boldsymbol{h}_s^H \boldsymbol{R}^{-1}\boldsymbol{h}_s)]\boldsymbol{R}^{-1}\boldsymbol{h}_s = \beta_1 \boldsymbol{w}_s$ where $\boldsymbol{r}_{\mathrm{xa}} = \mathrm{E}[\boldsymbol{x}_v(kT)a_k^*]$, $\pi_s = \mathrm{E}[|s_v(kT)|^2]$ is the power of the useful signal, $\boldsymbol{R}_x = E[\boldsymbol{x}_v(kT)\boldsymbol{x}_v(kT)^H] \approx \pi_s \boldsymbol{h}_s \boldsymbol{h}_s^H \pm R$ is correlation matrix of $\boldsymbol{x}_v(kT)$ and β_1 is a real scalar.

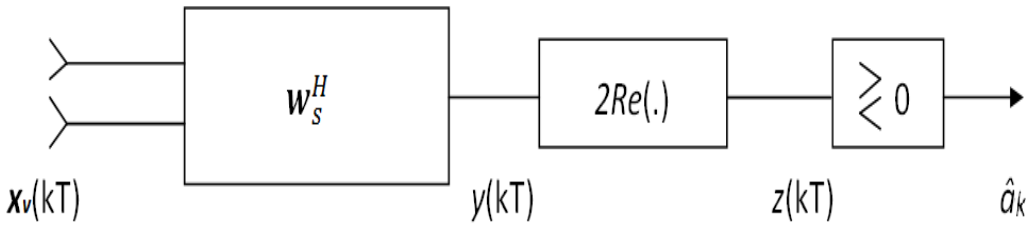

Figure 2-11: CIR-MLE receiver's structure for a BPSK signal.

The figure illustrates structure for $N = 2$ receiving antennas and BPSK modulation. This is the classical MLE receiver that minimizes the output sequence error rate.

In the case of $N = 1$ receiving antenna (Fig. 2-12) $h_s = |h_s|\mathrm{e}^{\jmath\phi_s}$ and the CIR-MLE receiver becomes reduced to a phase compensation of the useful signal, which thus becomes a real signal, followed by the removal of the imaginary part of the compensated observation.

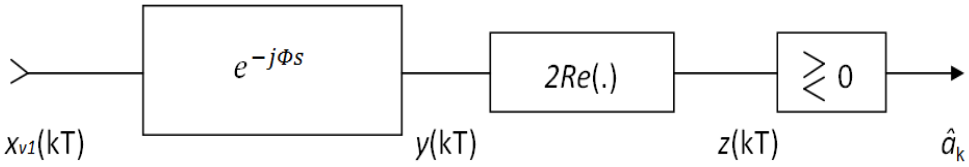

Figure 2-12: CIR-MLE receiver's structure for a BPSK signal and for $N = 1$.

The classical MLE receiver assumes a SO circular, Gaussian, and stationary vector $\boldsymbol{b}_{Tv}(kT)$ despite the fact that the interferences may be rectilinear and thus non Gaussian. In the absence of interference, CIR-MLE receiver is optimal and corresponds to the well-known maximal ratio combining(MCR) receiver. In the presence of noise, which does not satisfy the mentioned statistics this receiver becomes suboptimal.

Optimal receiver for an SO noncircular total noise

The optimal receiver for an SO noncircular total noise is depicted on Fig. 2-13. The figure illustrates structure for $N = 1$ receiving antennas and BPSK modulation. At the input of the filter we have the scalar signal $x_{v1}(kT)$ and its conjugated version $x_{v1}^*(kT)$, so that the output of the filter is given as

$$y(kT) \ = \tilde{\boldsymbol{w}}_s^H \ \tilde{\boldsymbol{x}}_v(kT)$$

where the 2×1 vectors $\tilde{\boldsymbol{x}}_v(kT)$ and $\tilde{\boldsymbol{h}}_s$ are defined by $\tilde{\boldsymbol{x}}_v(kT) \ = \ [x_{v1}(kT) \ x_{v1}^*(kT)]^T$ and $\tilde{\boldsymbol{h}}_s \ = \ [h_{s1} \ h_{s1}^*]^T$, respectively. The MLE receiver in SO noncircular, Gaussian and stationary total noise is denoted by NCIR-MLE receiver, and $\tilde{\boldsymbol{w}}_s$ is the so-called widely linear (WL) spatial matched filter (WL-SMF) defined by

$$\tilde{\boldsymbol{w}}_s = \boldsymbol{R}_b^{-1}\tilde{\boldsymbol{h}}_s \ ,$$

Where $\boldsymbol{R}_b \ = \ \mathrm{E}[\tilde{\boldsymbol{b}}_{Tv}(kT) \ \tilde{\boldsymbol{b}}_{Tv}^H(kT)] \ = \ \begin{bmatrix} \boldsymbol{R} & \boldsymbol{C} \\ \boldsymbol{C}^* & \boldsymbol{R}^* \end{bmatrix}$ is the correlation matrix of the total noise vector $\tilde{\boldsymbol{b}}_{Tv}(kT) = [b_{Tv1}(kT) \ b_{Tv1}^*(kT)]^T$, and $\boldsymbol{R}$ and $\boldsymbol{C}$ are the correlation and pseudo-

correlation matrices of the vector $\boldsymbol{b}_{Tv1}(kT)$, respectively. The output of WL receiver is real-values, and the symbol +1 (respectively, -1) is decided when $z(kT) > 0$ (respectively, <0).

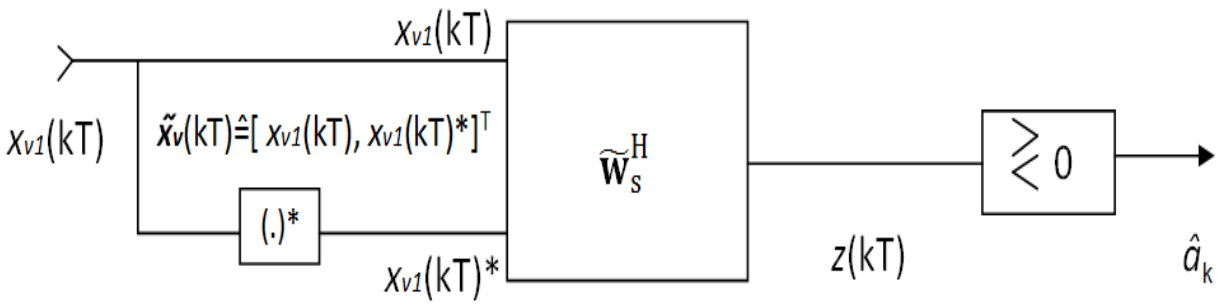

Figure 2-13: NCIR-MLE receiver's structure for a BPSK signal.

2.3.3 Performance of the CIR-MLE and NCIR-MLE receivers in the presence co-channel interference

In a radio communication networks, the interferences may be generated by the network itself (signals from neighboring cells using the same frequencies in a cellular network) and may be called internal. (In the considered scenario, the roles of the BSs are played by other users' equipments (UE).) This type of interference has the same waveform and modulation as the useful BPSK signal and it is non-Gaussian, rectilinear and stationary at the output of the matched filter after the sampling operation at the symbol rate. In this situation, the vector $\boldsymbol{b}_{Tv}(kT)$ can be written as

$$\boldsymbol{b}_{Tv}(kT) \approx \varphi_{1v}(kT)\boldsymbol{h}_1 + \mathbf{b}_{\mathrm{v}}(kT)$$

where $\boldsymbol{b}_v$ is the sampled background noise vector, assumed zero-mean, stationary, Gaussian, SO circular and spatially white, $\boldsymbol{h}_1$ is the channel impulse response vector of the interference, and φ_{1v} is the sampled complex envelope of the interference after the matched filtering operation. In the presence of this type of the interference, for $N = 1$ receiving antenna, spatial matched filter (SMF) $\boldsymbol{w}_{\mathrm{s}}$ reduces to a useful signal contribution in the real part of $y(kT)$. Then, the imaginary part of $y(kT)$, which contains no useful signal, is removed to generate $z(kT)$, which still contains the real part of interference plus background noise. Fig. 2-14 illustrates these steps on both the useful signal and interference constellations[2].
In the case WL-MLE receiver, for $N = 1$ receiving antenna, the complex response of the WL-SMF filter to the interference can be written as $\eta e^{j\psi}$, where η is a real quantity and ψ is defined by the phase of $h_s^* h_1$, which corresponds to equivalent phase difference between the interference and the useful signal $h_s = |h_s|\mathrm{e}^{\jmath\phi_s}$ and $h_1 = |h_1|\mathrm{e}^{\jmath\phi_1}$). WL-SMF filter approximately alignes the phase of the interference on the imaginary axis. In this way WL-SMF suppress the real part of the interference and thus its contribution in the output, while the useful signal's SNR becomes partly degraded. Fig. 2-15 illustrates these steps on both the useful signal and interference constellations.

[2] $\pi_{\mathrm{s}} = \mathrm{E}[|s_v(kT)|^2]$ is the power of the useful signal and $\pi_{\mathrm{s}} = \mathrm{E}[|j_v(kT)|^2]$ is the power of the interference signal.

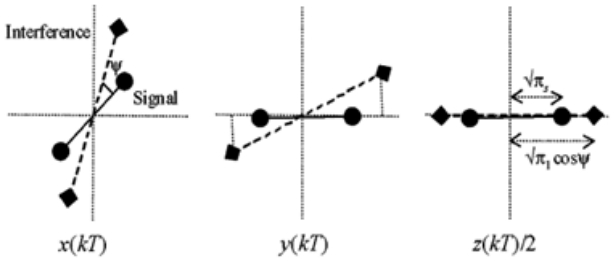

Figure 2-14: Constellations of BPSK useful signal and interference at the CIR-ML receiver output for

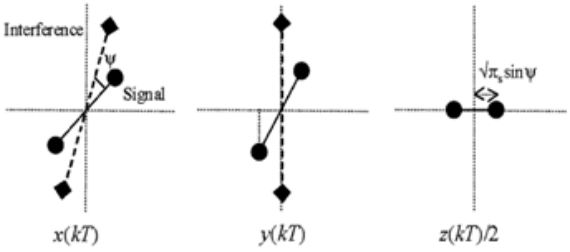

Figure 2-15: Constellation of BPSK useful signal and the Interference at the NCIR-MLE receiver output.

In difference to the rectilinear (PAM, BPSK) formats, in the case of the OQAM modulation format constellation is not composed from only two points. There are many points, which are arranged on a line and have Gaussian distribution This is illustrated in the Fig. 2-16, Fig. 2-17 and Fig. 2-18.

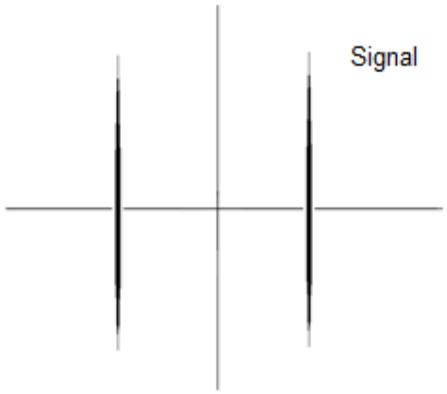

Figure 2-16: Constellation of a OFDM/OQAM subchannel signal for BPSK and ideal transmission channel.

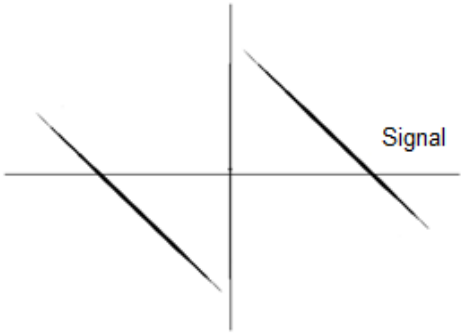

Figure 2-17: Constellation of OQAM useful signal in fading and the absence of interference.

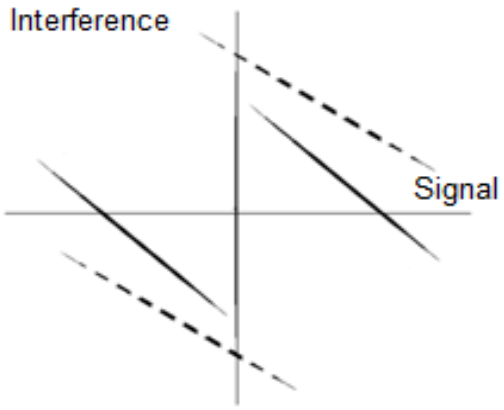

Figure 2-18: Constellation of OQAM useful signal flat in flat fading and the presence of interference.

Obviously, for the case of staggered both single-carrier and multi-carrier formats it can be concluded that the mere spatial matched filter WL-SMF, described above, can not suppress the interference with only the one-tap adjustment. For that reason it is need to include in the analysis the time dimension along with the space dimension, so that the phase/amplitude adjustments can be applied on the individual sets of frequency components. Spatiotemporal (ST) WL filter with more than one tap may mitigate the limitations of spatial WL filters by coping with the so-called intrinsic interference present in the modulation formats with I/Q staggering. (The FBMC, i.e. OFDM/OQAM situation in presence of co-channel interference and/or as used in the point-to-point (collocated) and distributed MIMO configurations may also require cross-subchannel structures in addition to SISO per-subchannel equalizers, as will be elaborated within D4.1.)

2.3.4 One-tap and multi-tap WLF equalizers

As has been indicated in the introductory part, the general multi-tap WLF equalizer configuration corresponds to those derived heuristically in [12], and through exhaustive analysis in [10] [11]. The WLF-based per-subchannel equalizer is presented here for only one-tap case, for both structures and recursive least-square (RLS) coefficients adaptation algorithm.

The input vector of the algorithm per subcarrier k and time instant i is defined as

$$\boldsymbol{u}_i(k) = \left[\begin{array}{cc} \mathrm{Re}\{R_i(k)\} & -\mathrm{Im}\{R_i(k)\} \end{array} \right]^T,$$

where $R_i(k)$ denotes the received symbols, and $\mathrm{Im}\{\cdot\}$ is the imaginary part of a complex number. The error signal for the RLS algorithm is defined as the difference of desired signal and the output of the projection of the filtered received signal,

$$E_i(k) = A_i(k) - \mathrm{Re}\{P_{i-1}(k)R_i(k)\} = A_i(k) - \boldsymbol{u}_i^T(k)\boldsymbol{p}_{i-1}(k)$$

where $\boldsymbol{p}_{i-1}(k) = \left[\begin{array}{cc} \mathrm{Re}\{P_{i-1}(k)\} & \mathrm{Im}\{P_{i-1}(k)\} \end{array} \right]^T$ is previously estimated equalizer coefficient vector, and $A_i\,(k)$ denotes the ideal real-valued BPSK signal.

In the following an MATLAB-like implementation of the RLS algorithm is provided for convenience of explicating the way of calculation of the corresponding adaptation gain AEX:

```
    wei = 0.9;
    Lm = ones(K,1) * 10^6;
for k = 1:K
    E(k) = A(k) - [real(R(k)) - imag(R(k))] * [real(P(k)) + imag(P(k))]';
    AEX = Lm(k) * conj(R(k))/(wei + R(k) * Lm(k) * conj(R(k)));
    Lm(k) = (Lm(k) - AEX * R(k) * Lm(k))/wei;
    P(k) = P(k) + AEX * E(k);
end
```

Extensions to multi-tap configuration is quite straightforward, in that the scalar coefficients are replaced by vectors, and the scalar Lm becomes a three-dimensional matrix, with the first two dimensions given by the number of equalizer coefficients.

2.3.5 Simulation results

The comparative evaluation results presented below are given for the case co-channel interference of the same power as the desired signal (SIR = 0 dB). The results are presented for BPSK and QPSK modulation formats, and illustrate the behavior of CP-OFDM (25 % cyclic prefix length) and FB-MC in delay-synchronized and unsynchronized scenarios as well as in frequency-synchronized and unsynchronized scenarios. The 3D diagrams illustrate the change of MSE as a function of time offset and frequency offset of interfering signal referred to the signal of interest (useful signal). Frequency offset is normalized by sub-channel spacing and time offset is indicated in the number of signal samples. All results are given for SNR = 20dB. Only frequency-flat, Rayleigh-distributed fading channel model was used, with for 1000 fading realization each pair of offsets, with sufficiently long equalizer training interval length (300 training intervals for CP-OFDM and 120 training intervals for FB-MC).

We compared results for CP-OFDM and FBMC for multi-carrier case with 48 active out of the total number of 64 subchannels.). Included also are the single-carrier cases, for one thing to serve as a reference, and for the other to possibly indicate the behavior of the formats if the parallel per-subchannel equalization configurations would have been used, to increase the available degrees of freedom in FBMC case to cope with the co-channel interfering signal. Namely, as discussed earlier, the staggered QAM single-carrier formats can use the fact that the quadrature component complementary to the one carrying the useful information does not have to be equalized to its (ideally) interpolated value. However, as the partially overlapping adjacent subchannels are introduced, the per-subchannel equalizer needs to compromise the suppression of both adjacent and co-channel interference. Only linear equalization is used - one-tap for CP-OFDM, and 8/4 DFE in FBMC case, without explicit compensation of the adjacent subchannels interference.

For illustration of the needed convergence times, and the need for its increase, in Fig.2-19 and Fig.2-22 are shown the averaged equalizer MSE values in dB for the case of CP-OFDM with FB-MC, for SNR = 20dB, and BPSK and QPSK modulation, respectively.

From Fig.2-19 it can be seen that the much longer adaptation time is needed in case with co-channel interference (CCI) than without it. The apparent absence of such effect in the FBMC case is quite likely related to lack of additional degrees of freedom (compensation of adjacent sub-channels interference), which should be taken into account in the assessment of the targeted simulation results. Yet, as seen fom Fig.2-20, although staying at relatively large MSE values, the MSE error for the FBMC case apparently does not change within the range of the inserted offsets, while the CP-OFDM MSE values increase quite rapidly. To gain a

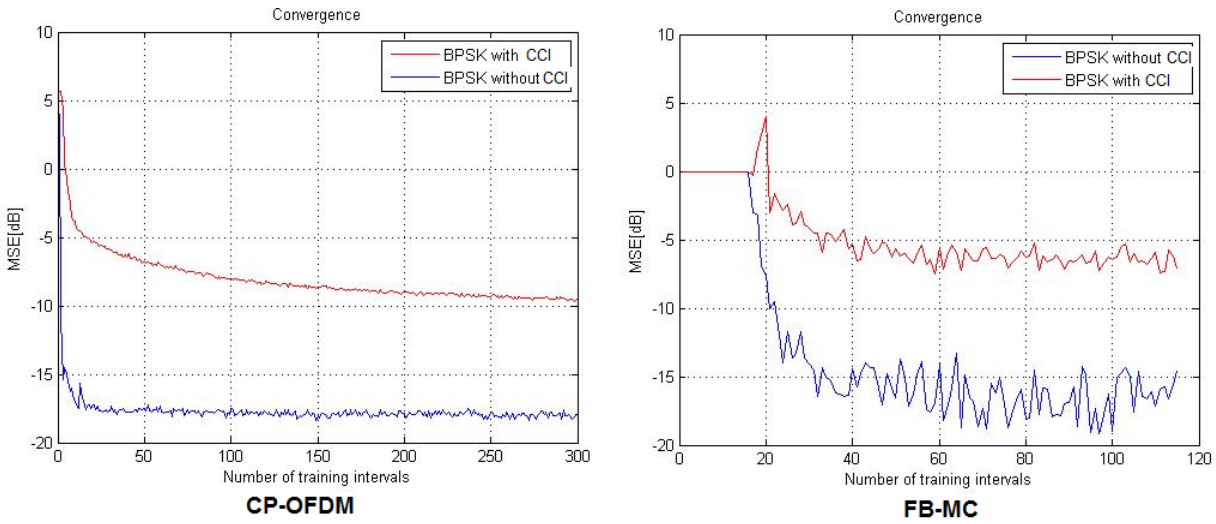

Figure 2-19: Comparison of convergence of CP-OFDM and FB-MC for BPSK case without frequency and time offsets in the co-channel interfering signals.

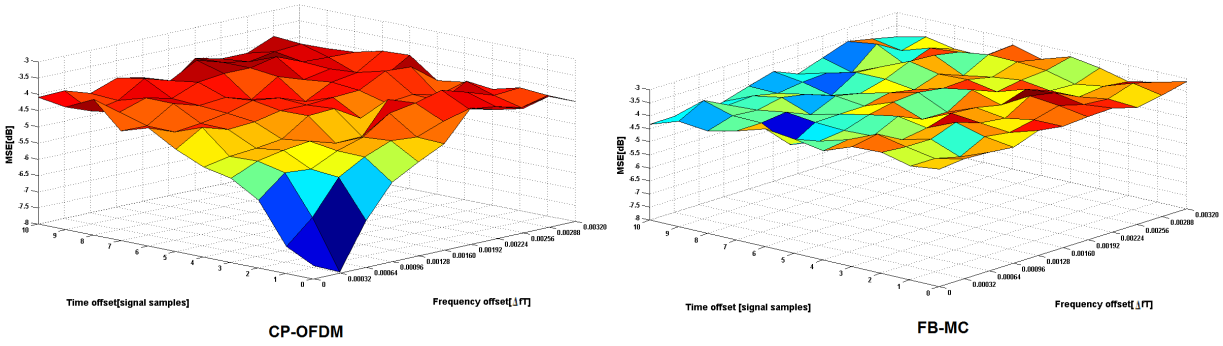

Figure 2-20: Variation of MSE as a function of time offset and frequency offsets of interfering signal referred to the 48 active out of the total number of 64 subchannels, the case for the BPSK modulation.

better insight into the possible limitation of this evaluation, in Fig.2-21 are shown the MSE variations for just single-carrier case. Interestingly, and quite unexpectedly, the FBMC case degrades performance in the presence of frequency offset, while for the time offsets they remain essentially unchanged. (Although the maximal amount of time-offset is less than the duration of CP, the multicarrier CP-OFDM format exhibits increase of the MSE degradation, compared to the case with just one subchannel.)

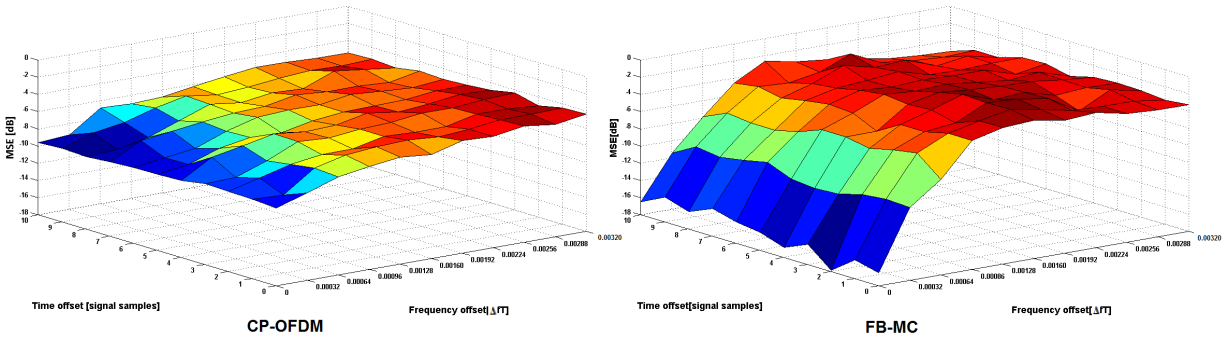

Figure 2-21: Variation of MSE as a function of time offset and frequency offsets of interfering signal referred to the useful signal for 1 active out of the total number of 64 subchannels, the case for the BPSK modulation.

The same set of simulation results is given bellow for the case of QPSK modulation in subchannels. Although it is expected that here the FBMC would perform better, as suggested also by the convergence plots shown in Fig.2-22, it is not reflected in the 3-D MSE results in terms of any appreciable difference in the MSE degradation rates, except that in the CP-OFDM case the better performance without time/frequency shifts exhibited in the BPSK case is now missing. This, actually, could be indicative of the inherent deficiency of the non-staggered QAM formats when it comes to the sensitivity to the presence of co-channel interference.

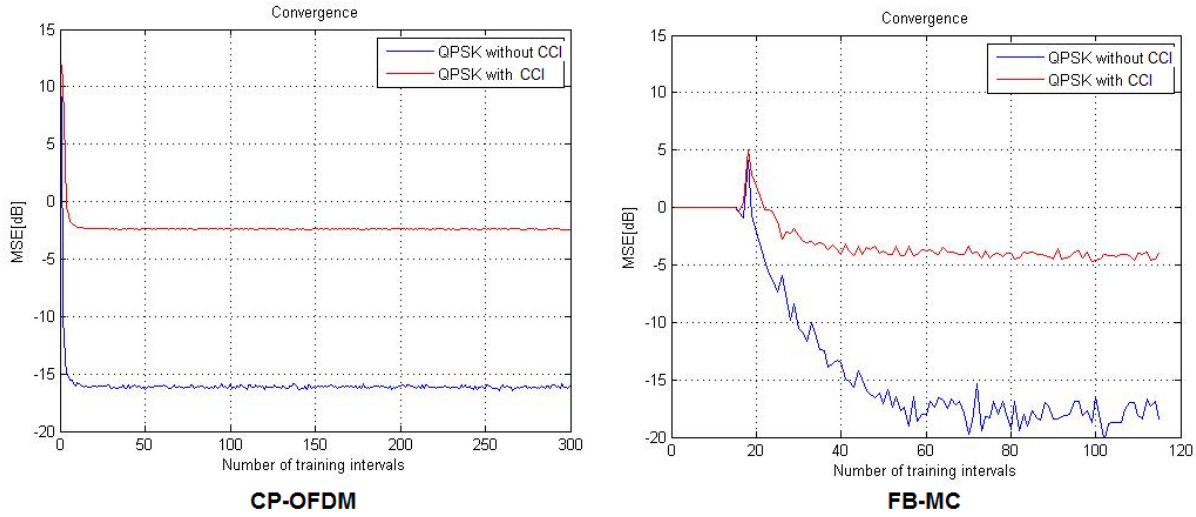

Figure 2-22: Comparison of convergence CP-OFDM with FB-MC for case without frequency and time offsets for QPSK modulation in the co-channel interfering signals

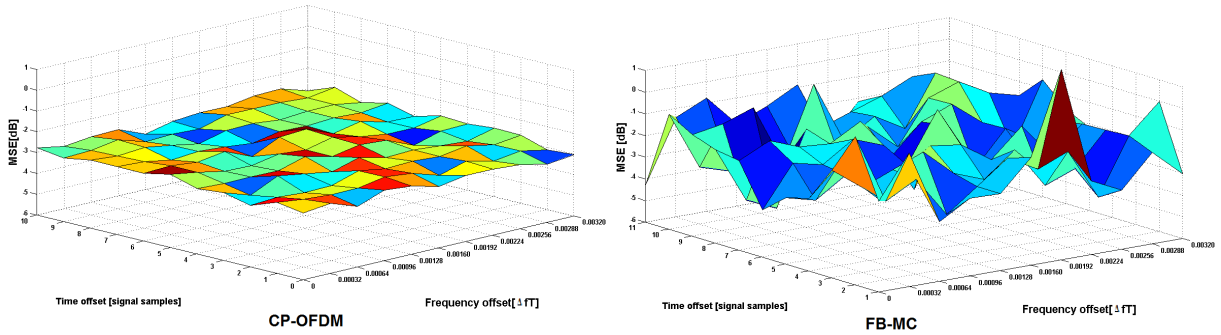

Figure 2-23: Variations of MSE as a function of time offset and frequency offsets of interfering signal referred to the useful signal for 48 active out of the total number of 64 subchannels, the case for the QPSK modulation.

The last of the set of the QPSK-related results may again confirm the (still) potential advantages of the FBMC formats in the presence of the time and/or frequency offsets.

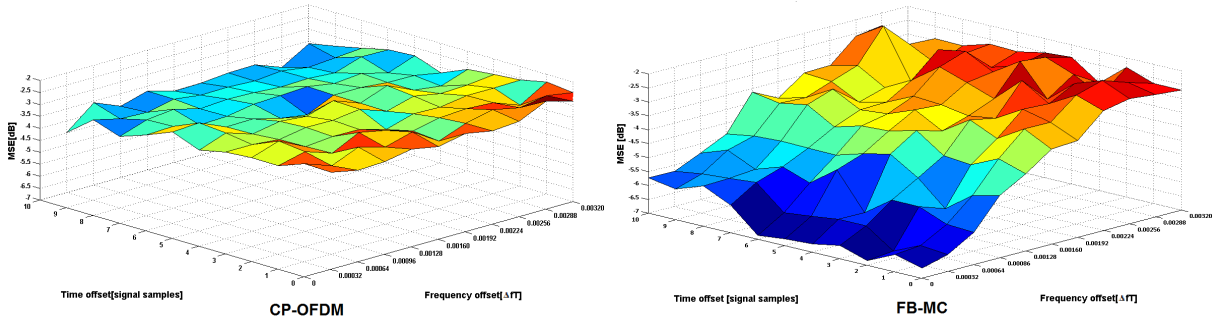

Figure 2-24: Variation of MSE as a function of time offset and frequency offsets of interfering signal referred to the useful signal for 1 active out of the total number of 64 subchannels, the case for the QPSK modulation.

2.3.6 Conclusions

With the above analysis and the accompanying simulation results it can be inferred an certain advantage of staggered multi-carrier modulation formats with spectrally shaped subchannels over the conventional CP-OFDM ones, in terms of the robustness in the presence of time-and frequency-unsynchronized co-channel interference. To arrive at such conclusion with possibly less uncertainty, along the appropriate support of explicit suppression of adjacent subchannel interference in FBMC case, much wider range of time-offsets should be used, It is expected that the forthcoming inclusion of the distributed MIMO configuration towards the preparation of the deliverable D4.1 may provide the right and most relevant and definitive insight into the expected differences in the robustness to inter-stream signals time and frequency offsets.

2.4 On the robustness of FBMC in delay asynchronous relay transmission

2.4.1 Multi-taps equalization of asynchronous relay transmission

2.4.1.1 System model

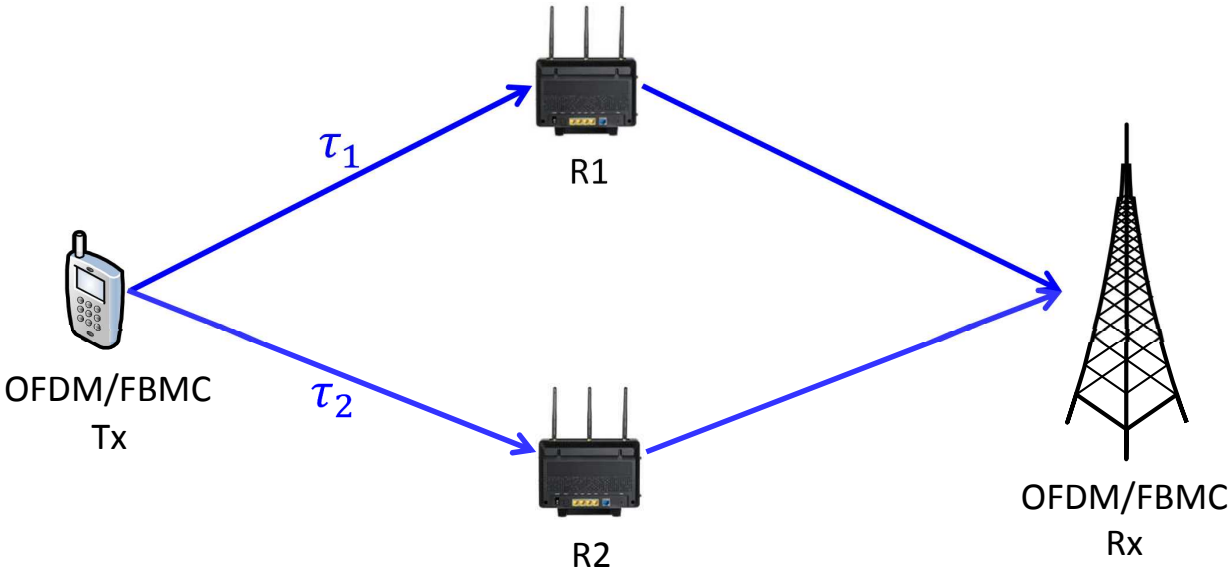

Figure 2-25: Asynchronous multicarrier based relay network

We consider a multicarrier based wireless network that consists in a source transmitter, two relay nodes R1 and R2, and a destination receiver as shown in Figure 2-25. All nodes have a single transmit antenna and also a single receive one. The relays are operating according to the Amplify and Forward (AF) protocol. We assume that there is no direct link between the source transmitter and the destination receiver due to the strong path-loss factor resulting from the large distance separating them.

Two multicarrier techniques are considered:

- the classical orthogonal frequency division multiplexing (OFDM) with a cyclic prefix duration (CP) $\Delta = T/8$ where T denotes the OFDM symbol period
- the filter bank based multicarrier (FBMC) one using using the prototype filter proposed in the European funded project "Physical Layer for Dynamic Access and Cognitive Radio-PHYDYAS" [15].

Since the transmitter is located at different distances from the relays, a different time delay is introduced on each source-relay-destination path. Let τ_1 and τ_2 be the delays associated to the signals received by the destination from relays R1 and R2, respectively. These delays are assumed to be uniformly distributed on the interval $[0, \tau_{\max}]$.

Consequently, we can express the composite signal at the destination receiver by the sum

of two delayed versions of the transmitted signal,

$$\begin{aligned} r(t) &= \sum_{i=1}^{L} h_{R_i \to D} \left(h_{S \to R_i} s(t-\tau_i) + n_i(t) \right) + n_D(t) \\ &= \sum_{i=1}^{L} \underbrace{h_{R_i \to D} h_{S \to R_i}}_{h_i} s(t-\tau_i) + \underbrace{h_{R_i \to D} n_i(t) + n_D(t)}_{n(t)} \end{aligned} \tag{2.7}$$

where,

- $h_{R_i \to D}$ stands for the complex channel gain between the relay R_i and the receiver destination
- $h_{S \to R_i}$ is the complex channel gain between the source transmitter and the relay R_i
- $n_i(t)$ and $n_D(t)$ denote respectively the additive white Gaussian noise (AWGN) at R_i and the receiver destination

Since the complex channel gains $h_{R_i \to D}$, $h_{S \to R_i}$ are independent Gaussian random variables, the product,

$$h_i = h_{R_i \to D} h_{S \to R_i} \tag{2.8}$$

follows the product-normal distribution with a probability density function,

$$f_X(x) = \frac{K_0(|x|)}{\pi} \tag{2.9}$$

where K_0 is the modified Bessel function of the second kind.
The received signal given in (2.7) can be rewritten in the following form,

$$r(t) = s(t) * \sum_{i=1}^{L} h_i \delta(t-\tau_i) + n(t) \tag{2.10}$$

Consequently, our system model can be reduced to OFDM/FBMC transmission through a multi-path channel with the following impulse response,

$$h(t) = \sum_{i=1}^{L} h_i \delta(t-\tau_i) \tag{2.11}$$

This latter becomes highly frequency selective when the timing offsets τ_i associated to each relay R_i path are very large.

OFDM case: When the maximum value of the timing offsets $\tau_{\max} = \max\{\tau_i, i = 1, ..., L\}$ does not exceed the cyclic prefix duration Δ, the orthogonality between the system subcarriers is preserved and the receiver is able to recover the useful signal free of inter-symbol interference (ISI) and inter-carrier interference (ICI) [16]. In this case, single complex coefficient per subcarrier equalizers provide the optimal performance. However when $\tau_{\max} > \Delta$, the orthogonality between the subcarriers is no longer maintained and a high amount of interference appears in all subcarriers [16]. This interference will strongly affect the system performance.

FBMC case: If the channel frequency response is assumed to be locally flat, that is,

$$\Omega_{\Delta m} = \{l, |l| \leq \Delta m \mid H(m_0 + l) \approx H(m_0)\} \tag{2.12}$$

where $\Omega_{\Delta m}$ be the neighborhood area around the subchannel m_0. It should be noticed that $\Omega_{\Delta m}$ depends on the coherence bandwidth B_c, i.e. on $\tau_{\max}$ [17], [18].
And if we consider that the prototype filter is well localized in both time and frequency domains [19], [20] meaning that, $\int_{-\infty}^{+\infty} f(t - nT/2) f(t - n_0 T/2) e^{j\frac{2\pi}{T}(m-m_0)t} dt$ immediately tends to zero when $|n - n_0|$ and $|m - m_0|$ increase. Therefore, a single tap per subcarrier equalization will achieve optimal performances.
However when $\tau_{\max}$ becomes non-negligible compared to the prototype filter length KT (here, K is the overlapping factor), the assumption that $f(t - \tau) \approx f(t)$ when $\tau \in [0, \tau_{\max}]$ is no longer valid and the orthogonality between the system subcarriers will be destroyed.
To deal with this problem, three main approaches have been proposed in the literature. The first one uses well localized waveforms that is, the pulse energy both in time and frequency domains are well contained to limit the effect on the neighborhood of a given symbol [20], [21], [19]. In this case, a basic equalizer structure of a single complex coefficient per subcarrier is considered.
The second approach uses FIR (finite impulse response) filters as subcarrier equalizers with cross connections between the adjacent subchannels to cancel the inter-carrier interference [22], [23].
The third approach applies a receiver filter bank structure providing over-sampled subcarrier signals to avoid the cross connections between the subchannels, and performs subcarrier equalization using FIR filters [24], [25], [26]. Recently, Waldhauser et al. have proposed MMSE (minimum mean square error) and decision feedback equalizer per subcarrier designed for FBMC/OQAM [27], [28]. Based on the same approach but using frequency sampling method, Ihalainen et al. have presented a multi-tap per-subcarrier equalizer in such a manner that the frequency response of the designed filter is forced to take the given target values at a set of considered frequency points within a subchannel [29].

2.4.1.2 Review of multi-taps equalizers design

The derivation of the equalizer coefficients is based on the principle that the equalizer of a subcarrier is designed to optimally compensate, at some points in the sub-band, the channel distortions and the timing offset between the transmitter and the receiver. More specifically, the equalizer coefficients are computed such that, the equalizer amplitude response meets perfectly the inverse of the channel amplitude response and the phase equalizer is equal to the negative phase of the channel response, at all considered frequency points.

In this section, we discuss the design of the 3-tap equalizer. It is worth noticing that any n-multi-tap equalizer can be computed in the same manner. In this case, three points of the inverse of the channel frequency are required to for each subchannel: $EQ(i)$ and two intermediate points $EQ1$, $EQ2$ (as depicted in Figure 2-26).

As previously mentioned, the frequency points $EQ(m)$, $EQ1$ and $EQ2$ for a given sub-

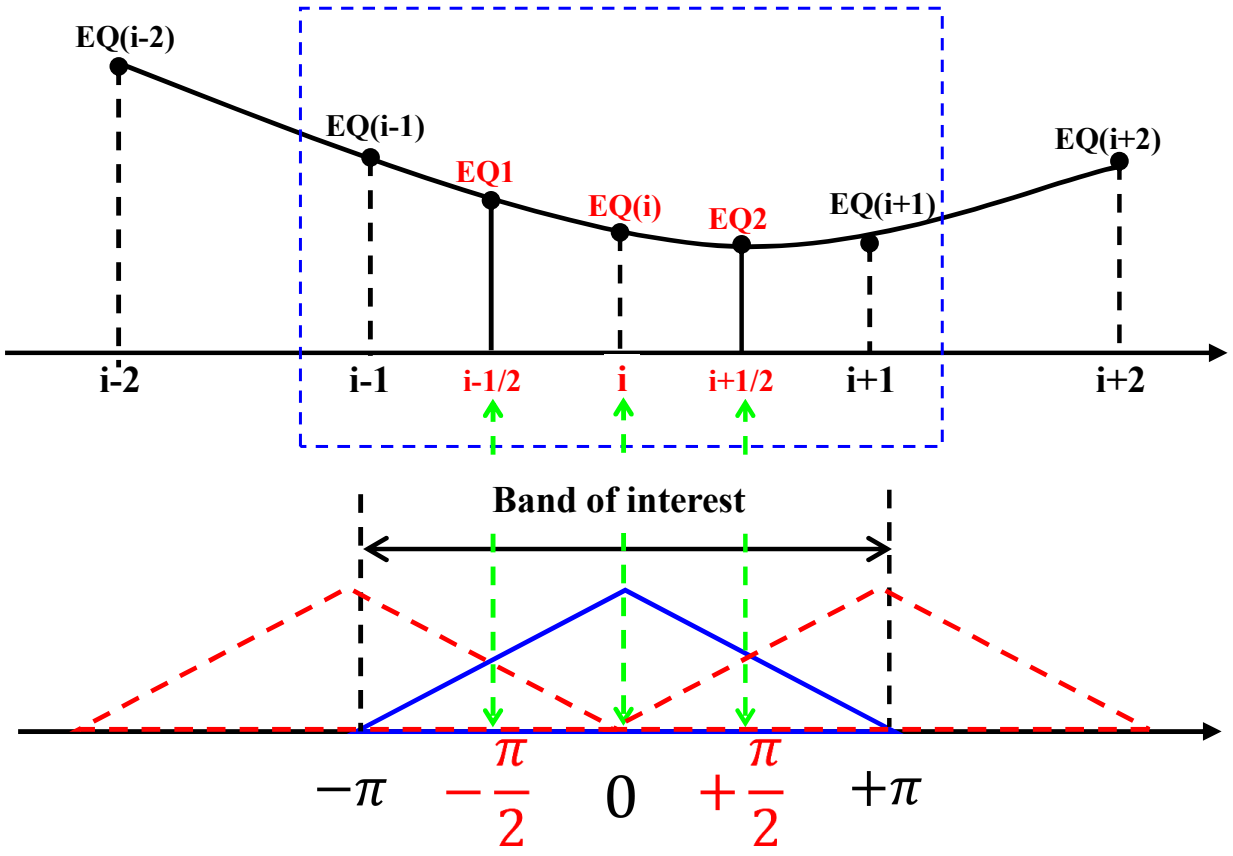

Figure 2-26: Points of the inverse subchannel frequency response used to compute the multi-tap equalizer

channel m are computed following the ZF (Zero-Forcing) criterion, that is,

$$\begin{aligned} EQ(m) &= \frac{H^*(e^{j2\pi m/N})}{|H(e^{j2\pi m/N})|^2} \\ EQ1 &= \frac{H^*(e^{j\pi(2m-1)/N})}{|H(e^{j\pi(2m-1)/N})|^2} \\ EQ2 &= \frac{H^*(e^{j\pi(2m+1)/N})}{|H(e^{j\pi(2m+1)/N})|^2} \end{aligned} \tag{2.13}$$

where, $H(e^{j2\pi m/N})$ is the channel frequency response at the subcarrier m, H^* stands for the conjugate of H and N denotes the number of subcarriers in the system.
Let $C_{\mathrm{eq,m}}(z)$ be the response of the equalizer of the subchannel m,

$$C_{\mathrm{eq,m}}(z) = c_{-1,m}z + c_{0,m} + c_{+1,m}z^{-1} \tag{2.14}$$

According to [29], the equalizer coefficients can be computed by resolving the following equations,

$$\begin{cases} C_{\mathrm{eq,m}}(e^{-j\pi/2}) = EQ1 \\ C_{\mathrm{eq,m}}(e^{-j0}) = EQ(m) \\ C_{\mathrm{eq,m}}(e^{+j\pi/2}) = EQ2 \end{cases} \text{(even subchannels) or } \begin{cases} C_{\mathrm{eq,m}}(e^{j\pi/2}) = EQ1 \\ C_{\mathrm{eq,m}}(e^{j\pi}) = EQ(m) \\ C_{\mathrm{eq,m}}(e^{j3\pi/2}) = EQ2 \end{cases} \text{(odd subchannels)} \tag{2.15}$$

We obtain then,

$$
\begin{aligned}
c_{-1,m} &= \pm\frac{1}{4}\left((2EQ(m) - EQ1 - EQ2) - j(EQ2 - EQ1)\right) \\
c_{0,m} &= \frac{1}{2}\left(EQ1 + EQ2\right) \\
c_{+1,m} &= \pm\frac{1}{4}\left((2EQ(m) - EQ1 - EQ2) + j(EQ2 - EQ1)\right)
\end{aligned} \tag{2.16}
$$

Note that the signs $+$ and $-$ correspond respectively to even and odd suchannels.

2.4.2 Cooperative MIMO relay for asynchronous multiuser transmission

2.4.2.1 System model

In this section, we consider a scenario of multiuser transmission in a multicarrier system with M subcarriers. We first consider the case of only two asynchronous users. We assume that the users occupy separate bands BW_u (u being the user index) according to the "subcarrier block assignment", and transmit to the same base station through two cooperative relays. Fig. 2-27 depicts the considered scenario. The signals of all users are received asynchronously by each relay. The delays $\tau_{i,j}$ between the ith user and the jth relay are random and uniformly distributed in the time interval $[0 \quad T]$, where T is the multicarrier period ($T = MT_s$, T_s being the sampling period). Each relay demodulates the signal of each user, and forwards them synchronously to the base station. It is worth noting that the relay is assumed to be able to be synchronized to each user and demodulate each user signal separately. The relays have the complete channel state information (CSI) from the users to the relays, and also from the relays to the base station. In order to increase the reliability, the relays cooperate to perform a maximum ratio transmitting (MRT). Hence, we can divide the scenario into two stages: the

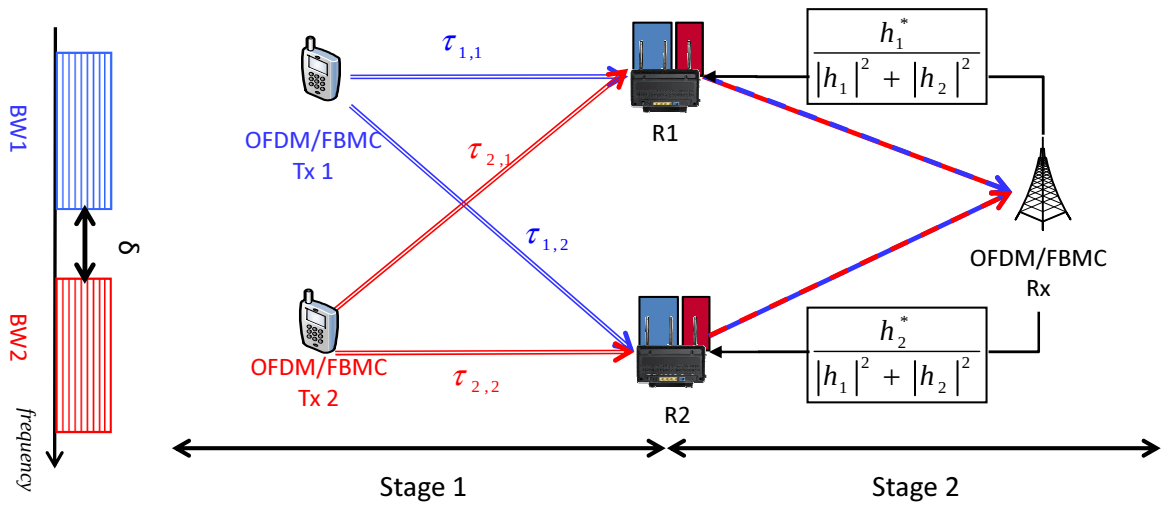

Figure 2-27: Description of the scenario

first one is the transmission between the users and the relays which is totally asynchronous. The second one is the link between the relays and the base station which is cooperative and

synchronous. It is assumed that the relays use two antennas for receiving but one transmit antenna. It is worth noticing that there is no diversity gain if two transmit antennas are used instead of one. This is because the performance of the whole system is limited by the first stage.

2.4.2.2 Asynchronous interference analysis

Let us assume that one of the relays is demodulating the signal from the user u. Since the other users are not synchronized with the considered one, the orthogonality between the subcarriers in BW_u and the others is lost, and an multiuser interference appears. The level of this interference is related to the spectrum shape of the signals and to the spectral distance. In order to minimize (or to avoid) the multiuser interference, a guard band of δ free subcarriers is introduced between each two adjacent users (*i.e.* BW_u and BW_{u+1}) [30].

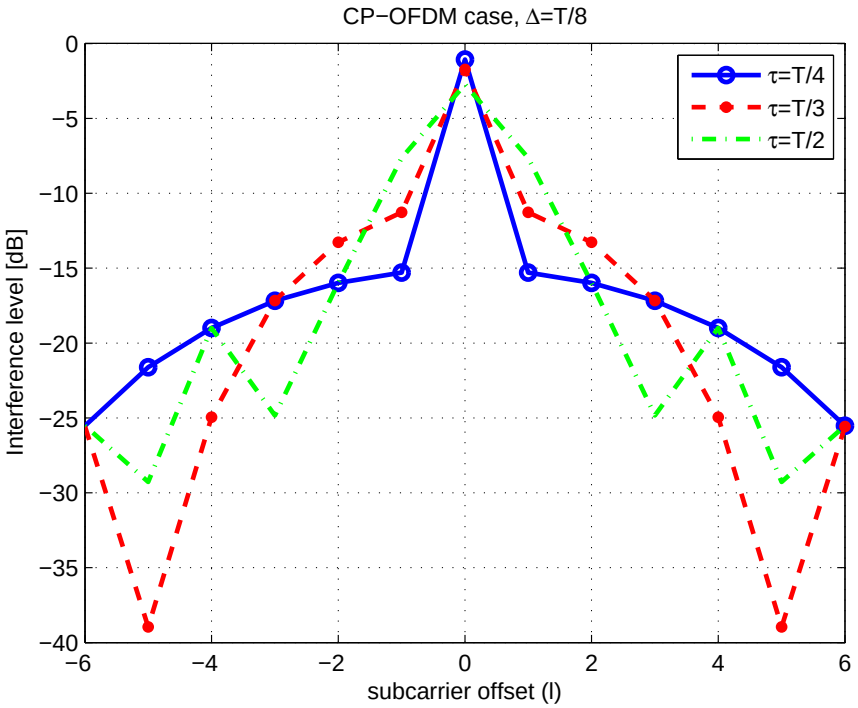

Figure 2-28: Description of the scenario

The interference power caused by one subcarrier on the others has been analyzed and evaluated in [31],[32] for OFDM and FBMC modulations. Fig. 2-28 and 2-29 depict the interference power (in dB) as a function of the spectral distance for some values of the asynchronism delay (τ), respectively for OFDM and FBMC using PHYDYAS filter. These values are calculated in a channel free case.

The demodulated received signal of the uth user can be written as

$$r_{k,n} = h_k(s_{k,n} + \sum_{k' \in BW_u} I_{k'}(0)) + \sum_{u'} \sum_{k' \in BW'_u} h_{k'} I_{k'}(\Delta_{uu'}) + b_{k,n}, \quad k \in BW_u \tag{2.17}$$

where h_k is the frequency response coefficient at the subcarrier k of the channel between the relay and user u such as $k \in BW_u$. Whereas, the coefficient $I_{k'}(\Delta_{uu'})$ represents the

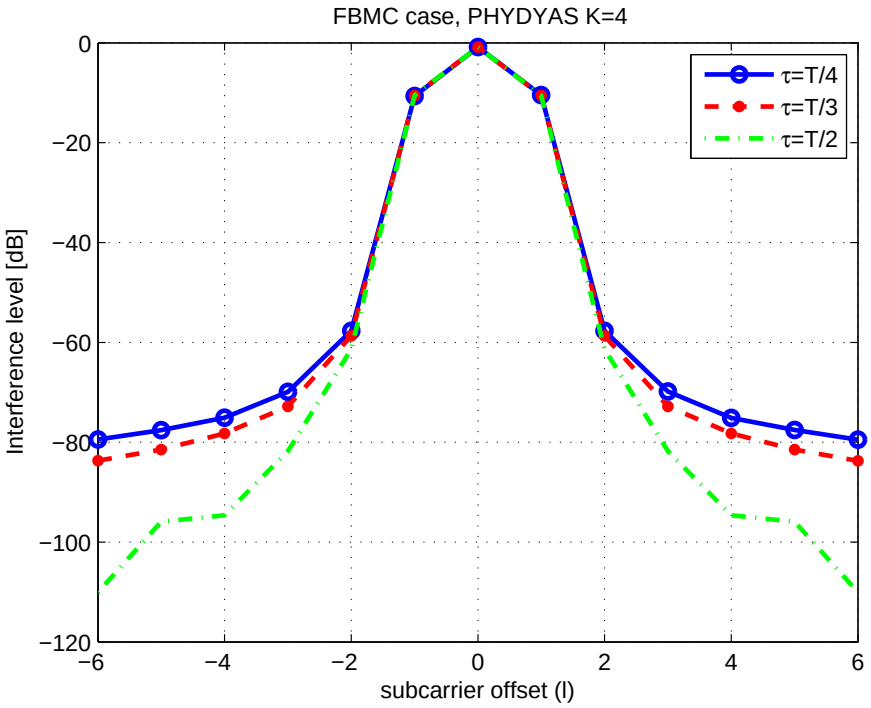

Figure 2-29: Description of the scenario

interference term caused by the signal in subcarrier k' on the subcarrier k and depends on the relative delay between the u'th and the uth users ($\Delta_{uu'} = \tau_{u'j} - \tau_{uj}$). It is worth pointing out that the equation above takes into account the fact that the subcarriers from the same user does not cause interference in OFDM case (*i.e.* $I_{k'}(0) = 0$). Whereas, in FBMC case, the term $I_{k'}(0)$ is purely imaginary (if we consider that $s_{k,n}$ are always real valued). Therefore, the performance of such a system depends strongly on the interference power. Let us denote the latter by $\rho_k(\Delta) = E\{|I_{k'}(\Delta)|^2\}$, some values of $\rho_{k'-k}(\Delta)$ are depicted in Fig. 2-28 and Fig. 2-29.

As we have aforementioned, since the interference from the same user is null, the considered user subcarriers which are the most exposed to the interference are the ones on the border of the block BW_u. In OFDM case, we can see from Fig. 2-28 that $\rho_{\pm 1}(\Delta)$ can reach up to $-8dB$ (when $\Delta = T/2$). When the spectral distance $|d| = |k' - k| = 6$, we only have $\rho_{\pm 6}(\Delta) = -25dB$. That is, if two user bands are separated by 6 subcarriers, the interference may exceed $-25dB$ at the border subcarriers (assuming all the channel coefficients are unit $h_{k'} = 1$). The total interference power in a subcarrier $k \in BW_u$ belonging to the block BW_u is obtained by the weighted sum of $\rho_{k'}(\Delta)$ and the channel coefficients $|h_{k'}|^2$, hence we can write:

$$P_{interf}(k) = \sum_{u'} \sum_{k' \in BW_{u'}} \rho_{k'-k}(\Delta_{uu'})|h_{k'}|^2, \quad k \in BW_u. \tag{2.18}$$

In the case where FBMC modulation is considered, Fig. 2-29 shows that practically $\rho_d(\Delta)$ is independent of the relative asynchronism delay Δ (The values below $-60dB$ are neglected). Moreover, it is quite clear that the interference is less than $-60dB$ for $|d| \geq 2$. That is, a guard band of only one subcarrier between the different users is sufficient to guarantee a negligible interference whatever the amount of the asynchronism delay.

Since the relays are equipped by two receive antennas, a maximum ratio combining is performed in each relay. The symbols at demodulator output of the lth relay is

$$\begin{aligned} y_{k,n,l} =& s_{k,n} + \sum_{k' \in BW_u} I_{k'}(0) + \frac{h^*_{k,l,1}}{|h_{k,l,1}|^2 + |h_{k,l,2}|^2} \sum_{u'} \sum_{k' \in BW'_u} h_{k',l,1} I_{k'}(\Delta_{uu'}) \\ &+ \frac{h^*_{k,l,2}}{|h_{k,l,1}|^2 + |h_{k,l,2}|^2} \sum_{u'} \sum_{k' \in BW'_u} h_{k',l,2} I_{k'}(\Delta_{uu'}) + \frac{h^*_{k,l,1} b_{k,n,l,1} + h^*_{k,l,2} b_{k,n,l,2}}{|h_{k,l,1}|^2 + |h_{k,l,2}|^2}, \quad k \in BW_u \end{aligned} \tag{2.19}$$

Hence,

$$\begin{aligned} y_{k,n,l} =& s_{k,n} + \sum_{k' \in BW_u} I_{k'}(0) + \sum_{u'} \sum_{k' \in BW'_u} \frac{h^*_{k,l,1} h_{k',l,1} + h^*_{k,l,2} h_{k',l,2}}{|h_{k,l,1}|^2 + |h_{k,l,2}|^2} I_{k'}(\Delta_{uu'}) \\ &+ \frac{h^*_{k,l,1} b_{k,n,l,1} + h^*_{k,l,2} b_{k,n,l,2}}{|h_{k,l,1}|^2 + |h_{k,l,2}|^2}, \quad k \in BW_u \end{aligned} \tag{2.20}$$

where $h_{k,l,i}$ is the channel coefficient at the subcarrier k between the uth user ($k \in BW_u$) and the ith antenna of the lth relay. Therefore, we obtain for OFDM the latter expression with $\sum_{k' \in BW_u} I_{k'}(0) = 0$, and for FBMC after retreaving the real part of the demodulated symbol:

$$\begin{aligned} \mathfrak{Re}\{y_{k,n,l}\} =& s_{k,n} + \mathfrak{Re}\left\{ \sum_{u'} \sum_{k' \in BW'_u} \frac{h^*_{k,l,1} h_{k',l,1} + h^*_{k,l,2} h_{k',l,2}}{|h_{k,l,1}|^2 + |h_{k,l,2}|^2} I_{k'}(\Delta_{uu'}) \right\} \\ &+ \mathfrak{Re}\left\{ \frac{h^*_{k,l,1} b_{k,n,l,1} + h^*_{k,l,2} b_{k,n,l,2}}{|h_{k,l,1}|^2 + |h_{k,l,2}|^2} \right\}, \quad k \in BW_u \end{aligned} \tag{2.21}$$

In the transmitting phase, the relays only use one antenna (for each relay) to transmit the whole users data to the base station. Since we assumed that the relays have the information about the channel between the relays and the base station, the relays can perform a maximum ratio transmission to exploit the diversity. Note that the assumption of perfect CSI at the relay sides may be relaxed by assuming that the base station calculates and only sends the weigh coefficients to the relays. It should be noted that the relays transmit the soft demodulated and equalized symbols without making hard decisions. Therefore, the received symbols of the whole users are given by:

$$z_{k,n} = \frac{|\mathfrak{h}_{k,1}|^2 y_{k,n,1} + |\mathfrak{h}_{k,2}|^2 y_{k,n,2}}{\sqrt{|\mathfrak{h}_{k,1}|^2 + |\mathfrak{h}_{k,2}|^2}} + \gamma_{k,n} \tag{2.22}$$

Hence, in general and after processing, we obtain

$$z_{k,n} = \underbrace{\sqrt{|\mathfrak{h}_{k,1}|^2 + |\mathfrak{h}_{k,2}|^2} s_{k,n} + \gamma_{k,n}}_{t_1} + \underbrace{\sum_{u'} \sum_{k' \in BW'_u} H_{k,k'} I_{k'}(\Delta_{uu'}) + \Gamma_{k,n}}_{t_2}, \tag{2.23}$$

where

$$H_{k,k'} = \frac{|\mathfrak{h}_{k,1}|^2 \left(h^*_{k,1,1} h_{k',1,1} + h^*_{k,1,2} h_{k',1,2} \right)}{\sqrt{|\mathfrak{h}_{k,1}|^2 + |\mathfrak{h}_{k,2}|^2 \left(|h_{k,1,1}|^2 + |h_{k,1,2}|^2 \right)}} + \frac{|\mathfrak{h}_{k,2}|^2 \left(h^*_{k,2,1} h_{k',2,1} + h^*_{k,2,2} h_{k',2,2} \right)}{\sqrt{|\mathfrak{h}_{k,1}|^2 + |\mathfrak{h}_{k,2}|^2 \left(|h_{k,2,1}|^2 + |h_{k,2,2}|^2 \right)}} \tag{2.24}$$

and the noise term $\Gamma_{k,n}$ is given by

$$\Gamma_{k,n} = \frac{|\mathfrak{h}_{k,1}|^2 \left(h^*_{k,1,1} b_{k,n,1,1} + h^*_{k,1,2} b_{k,n,1,2}\right)}{\sqrt{|\mathfrak{h}_{k,1}|^2 + |\mathfrak{h}_{k,2}|^2}\left(|h_{k,1,1}|^2 + |h_{k,1,2}|^2\right)} + \frac{|\mathfrak{h}_{k,2}|^2 \left(h^*_{k,2,1} b_{k,n,2,1} + h^*_{k,2,2} b_{k,n,2,2}\right)}{\sqrt{|\mathfrak{h}_{k,1}|^2 + |\mathfrak{h}_{k,2}|^2}\left(|h_{k,2,1}|^2 + |h_{k,2,2}|^2\right)} \tag{2.25}$$

The first term t_1 in equation (2.23) is the classical expression of an MRT interference-free received signal, whereas the second term t_2 represents the effect of the interference and noise from the first stage (*i.e.* at the relay side). The interference terms involving $H_{k,k'}$ can be avoided in FBMC by introducing a guard band of one subcarrier between the users because the terms $I_{k'}(\Delta_{uu'})$ would be very small ($I_{k'}(\Delta_{uu'}) \approx 0$). However, the noise term $\Gamma_{k,n}$ will remain. If we assume that the noise power at the relays is constant, a BER floor will appear in high SNR at the base station. However, if we evaluate the system performance assuming that the noise level is the same in the relays and in the base station (or even up to a factor), we only obtain an SNR loss in BER performance without affecting the diversity.

2.4.3 Simulation results

We first analyze the bit error rate (BER) of the uplink transmission in OFDM/FBMC based network with a source, a destination and two relays nodes (see Figure 2-25). We assume that the multicarrier system has $N = 128$ with a sampling frequency $f_s = 1.92$ MHz thus the corresponding OFDM/FBMC symbol period is $T = 66.67\mu s$. The length of cyclic prefix is N/8=16, i.e. $\Delta = 8.33\mu s$. The transmitted data is QPSK modulated. The timing offsets τ_i associated to each relay-path are randomly chosen from [0,$\tau_{\max}$] with a uniform distribution. The channel state information (CSI) is assumed to be perfectly known at the destination. It is worth mentioning that the following results are compared to the perfect synchronized scenario in which the orthogonality between the different subchannels is maintained.

In Figure 2-30, we investigate the robustness of OFDM and FBMC (with different multi-tap equalizers) to the delay asynchronism with different timing offset intervals $[0, T/8]$ and $[0, T/4]$. The BERs of OFDM and FBMC are plotted against the signal-to-noise-ratio (SNR).

In the OFDM case, the system provides the optimal performance when $\tau_{\max} = T/8 = \Delta$. However, we observe a severe degradation when $\tau_{\max} = T/4$. We can explain this result as follows: when the timing offset is lower than the cyclic prefix duration $\tau_{\max} 0 \leq \Delta$, the orthogonality between the system subcarriers is maintained; otherwise the transmission performance will be affected by the ISI and the ICI resulting from the timing offsets $\tau_{1,2} \in [T/8, T/4]$. Since the timing offset is a uniform random variable, the probability of obtaining the performance of the perfect synchronized case is given by the CP duration over the whole timing offset interval (Δ/τ_{max}). The probability of the orthogonality decreases as τ_{max} increases. Therefore, the error probability becomes higher.

In the FBMC case, we can see that the single tap equalization presents is a slight loss with respect to the optimal performance when $\tau_{1,2} \in [0, T/8]$. Moreover, the multi-taps equalizers provide almost the optimal performance. Such a result can be explained by the fact that the equivalent propagation channel has a weakly frequency selective response which can be decomposed as locally flat subchannels ($\{l, |l| \leq 1 \mid H(m_0 + l) \approx H(m_0)\}$). Since each subchannel overlaps only with its immediate neighbors, a single tap equalization is able to reach the optimal performance.

However when $\tau_{1,2} \in [0, T/4]$, we observe a large gap between the single-tap equalizer performance and the optimal one. Such a behavior is due to the fact that each subchannel is no

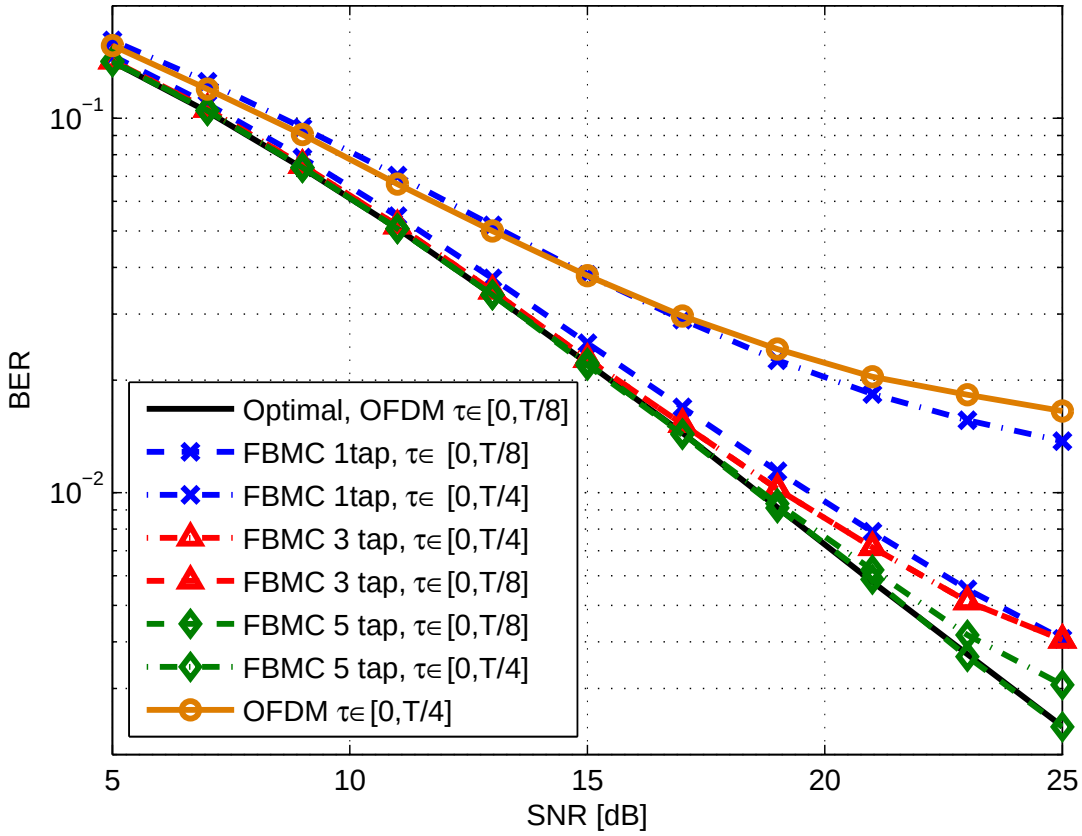

Figure 2-30: OFDM, 1,3 and 5-tap-FBMC BER performances with $\tau_{\max} = 0, T/8$ and $T/4$

longer considered as flat which implies that the orthogonality between the system subcarriers is destroyed even after the equalization. Furthermore, we can see that the 3 and 5 taps-equalizers are able to restore the orthogonality between subcarriers and provide practically the optimal performances.

In the following we present performance comparison results of OFDM and FBMC in the scenario depicted in Fig. 2-27. We show in Fig. 2-31 the impact of the guard band size δ introduced between the different user subcarrier blocks. We compare the BER performance of CP-OFDM and FBMC with different values of δ. The optimal curve shown in the figure corresponds to the optimal case where OFDM is used with all synchronized users (*i.e.* the subcarrier orthogonal is maintained). We recall that the asynchronism delay between the users is uniformly distributed in the time interval $[0, \quad T]$. The curves with red color and circle marker represent the OFDM performance curves, whereas the blue ones with triangle marker are those of FBMC.

According to this figure, we can remark that when $\delta = 0$ (*i.e.* there is no guard band between the users blocks), a BER floor appears for both OFDM and FBMC (solid curves). For OFDM, the BER floor level is of about 3×10^{-4}, whereas it is of about 10^{-4} for FBMC. However, when one subcarrier is introduced as guard band ($\delta = 1$) between the user blocks, the situation is different for FBMC. We can see that the obtained FBMC performance is the same as the optimal one. That is, one subcarrier as a guard band is enough to avoid interference between all the asynchronous users. Nevertheless, OFDM still suffer from multiuser interference

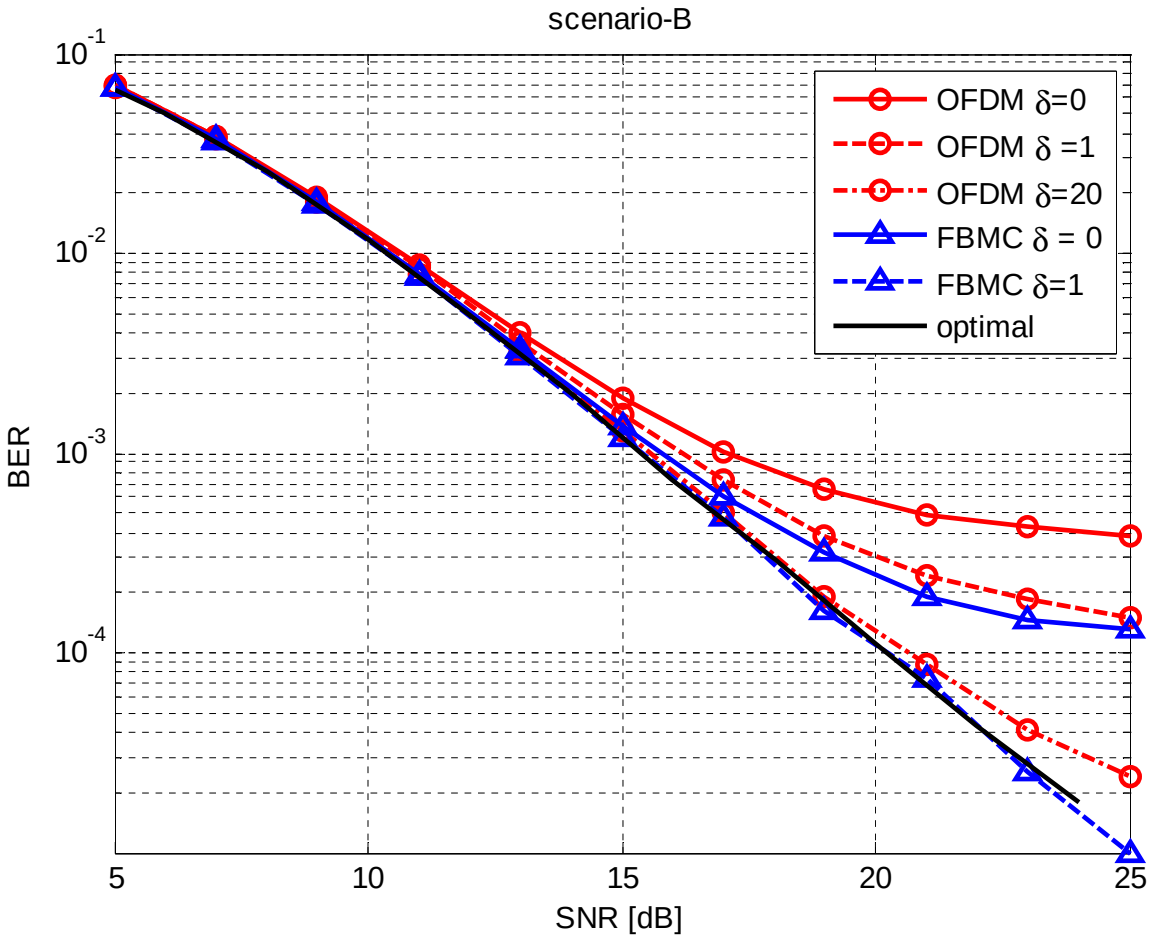

Figure 2-31: Impact of the guard-band length

when $\delta = 1$, and -as we can see in the figure- the BER floor appears above 10^{-4}. In order to reach almost the optimal performance at $SNR = 20dB$, we have to set the guard band size at around $\delta = 20$ (according to the figure) which is very large.

In Fig. 2-32, we are interested in the sensitivity of OFDM and FBMC to the maximal asynchronism delay τ_{max}. That is, the actual delay τ is uniformly distributed in the time interval $[0, \quad \tau_{max}]$. As we have seen that FBMC has optimal performance when $\delta \geq 1$, then we set for this simulation that $\delta = 0$ in order to be able to observe the effect of τ_{max} on the BER performance. Therefore, we show the BER performance of FBMC and OFDM for diffident values of $\tau_{max} \in \{T, T/4, T/7\}$. According to the simulation results, we observe that the FBMC BER performance does not change whatever the values of τ_{max}. However, OFDM is sensitive to the maximal asynchronism delay. Obviously, the OFDM BER floor lowers with the decrease in asynchronism delay (τ_{max}). In fact, if the asynchronism delay is equal or less than the cyclic prefix size, the CP-OFDM BER performance is optimal.

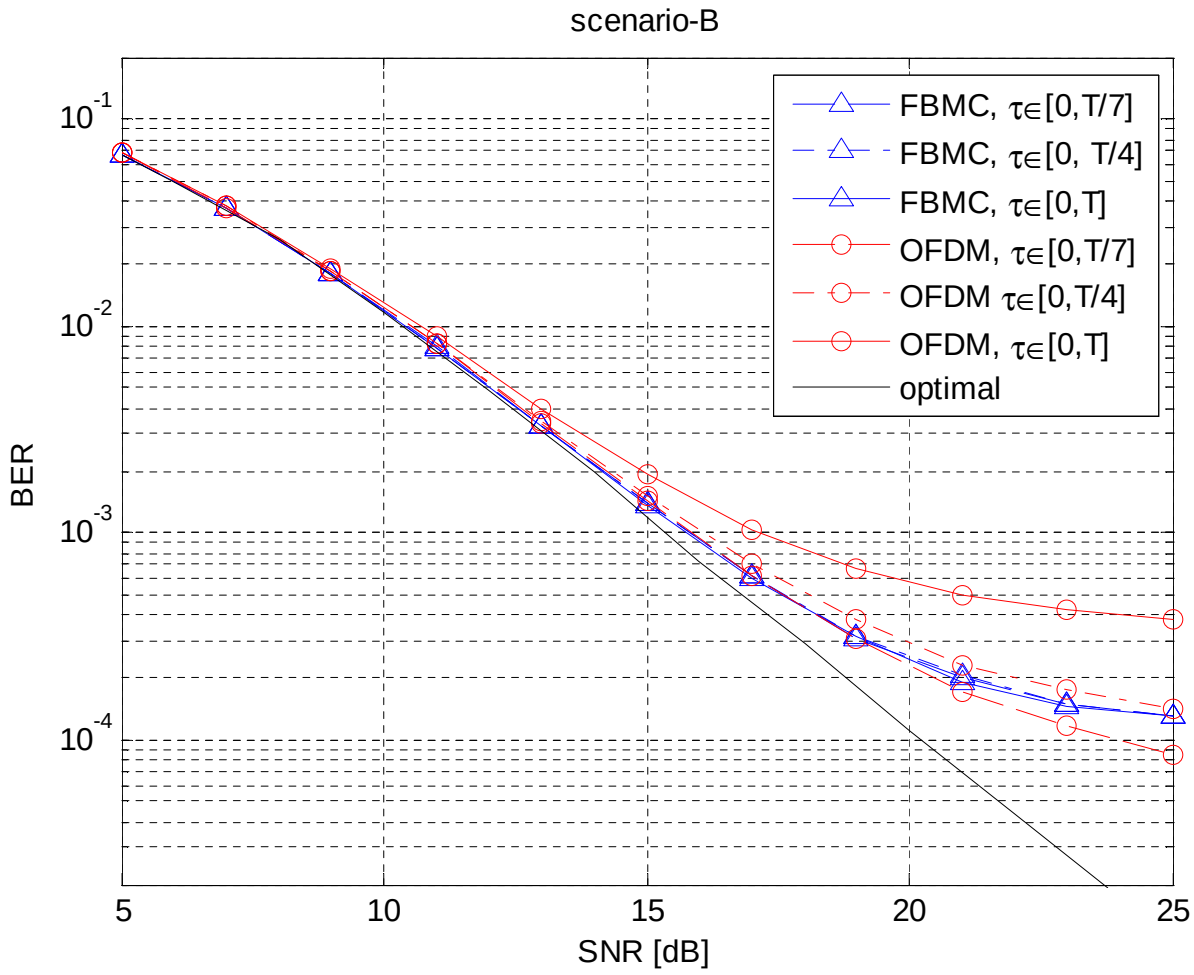

Figure 2-32: Impact of the maximum asynchronism delay

2.4.4 Conclusion

In the first part of this section, we have analyzed the performance of asynchronous OFDM/FBMC based relay networks. We have shown that asynchronous OFDM performances are subjected to a severe degradation. Such a result is explained by the high amount of interference resulting from the loss of the orthogonality which is caused by the timing offset exceeding the cyclic prefix duration. On the other hand, we have proposed different multi-taps subchannel equalizers to counteract the detrimental effects of timing asynchronism on the FBMC performances. From simulation results, it has been demonstrated that multi-tap equalizations are able to restore the orthogonality between the system subcarriers and significantly outperform the conventional single-tap equalization when the timing offset is too large. Moreover, the obtained results show that the 5-taps per subchannel equalization is able to absorb large timing offsets offering thus a strong robustness of FBMC against timing synchronization errors.

In the second part, we have considered a scenario with two time-asynchronous users occupying two different frequency bands. We have shown that when OFDM is used, the users orthogonality is lost due to the time asynchronism leading to a high multi-user interference level. We have seen that a guard band larger than 20 subcarriers has to be inserted between

the users to avoid the multi-user interference effect in OFDM. Obviously, a such guard band is very high and causes a large spectral efficiency loss. As for the FBMC modulation, the situation is different. Indeed, a band guard of only one subcarrier is sufficient to avoid multi-user interference thanks to the spectrum well-localization of the used pulse shape. Thus, this feature allows the FBMC systems to operate properly in asynchronous scenarios and outperform the OFDM.

3. Channel estimation in cooperative communications using FB-MC

FBMC/OQAM systems suffer from an imaginary intercarrier/intersymbol interference, that complicates signal processing tasks at the receiver, including channel estimation [33]. A multitude of training designs and associated channel estimation methods have been proposed for such systems [33]. The design of optimal FBMC/OQAM preambles for the purpose of estimating the channel in single-antenna single-link channels was investigated in [34] (see also [33, 35]). Both full (i.e., with pilots at all the subcarriers) and sparse (i.e., with isolated pilot subcarriers surrounded by nulls) preambles were considered and their performances were analyzed.

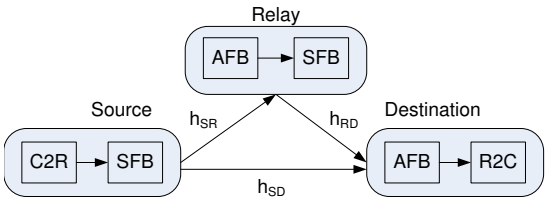

Figure 3-1: The cooperative system under consideration.

The goal, here, is to address the above problem *for the first time* in the context of a simple cooperative network as the one given in Fig. 3-1. Single-antenna transmitters and receivers are assumed, while a single one-way relay is employed to assist the transmission, following a simple amplify-and-forward (AF) protocol. The system operates in two phases, with the source transmitting to the destination in both of them. In the second phase, the relay forwards to the destination an amplified version of the signal transmitted by the source in the first phase. This allows the first phase signal to be received through two different links, thus enhancing the diversity. In a manner analogous to a Cyclic-Prefix (CP) OFDM-based system, filter banks are employed at the relay terminal to help amplify the received signal *per subcarrier*. It is desired to estimate the channels in both of the paths leading to the destination node. The problem of optimally designing the preambles in the two phases is investigated for Least-Squares (LS) channel estimation, where optimality is in the sense of the minimum Mean Square Error (MSE) estimation subject to transmit energy constraints.

In the following, the single-input single-output system model for a FBMC/OQAM system will be presented along with the assumptions and the specific details of the preamble structures that are used for channel estimation (i.e. sparse and full preamble cases). Then, the preambles will be casted into the cooperative system under study and finally simulation results will be provided to support the theoretical analysis.

3.1 System model

The FBMC/OQAM synthesis filter bank (SFB) output signal is given by [36]

$$s(l) = \sum_{m=0}^{M-1} \sum_{n} a(m,n) g_{m,n}(l) \tag{3.1}$$

where $a(m,n)$ are real OQAM symbols, produced by the complex to real OQAM modulator (C2R block in Fig. 3-1) and

$$g_{m,n}(l) = g\left(l - n\frac{M}{2}\right) e^{j\frac{2\pi}{M}m\left(l-\frac{L_g-1}{2}\right)} e^{j\phi(m,n)}, \tag{3.2}$$

with g being a real symmetric prototype filter impulse response of length $L_g = MK$ and unit energy. M is the (even) number of subcarriers, K is the overlapping factor and $\phi(m,n) = \phi_0 + \frac{\pi}{2}(m+n)$. ϕ_0 can be arbitrarily chosen, e.g. $\phi(m,n) = (m+n)(\pi/2) - mn\pi$ [36]. Finally, the pair (m,n) is the frequency-time (FT) point with subcarrier index m and time index n.

The signal $s(l)$ is transmitted through a frequency selective channel that is modeled by the $L_h \times 1$ vector $\boldsymbol{h}$. Applying the commonly used assumptions that the channel is (approximately) frequency flat at each subcarrier and constant over the duration of the prototype filter $g(.)$ [37], the signal at FT point (p,q), after the receiver's analysis filter bank (AFB), is given by [34]

$$y(p,q) = H(p)a(p,q) + j\sum_{m=0}^{M-1}\sum_{(n\neq m)=0}^{N-1} H(m)a(m,n)u_{m,n}^{p,q} + \eta(p,q), \tag{3.3}$$

where $H(p)$ is the channel frequency response (CFR) at the point (p,q) and $\eta(p,q) \sim \mathcal{CN}(0,\sigma^2)$ is an additive noise term [34]. The summation term in (3.3) is the associated interference due to the factors

$$\sum_l g_{m,n}(l)g_{p,q}^*(l) = ju_{m,n}^{p,q}, \tag{3.4}$$

known as intrinsic interference [38].

For well FT localized pulses $g(.)$, the interference is limited to the first-order neighborhood $\Omega_{p,q}$ around (p,q), i.e. $\Omega_{p,q} \in \{(p,q\pm1),(p\pm1,q),(p\pm1,q\pm1)\}$, and (3.3) can be written as

$$y(p,q) = H(p)a(p,q) + j\sum_{(m,n)\in\Omega_{p,q}} H(m)a(m,n)u_{m,n}^{p,q} + \eta(p,q). \tag{3.5}$$

For channel estimation, the transmitter sends either a full or a sparse preamble at the beginning of a data frame, to assist the receiver. The preambles will be assumed to consist of two FBMC/OQAM symbols. The first one is a vector of pilot symbols $a(p,0)$ while the second one is a zero vector, i.e. $a(p,1) = 0$, for all p, which serves as a guard against interference from the data. For the sake of the analysis, and without loss of generality, the all zeros FBMC symbol that is also commonly sent before the pilots will be omitted here (as in [35]).[1]

In view of the above, when a sparse-preamble is sent, the interference term (3.5) is set to zero because the non-zero pilot symbols are surrounded by zeros. Let $p \in \{p_1,p_2,\ldots,p_L\} = \mathcal{P}$ be the subchannel indexes in which the non-zero pilot symbols $a(p,0)$ are assigned by the transmitter and L the minimum required number of pilot symbols. This means that the input-output signals, focusing on the pilot positions, are

$$y(p,0) = H(p)a(p,0) + \eta(p,0). \tag{3.6}$$

In the full-preamble case, the pilot symbol at position p is interfered only by those at $p-1$ and $p+1$. Moreover, with a slight abuse of the OQAM definition, we incorporate, as in [35], the phase factors $e^{j\phi(p,0)}$ in the training symbols, getting $x(p,0) = a(p,0)e^{j\phi(p,0)}$, with the associated minor modification to the $g_{m,0}(\cdot)$ definition. This results in $\sum_l g_{m+1,0}(l)g_{m,0}^*(l) = \sum_l g_{m-1,0}(l)g_{m,0}^*(l) = \beta$, i.e., the interference corresponding to $ju_{m,0}^{p,0}$ in (3.4) for $m = p\pm1$ is then purely real with $\beta > 0$ defined in [33]. In light of the above, (3.5), for $q = 0$, can be written as

$$y(p,0) = H(p)x(p,0) + H(p-1)x(p-1,0)\beta + H(p+1)x(p+1,0)\beta + \eta(p,0). \tag{3.7}$$

[1] Its absence, in practice, can be justified, for example in wireless transmissions that involve inter-frame gaps.

By collecting all $y(p,0)$ into a single vector $\boldsymbol{y} = [\ y(0,0) \quad y(1,0) \quad \cdots \quad y(M-1,0)\ ]^T$, the following linear system can be written [35]

$$\boldsymbol{y} = \boldsymbol{B}\boldsymbol{X}\boldsymbol{H} + \boldsymbol{\eta}, \tag{3.8}$$

where $\boldsymbol{B}$ is a circulant matrix with first row equal to $[\ 1 \quad \beta \quad 0 \quad \cdots \quad 0 \quad \beta\ ]$, $\boldsymbol{X} = \mathrm{diag}\Big(x(0,0), x(1,0), \ldots, x(M-1,0)\Big)$, $\boldsymbol{H} = [\ H(0) \quad H(1) \quad \cdots \quad H(M-1)\ ]^T$ and

$$\boldsymbol{\eta} = [\ \eta(0,0) \quad \eta(1,0) \quad \cdots \quad \eta(M-1,0)\ ]^T \tag{3.9}$$

with $\boldsymbol{\eta} \sim \mathcal{CN}(\boldsymbol{0}, \sigma^2\boldsymbol{B})$.

The input-output relation in (3.7) can be further simplified if the channel constancy assumption (CC) is made (e.g. [37]), i.e. the neighboring CFRs are assumed equal to each other ($H(p) \simeq H(p-1) \simeq H(p+1)$). This is the case when the channel order is much smaller than the number of subchannels. In this case, (3.7) can be written as

$$y(p,0) = H(p)b(p,0) + \eta(p,0). \tag{3.10}$$

where $b(p,0) = x(p,0) + x(p-1,0)\beta + x(p+1,0)\beta$. The problem of training design based on (3.7) has been tackled in [35] for a single-link system with and without the CC assumption. Here, the corresponding problem will be studied for a cooperative system.

In the following sections, the design of the sparse-preamble will be described first. Then, the full-preamble case will be presented with the channel constancy assumption. The analysis will be completed by dropping this assumption (referred to as NoCC in the following).

3.2 The sparse-preamble case

In the sparse preamble case, the associated interference is suppressed by setting to zero the neighborhood of isolated pilot symbols (see (3.5) along with (3.6)). Optimal conditions are derived in [39], for the energy allocations and positions of the pilot symbols. In the following, the associated design problem along with the derived solution will be described (the interested reader is referred to [39] for more information). The resulting conditions are analogous to those derived in [40] for CP-OFDM and dictate that the source should allocate the *whole* of the training energy in the first phase, to *equispaced and equipowered pilots*. Moreover, the relay should also uniformly allocate its energy to forward the corresponding training signal. As a byproduct, a relay-induced interference term is identified at the destination node and a simple cancellation procedure is proposed and evaluated. Simulation results are reported that corroborate the analysis and provide a comparison with the corresponding CP-OFDM system.

As already mentioned in the previous section, the source sends a sparse preamble vector (at time index 0) followed by an all zeros one (at time index 1) in each phase. Assuming well-localized prototype filters in time and frequency, as is the case here, the induced interference in the frequency-time point (p,q) comes only from its first order neighbors. The all zeros vector along with the assumed sparse preamble structure protects the transmitted pilot symbols for this interference [33]. The channel impulse responses $\boldsymbol{h}_i$ are modeled as $L_i \times 1$ complex Gaussian random vectors with independent elements for $i \in \{\mathrm{SD}, \mathrm{SR}, \mathrm{RD}\}$. In the sparse preamble case, the destination is going to estimate the overall channel $\boldsymbol{h} = [\boldsymbol{h}_{\mathrm{SD}}^T,\ \boldsymbol{h}_{\mathrm{R}}^T]^T$, where $\boldsymbol{h}_{\mathrm{R}}$ is the S-R-D channel impulse response of length $L = L_{\mathrm{SR}} + L_{\mathrm{RD}} - 1$.

The received signals (associated with (3.6)) that the destination uses for channel estimation, focusing on the pilot positions $p \in \mathcal{P}$, are

$$y_{\mathrm{D}_1}(p,0) = H_{\mathrm{SD}}(p)a_1(p,0) + \eta_{\mathrm{D}_1}(p,0), \quad (3.11)$$

$$y_{\mathrm{D}_2}(p,0) = H_{\mathrm{SD}}(p)a_2(p,0) + \lambda(p,0)H_{\mathrm{R}}(p)a_1(p,0) + w_2(p,0), \quad (3.12)$$

respectively. In (3.11), (3.12), $H_{\mathrm{SD}}(p)$ and $H_{\mathrm{R}}(p)$ are the channel frequency responses (CFR) at the pilot subchannels of the SR and SRD channels, which are assumed constant for the duration of the preamble, and $\eta_{\mathrm{D}_1}(p,0)$, $w_2(p,0)$ are appropriately defined noise terms [39]. Finally, $\lambda(p,0)$ is the amplification factor used by the relay to forward the received signal of the p-th subchannel by assigning the per subchannel energy $e_{\mathrm{R}}(p,0)$. Based on those signals, an LS channel estimator can be defined, and denoting by $\boldsymbol{C}_{\hat{\boldsymbol{h}}}$ the covariance matrix of the estimation error, the sparse-preamble design is based on the following minimization problem:

$$\min_{\boldsymbol{e}_1,\boldsymbol{e}_2,\boldsymbol{e}_{\mathrm{R}},E_1,E_2,\mathcal{P}} \frac{1}{2L}\mathrm{Tr}(\boldsymbol{C}_{\hat{\boldsymbol{h}}}) \quad (3.13)$$

such that

$$E_1 + E_2 = E_{\mathrm{S}}, \sum_{p\in\mathcal{P}} e_1(p,0) = E_1, \sum_{p\in\mathcal{P}} e_2(p,0) = E_2, \sum_{p\in\mathcal{P}} e_{\mathrm{R}}(p,0) = E_{\mathrm{R}},$$

where $\boldsymbol{e}_k$ and $\boldsymbol{e}_{\mathrm{R}}$ are $L\times 1$ vectors containing the energies $e_k(p,0) = |a_k(p,0)|^2$'s and $e_{\mathrm{R}}(p,0)$'s, respectively, E_k is the energy allocated to training in phase k and $E_{\mathrm{R}}, E_{\mathrm{S}}$ are given energy budgets. The optimal placement of the pilot symbols $\mathcal{P}$ is also to be optimized.

The solution of (3.13) dictates that $E_1 = E_{\mathrm{S}}$ and $E_2 = 0$ which means $e_2(p,0) = 0$. Moreover, $e_1(p,0) = E_{\mathrm{S}}/L$, $e_{\mathrm{R}}(p,0) = E_{\mathrm{R}}/L$ and the positions $p_l = \frac{M}{L}(l-1)$, for $l = 1,2,\ldots,L$, i.e. at the source, all energy is uniformly allocated to equispaced pilot symbols at the first phase and the relay, similarly, allocates uniformly its energy to forward the pilot signals during the second phase.

3.3 The full-preamble case

In order to further extend this study, the so-called full preamble design (i.e., with all tones carrying pilot symbols) is also addressed. In sparse preambles, the pilot symbols are guarded by the surrounding nulls and do not interfere with each other. As a result, no pilot symbol energy increase is present at the received signals (as observed in the case of full-preambles) and the system is similar to CP-OFDM in terms of design conditions and estimation performance. Here, the same problem is considered for the full preamble case. Because neighboring pilot symbols interfere with each other, there is effectively an energy increase of each pilot symbol at the receiver. It has been been shown in the single-link case [35] that equal symbols (optimally) maximize this energy increase and that FBMC/OQAM has a superior estimation performance than CP-OFDM.

Here, the full preamble design will be considered first under the common assumption of CC (e.g. [37]). It is reminded that CFRs at neighboring subchannels are then assumed to be equal. The conditions that are derived [41] are analogous to the ones observed in [35]. Moreover, as a byproduct, the optimal full preamble design for the CP-OFDM-based cooperative system will be derived, through its connection to the FBMC/OQAM system. Simulation results are presented for both mildly and highly frequency selective channels, which corroborate the analysis and demonstrate significant performance gains of FBMC/OQAM over its CP-OFDM counterpart,

particularly at practical signal-to-noise ratio (SNR) values. Second, the CC assumption will be dropped (i.e., we move to the NoCC case) and, hence, the neighboring CFR values are considered unequal. The outcome that is observed is similar to the one in [35] for the single-link case.

3.3.1 With the channel constancy assumption

Here, the design problem along with the derived solution will be described (the interested reader is referred to [41] for more information). The received signals (that are associated with (3.10)), during the two phases, at the destination are given by

$$y_{\mathrm{D}_1}(p,0) = H_{\mathrm{SD}}(p)b_1(p,0) + \eta_{\mathrm{D}_1}(p,0), \tag{3.14}$$

$$y_{\mathrm{D}_2}(p,0) = H_{\mathrm{SD}}(p)b_2(p,0) + H_{\mathrm{R}}(p)b_3(p,0) + w_2(p,0), \tag{3.15}$$

respectively. Here, $p = 0, 1, \ldots, M-1$, i.e. all subchannels are loaded with pilots. Moreover,

$$b_k(p,0) = x_k(p,0) + x_k(p-1,0)\beta + x_k(p+1,0)\beta, \tag{3.16}$$

for $k = 1, 2$ are the received pseudo-pilots, i.e. the pilot symbol $x_k(p,0)$ at the p-th subchannel is interfered by $x_k(p \pm 1, 0)$ and β is a known interference factor [33]. Additionally,

$$b_3(p,0) = \lambda(p,0)b_1(p,0) + \lambda(p-1,0)b_1(p-1,0)\beta + \lambda(p+1,0)b_1(p+1,0)\beta, \tag{3.17}$$

where, again, $\lambda(p,0)$ is the amplification factor used by the relay to forward the received signal of the p-th subchannel by assigning the per subchannel energy $e_{\mathrm{R}}(p,0)$. The aim here is to estimate the overall channel frequency response $\boldsymbol{H} = [\boldsymbol{H}_{\mathrm{SD}}^T, \boldsymbol{H}_{\mathrm{R}}^T]^T$.

The preamble design in this case in based on the following minimization problem:

$$\min_{\boldsymbol{x}_1, \boldsymbol{x}_2, \boldsymbol{e}_{\mathrm{R}}, \mathcal{E}_1, \mathcal{E}_2} \frac{1}{2M}\mathrm{Tr}(\boldsymbol{C}_{\hat{\boldsymbol{H}}}) \tag{3.18}$$

subject to

$$\sum_{p=0}^{M-1} \Big[|x_k(p,0)|^2 + \beta x_k(p,0)x_k^*(p-1,0) + \beta x_k(p,0)x_k^*(p+1,0)\Big] \leq \mathcal{E}_k,\ k = 1,2 \tag{3.19}$$

$$E\Big\{ \sum_{p=0}^{M-1} \Big[|x_{\mathrm{R}}(p,0)|^2 + \beta x_{\mathrm{R}}(p,0)x_{\mathrm{R}}^*(p-1,0) + \beta x_{\mathrm{R}}(p,0)x_{\mathrm{R}}^*(p+1,0)\Big]\Big\} \leq \mathcal{E}_{\mathrm{R}} \tag{3.20}$$

$$\mathcal{E}_1 + \mathcal{E}_2 = \mathcal{E}_{\mathrm{S}}, \tag{3.21}$$

where $\boldsymbol{x}_k$ and $\boldsymbol{e}_{\mathrm{R}}$ are $M \times 1$ vectors containing the $x_k(p,0)$'s and $e_{\mathrm{R}}(p,0)$'s, respectively, $\mathcal{E}_k$ is the source energy allocated to training in phase k and $\mathcal{E}_{\mathrm{R}}, \mathcal{E}_{\mathrm{S}}$ are given energy budgets referring to the SFB outputs (see also [35]). In this case, the input and output energies are not equal as it is the case with the sparse preambles. In (3.20), the relay energy is constrained in the mean sense and $x_{\mathrm{R}}(p,0)$ is the input signal at the p-th subchannel of the relay SFB.

The above problem can be solved optimally as far as $\mathcal{E}_1$, $\mathcal{E}_2$ are concerned, leading to the conclusion that the source should assign all available energy to the first phase, i.e. $\mathcal{E}_1 = \mathcal{E}_{\mathrm{S}}$ and $\mathcal{E}_2 = 0$ or $\boldsymbol{x}_2 = 0$. For the remaining variables, i.e. $\boldsymbol{x}_1$, $\boldsymbol{e}_{\mathrm{R}}$, two cases are studied. In the first, the three λ factors in (3.17) are assumed equal to each other. In the second one, a high SNR regime is assumed at the relay. In both cases, the source should use equal symbols (not only equal in energy) and the relay should assign uniformly its available energy. It is interesting to recall that this is in line with the optimal preamble design in single-link FBMC/OQAM systems [33], where it was shown to maximize the pseudo-pilot energies in (3.16). Moreover, this choice of the pilot symbols, in conjunction with the uniform energy allocation at the relay, also leads to all equal λ's, something that was only assumed in the first approach.

3.3.2 Without the channel constancy assumption

First, the input-output signals for channel estimation will be presented and then the training design will be described.

3.3.2.1 Input-ouput signals

The channel impulse responses $\boldsymbol{h}_i$ are modeled as in the previous section, namely as $L_i \times 1$ complex Gaussian random vectors with independent elements, i.e. $\boldsymbol{h}_i \sim \boldsymbol{\mathcal{CN}}(\boldsymbol{0}, \boldsymbol{C}_i)$, where $\boldsymbol{C}_i$ is diagonal and $i \in \{\mathrm{SD}, \mathrm{SR}, \mathrm{RD}\}$.

As already mentioned, a two-phase transmission protocol is used for the transmission of information between the source S and the destination D with the assistance of the relay R. In more detail, during the first phase and focusing on the first (non-zero) preamble FBMC symbol, S transmits the symbols $x_1(p,0)$ to R and D. When no CC is assumed, these are received as

$$\boldsymbol{y}_{\mathrm{R}} = \boldsymbol{B}\boldsymbol{X}_1\boldsymbol{H}_{\mathrm{SR}} + \boldsymbol{\eta}_{\mathrm{R}}, \tag{3.22}$$

$$\boldsymbol{y}_{\mathrm{D}_1} = \boldsymbol{B}\boldsymbol{X}_1\boldsymbol{H}_{\mathrm{SD}} + \boldsymbol{\eta}_{\mathrm{D}_1}, \tag{3.23}$$

respectively. The noise terms are described as $\boldsymbol{\eta}_{\mathrm{R}} \sim \mathcal{CN}(\boldsymbol{0}, \sigma_{\mathrm{R}}^2\boldsymbol{B})$ and $\boldsymbol{\eta}_{\mathrm{D}_1} \sim \mathcal{CN}(\boldsymbol{0}, \sigma_{\mathrm{D}}^2\boldsymbol{B})$. The remaining terms in (3.22), (3.23) are defined as in (3.8).

The received signal at R is first multiplied by $\boldsymbol{B}^{-1}$. It is pointed out here that this multiplication can be performed by exploiting the circulant nature of $\boldsymbol{B}^{-1}$, i.e. by utilizing FFT/IFFT operations and the (known) eigenvalues of the matrix. Finally, R amplifies the outcome by the diagonal matrix $\boldsymbol{\Lambda} = \mathrm{diag}\Big(\lambda(0,0), \lambda(1,0), \ldots, \lambda(M-1,0)\Big)$ with the aim to set the mean energy per subcarrier p at the input of R's SFB, namely, R "regulates" the mean energy that is allocated to the signals that are fed into each subchannel by the factors $\lambda(p,0)$ (to be defined shortly). Specifically,

$$\boldsymbol{x}_{\mathrm{R}} = \boldsymbol{\Lambda}\boldsymbol{B}^{-1}\boldsymbol{y}_R = \boldsymbol{\Lambda}\Big(\boldsymbol{X}_1\boldsymbol{H}_{\mathrm{SR}} + \boldsymbol{B}^{-1}\boldsymbol{\eta}_{\mathrm{R}}\Big) = \boldsymbol{\Lambda}\Big(\boldsymbol{X}_1\boldsymbol{H}_{\mathrm{SR}} + \boldsymbol{\eta}'_{\mathrm{R}}\Big), \tag{3.24}$$

where $\boldsymbol{\eta}'_{\mathrm{R}} = \boldsymbol{B}^{-1}\boldsymbol{\eta}_{\mathrm{R}} \sim \mathcal{CN}(\boldsymbol{0}, \sigma_R^2\boldsymbol{B^{-1}})$. Each element of $\boldsymbol{\eta}_{\mathrm{R}}$ is zero mean with identical variance, i.e. $\sigma'^2_{\mathrm{R}} = [\sigma_{\mathrm{R}}^2\boldsymbol{B}^{-1}]_{ii}$. This is a direct consequence of the fact that $\boldsymbol{B}$, and hence $\boldsymbol{B}^{-1}$, is a circulant matrix.

By defining the energy allocations $e_{\mathrm{R}}(p,0)$ for each element of $\boldsymbol{x}_{\mathrm{R}}$, the p-th element $\lambda(p,0)$ of the diagonal matrix $\boldsymbol{\Lambda}$ is given by

$$\lambda(p,0) = \sqrt{\frac{e_{\mathrm{R}}(p,0)}{\theta_{\mathrm{SR}}^2 e_1(p,0) + \sigma'^2_R}}, \tag{3.25}$$

where θ_{SR}^2 is the mean energy of $H_{\mathrm{SR}}(p)$ and it is given by $\theta_{\mathrm{SR}}^2 = \mathcal{E}(|H_{\mathrm{SR}}(p)|^2) = \mathrm{Tr}(\boldsymbol{C}_{\mathrm{SR}})$, which is independent of p (for channels with uncorrelated scattering, as the ones that are considered here). Moreover, it is defined that $e_1(p,0) = |x_1(p,0)|^2$ and for future reference that $e_2(p,0) = |x_2(p,0)|^2$ (i.e. the source energy per training symbol during the first and second phase, respectively).

During the second phase and focusing again on the first (non-zero) preamble FBMC symbol, S transmits the symbols $x_2(p,0)$ to D and R transmits the symbols $x_{\mathrm{R}}(p,0)$, i.e. the elements of $\boldsymbol{x}_{\mathrm{R}}$. The received signal is

$$\begin{aligned}
\boldsymbol{y}_{\mathrm{D}_2} &= \boldsymbol{B}\boldsymbol{X}_2\boldsymbol{H}_{\mathrm{SD}} + \boldsymbol{B}\boldsymbol{X}_{\mathrm{R}}\boldsymbol{H}_{\mathrm{RD}} + \boldsymbol{\eta}_{\mathrm{D}_2} \\
&= \boldsymbol{B}\boldsymbol{X}_2\boldsymbol{H}_{\mathrm{SD}} + \boldsymbol{B}\boldsymbol{\Lambda}\boldsymbol{X}_1\boldsymbol{H}_{\mathrm{R}} + \boldsymbol{B}\boldsymbol{\Lambda}\mathrm{diag}\Big(\boldsymbol{H}_{\mathrm{RD}}\Big)\boldsymbol{\eta}'_R + \boldsymbol{\eta}_{\mathrm{D}_2} \\
&= \boldsymbol{B}\boldsymbol{X}_2\boldsymbol{H}_{\mathrm{SD}} + \boldsymbol{B}\boldsymbol{\Lambda}\boldsymbol{X}_1\boldsymbol{H}_{\mathrm{R}} + \boldsymbol{w}_2,
\end{aligned} \tag{3.26}$$

where $\boldsymbol{w}_2 = \boldsymbol{B}\boldsymbol{\Lambda}\text{diag}\Big(\boldsymbol{H}_{\text{RD}}\Big)\boldsymbol{\eta}'_R + \boldsymbol{\eta}_{\text{D}_2}$ and $\boldsymbol{H}_{\text{R}} = \boldsymbol{H}_{\text{SR}} \odot \boldsymbol{H}_{\text{RD}}$ (with $\odot$ meaning element-wise multiplication). Finally, $\boldsymbol{\eta}_{\text{D}_2} \sim \mathcal{CN}(\boldsymbol{0}, \sigma_D^2\boldsymbol{B})$.

The destination uses (3.23), (3.26) in order to estimate the channel $\boldsymbol{H} = [\ \boldsymbol{H}_{SD}^T \quad \boldsymbol{H}_R^T\ ]^T$. Specifically, the following input-output relation can be written, after multiplying each equation with $\boldsymbol{B}^{-1}$, i.e. $\boldsymbol{y}'_{\text{D}_i} = \boldsymbol{B}^{-1}\boldsymbol{y}_{\text{D}_i}$ for $i = 1, 2$, as

$$\begin{bmatrix} \boldsymbol{y}'_{\text{D}_1} \\ \boldsymbol{y}'_{\text{D}_2} \end{bmatrix} = \begin{bmatrix} \boldsymbol{X}_1 & \boldsymbol{0} \\ \boldsymbol{X}_2 & \boldsymbol{\Lambda}\boldsymbol{X}_1 \end{bmatrix} \begin{bmatrix} \boldsymbol{H}_{\text{SD}} \\ \boldsymbol{H}_{\text{R}} \end{bmatrix} + \begin{bmatrix} \boldsymbol{\eta}'_{\text{D}_1} \\ \boldsymbol{w}'_2 \end{bmatrix}, \tag{3.27}$$

where $\boldsymbol{\eta}'_{\text{D}_1} = \boldsymbol{B}^{-1}\boldsymbol{\eta}_{\text{D}_1} \sim \mathcal{CN}(\boldsymbol{0}, \sigma_D^2\boldsymbol{B}^{-1})$ and $\boldsymbol{w}'_2 = \boldsymbol{B}^{-1}\boldsymbol{w}_2 = \boldsymbol{\Lambda}\text{diag}\Big(\boldsymbol{H}_{\text{RD}}\Big)\boldsymbol{\eta}'_R + \boldsymbol{\eta}'_{\text{D}_2}$ and $\boldsymbol{\eta}'_{\text{D}_2} = \boldsymbol{B}^{-1}\boldsymbol{\eta}_{\text{D}_2} \sim \mathcal{CN}(\boldsymbol{0}, \sigma_D^2\boldsymbol{B}^{-1})$. The noise term $\boldsymbol{w}'_2$ is a zero mean random vector and its p-th element has variance equal to $\sigma^2_{\boldsymbol{w}'_2}(p) = \lambda^2(p,0)\theta^2_{RD}\sigma'^2_R + \sigma'^2_D$. It is noted that $\sigma'^2_{\text{D}} = [\sigma^2_{\text{D}}\boldsymbol{B}^{-1}]_{ii}$ similarly with σ'^2_R and θ^2_{RD} is defined similarly with θ^2_{SR}.

In compact form with direct matching of terms, (3.27) can be written as

$$\boldsymbol{y}' = \boldsymbol{\mathcal{X}}\boldsymbol{H} + \boldsymbol{w} \tag{3.28}$$

The noise term $\boldsymbol{w}$ is zero mean with covariance $\boldsymbol{C}_{\boldsymbol{w}} = \text{diag}\Big(\boldsymbol{C}_{\boldsymbol{\eta}'_{\text{D}_1}}, \boldsymbol{C}_{\boldsymbol{w}'_2}\Big)$. The diagonal blocks of $\boldsymbol{C}_{\boldsymbol{w}}$ are not diagonal matrices. However, as it will be observed later on, we are only interested in their diagonal elements, which are $[\boldsymbol{C}_{\boldsymbol{\eta}'_{\text{D}_1}}]_{pp} = \sigma'^2_{\text{D}}$ and $[\boldsymbol{C}_{\boldsymbol{w}'_2}]_{pp} = \sigma^2_{\boldsymbol{w}'_2}(p)$, respectively.

Finally, the LS estimate of $\boldsymbol{H}$ and the associated error covariance matrix are given by

$$\hat{\boldsymbol{H}} = \boldsymbol{\mathcal{X}}^{-1}\boldsymbol{y}, \quad \boldsymbol{C}_{\hat{\boldsymbol{H}}} = \boldsymbol{\mathcal{X}}^{-1}\boldsymbol{C}_{\boldsymbol{w}}\boldsymbol{\mathcal{X}}^{-H} \tag{3.29}$$

3.3.2.2 Preamble design

The training design consists of a) determining the source training symbols $x_k(p,0) = a_k(p,0)e^{j\phi_k(p,0)}$, $k = 1, 2$, b) the relay energies $e_{\text{R}}(p,0)$ per subcarrier in the second phase, and c) the source training energy allocation between the two transmission phases. The preamble optimization criterion will be to minimize the mean squared error $\text{MSE} = \frac{1}{2M}\text{Tr}(\boldsymbol{C}_{\hat{\boldsymbol{H}}})$ subject to *sum* energy constraints at the source and the relay, namely

$$\min_{\boldsymbol{x}_1, \boldsymbol{x}_2, \boldsymbol{e}_{\text{R}}, \mathcal{E}_1, \mathcal{E}_2} \ \frac{1}{2M}\text{Tr}(\boldsymbol{C}_{\hat{\boldsymbol{H}}}) \tag{3.30}$$

s.t.

$$\sum_{p=0}^{M-1} \Big[|x_k(p,0)|^2 + \beta x_k(p,0)x_k^*(p-1,0) + \beta x_k(p,0)x_k^*(p+1,0)\Big] \le \mathcal{E}_k,\ k = 1, 2 \tag{3.31}$$

$$\mathcal{E}\Big\{ \sum_{p=0}^{M-1} \Big[|x_{\text{R}}(p,0)|^2 + \beta x_{\text{R}}(p,0)x_{\text{R}}^*(p-1,0) + \beta x_{\text{R}}(p,0)x_{\text{R}}^*(p+1,0)\Big]\Big\} \le \mathcal{E}_{\text{R}} \tag{3.32}$$

$$\mathcal{E}_1 + \mathcal{E}_2 = \mathcal{E}_{\text{S}}, \tag{3.33}$$

where $\boldsymbol{x}_k$, $\boldsymbol{e}_{\text{R}}$, $\mathcal{E}_k$, $\mathcal{E}_{\text{R}}$ and $\mathcal{E}_{\text{S}}$ are defined as in (3.18).

It will be convenient to re-write the cost function above in an alternative form. Specifically, by applying the matrix inversion lemma to the 2×2 block matrix $\boldsymbol{\mathcal{X}}^{-1}$ with diagonal blocks, it can be shown that the trace in (3.30) is applied on a sum of diagonal matrices. The MSE can then be written as $\text{MSE} = \frac{1}{2M}\sum_{p=0}^{M-1} v_p$, where

$$v_p = \frac{\sigma'^2_{\text{D}} + \sigma'^2_{\text{R}}\theta^2_{\text{RD}}}{e_1(p,0)} + \frac{\sigma'^2_{\text{D}}\theta^2_{\text{SR}}e_2(p,0)}{e_{\text{R}}(p,0)e_1(p,0)} + \frac{\sigma'^2_{\text{D}}\sigma'^2_{\text{R}}e_2(p,0)}{e_{\text{R}}(p,0)e_1^2(p,0)} + \frac{\sigma'^2_{\text{D}}\theta^2_{\text{SR}}}{e_{\text{R}}(p,0)} + \frac{\sigma'^2_{\text{D}}\sigma'^2_{\text{R}}}{e_{\text{R}}(p,0)e_1(p,0)} \tag{3.34}$$

Some comments concerning the energies are in order. First, the constraints of the minimization problem correspond to the energies at the *output* of the SFBs of the source or the relay. Second, due to the stability of the SFBs, the energies at the inputs of the SFBs can be constrained as $\sum_{p=0}^{M-1} e_1(p,0) \leq E_1$ and $\sum_{p=0}^{M-1} e_2(p,0) \leq E_2$ for the source and $\sum_{p=0}^{M-1} e_{\mathrm{R}}(p,0) \leq E_{\mathrm{R}}$ for the relay (see also [34, 35]). Finally, $E_1 + E_2 \leq E_S$.

The minimization problem using the alternative cost-function that is based on (3.34) along with the constraints at the inputs of the SFBs at the source and the relay, is identical to the corresponding problem that is defined for the CP-OFDM case as explained in [41]. This is a direct consequence of the $\boldsymbol{B}^{-1}$ operation at the relay which removes the interchannel interference that is commonly present in FMBC/OQAM systems. The solution to those problems dictates that the source should allocate uniformly all each training energy to the first phase. Moreover, the relay should allocate uniformly its energy at each subchannel for forwarding the pilot signals. In more detail, the source should set $E_1 = E_S$, $E_2 = 0$, $x_1(p,0) = \sqrt{E_S/M}e^{j\phi_1(p,0)}$, $x_1(p,0) = \sqrt{E_S/M}e^{j\phi_1(p,0)}$ and $x_2(p,0) = 0$. Moreover, the relay should set $e_R(p,0) = \sqrt{E_R/M}$.

Finally, the aforementioned solution is also the solution to the original problem i.e. with the constraints at the outputs of the SFBs if those constraints are tight, namely they hold with equality as it is argued in [35]. This is true if additionally the phases of the pilot symbols are equal to each other making the pilot symbols also equal to each other (i.e. not only equal in energy). To see this, let us focus on the energy constraint at the output of the SFB of the source. It is easy to prove, using the fact that the pilot symbols have the same energy, that

$$\sum_{p=0}^{M-1} \left[|x_1(p,0)|^2 + \beta x_1(p,0)x_1^*(p-1,0) + \beta x_1(p,0)x_k^*(p+1,0) \right] \leq E_S(1+2\beta). \quad (3.35)$$

The equality holds when the phases of the pilot symbols are set equal to each other and hence $E_S(1+2\beta) = \mathcal{E}$ (a similar result can be seen in [35]). So, the source pilot symbols are set as $x_1(p,0) = \sqrt{E_S/M}e^{j\phi}$, i.e. $\phi_1(p,0) = \phi$ for all p.

It is interesting to note here that the MSE function depends only on the energies of the training symbols at the input of the SFB (like the case of CP-OFDM) and no pseudo-pilots are actually created which could result in an energy increase.

3.4 Simulation results

In this section, some simulation results are presented that support the preamble designs that were briefly described in the previous sections. First, the results for the sparse-preamble and then for the full preamble case are presented.

3.4.1 The sparse preamble case

Filter banks with $M = 256$, $K = 3$ were used, employing the prototype filter designed in [42]. All channels were generated to undergo Rayleigh block fading with an exponential profile and lengths $L_{\mathrm{SD}} = 32$, $L_{\mathrm{SR}} = 16$ and $L_{\mathrm{RD}} = 17$ (thus, in this case, $L = 32$). The energy budgets were chosen as $E_{\mathrm{S}} = E_{\mathrm{R}} = L$, so as to have mean energy per pilot symbol equal to 1. QPSK data were transmitted (with a unit energy per bit). Moreover, as usually assumed, the destination and the relay have the same noise variance. The performance of the corresponding CP-OFDM system is included, for the sake of the comparison, where a CP of minimum length (equal to the channel order) was assumed.

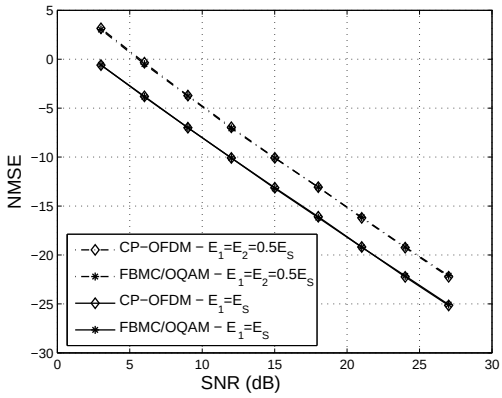

(a) NMSE performance of the optimal and suboptimal energy allocation between the two phases for $M = 256$, $K = 3$, and $L = 32$.

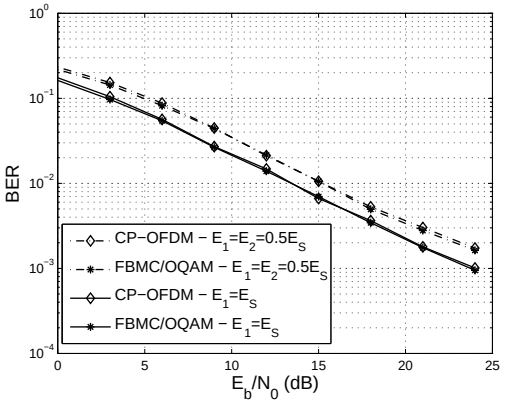

(b) BER for the (QPSK) data transmitted in the first phase. Optimal and suboptimal energy allocation schemes are compared.

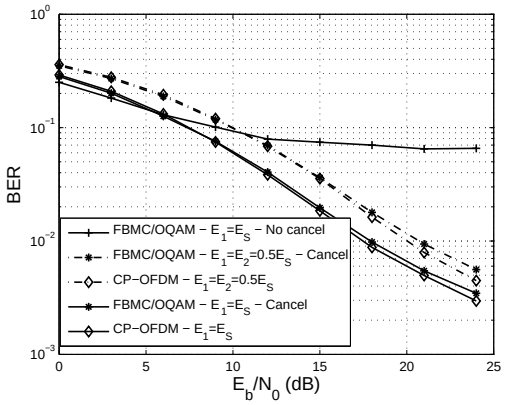

(c) As in Fig. 3.2(b), for the second phase transmission.

Figure 3-2: The sparse preamble case.

In Fig. 3.2(a), the normalized MSE (NMSE) ($E(\|\boldsymbol{h} - \hat{\boldsymbol{h}}\|^2/\|\boldsymbol{h}\|^2)$) performance is depicted versus the signal to noise ratio (SNR), for both optimal ($E_1 = E_{\rm S}$) and suboptimal ($E_1 = E_2 = 0.5E_{\rm S}$) source energy allocations between the two phases. All other training conditions hold as dictated by the optimal training design. As expected, the performance is significantly better when the optimal design is employed. Moreover, the two multicarrier systems perform similarly.

In Figs. 3.2(b), 3.2(c), the (uncoded) bit error rate (BER) performances at the destination detector with QPSK input are shown for phases 1 and 2, respectively. The SNR loss incurred by the CP redundancy in CP-OFDM was taken into account when calculating the corresponding BER. In the FBMC/OQAM-based relay, the amplification factors were chosen so as to have unit energy per information bit at the channel inputs of the S-R-D chain. One can observe a significant performance gain (of about 2-3 dB) over the suboptimal source energy allocation. Moreover, and not unexpectedly, the two multicarrier systems perform similarly in the detection of the first phase data (cf. Fig. 3.2(b)). In Fig. 3.2(c), the destructive effect of the identified interference term [39] and the importance of its (approximate) cancellation are demonstrated. Observe the severe error floor in the optimal case without cancellation. On the other hand, no cancellation seems to be the best choice at low SNR values, because of the errors incurred then at the interference approximation due to channel estimatior errors and a_1 decision error

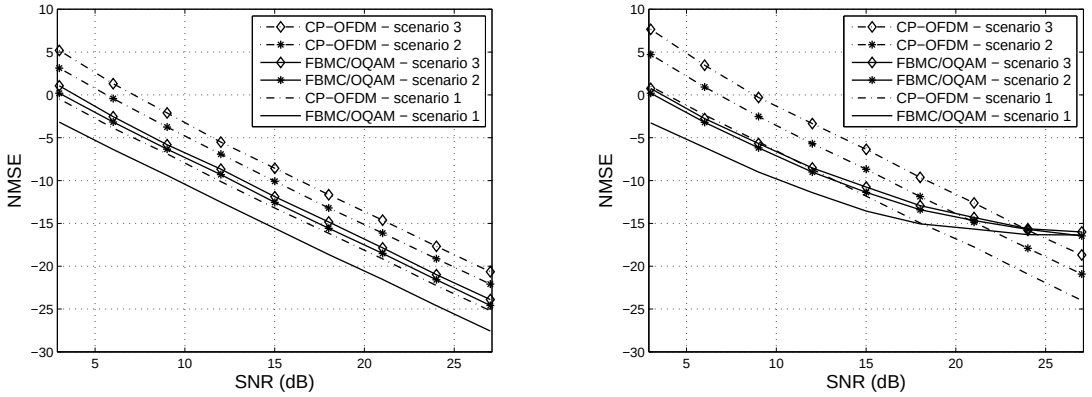

(a) Estimation performance for channels of low to mild frequency selectivity. $M = 64$, $K = 3$.

(b) As in Fig. 3.3(a), for highly frequency selective channels.

Figure 3-3: The full preamble case with the CC assumption.

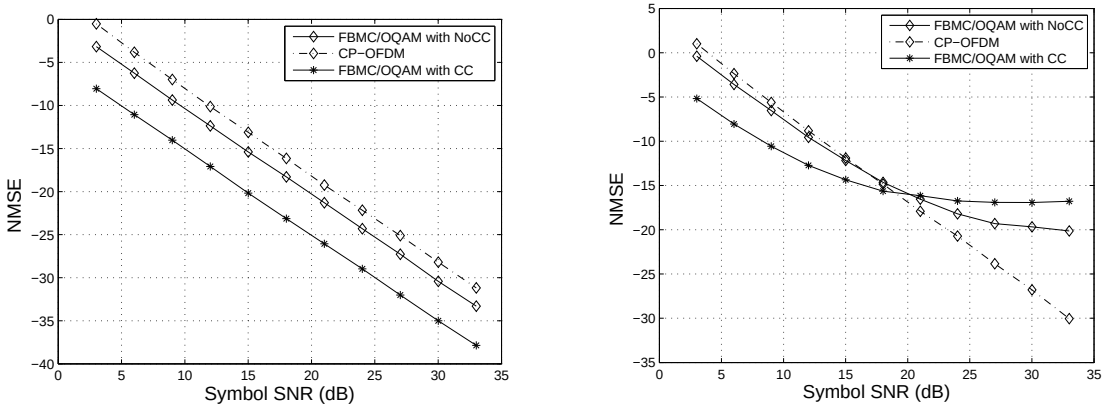

(a) Estimation performance for channels of low to mild frequency selectivity. $M = 64$, $K = 3$.

(b) As in Fig. 3.4(a), for highly frequency selective channels.

Figure 3-4: The full preamble case without the CC assumption.

propagation. The somewhat worse than CP-OFDM performance of the cancellation-based equalizer at higher SNRs could be attributed to the composite noise term $w_2(p, 0)$ in (3.12) at the FBMC/OQAM destination receiver because of the interference effect [39]. One should add to this, the effect of the residual interference caused by the fact that the subchannels in (3.11) and (3.12) are only approximately frequency flat [39].

3.4.2 The full preamble case

In this section, simulation results are reported for the full preamble case. Filter banks designed as in [42] were employed, with $M = 64$ and $K = 3$. Results are shown for two cases, corresponding to low/mild and severe frequency selectivity. In the first case, all channels were generated to undergo Rayleigh block fading with an exponential profile and lengths $L_{\rm SD} = 4$, $L_{\rm SR} = 3$, and $L_{\rm RD} = 2$, that is, quite small compared to M. The ITU Veh-A profile was assumed in the second case for all channels involved, giving rise to channels of lengths $L_{\rm SR} = L_{\rm RD} = L_{\rm SD} = 29 \approx \frac{M}{2}$. (The S-R-D channel has length $57 \approx M$.) The energy budgets were chosen as $\mathcal{E}_{\rm S} = \mathcal{E}_{\rm R} = M$, so that the mean energy per pilot symbol be equal to 1. Moreover, the noise variance at

the destination and the relay are assumed equal. The performance of the corresponding CP-OFDM system was also tested, where a CP of minimum length (equal to the channel order) was assumed. It should be mentioned here that appropriate scalings were performed wherever necessary to ensure equal transmit powers at all cases.

3.4.2.1 With the CC assumption

Three scenarios were examined when the CC assumption is made. In the first one, the derived optimal training conditions were respected. In the second and third scenarios, $E_1 = E_2$. The third scenario also permits the relay to depart from the uniform energy allocation and employ randomly chosen λ's. The results are depicted in Figs. 3.3(a) and 3.3(b), for the two channel models, respectively. The normalized MSE performance is plotted versus SNR. As expected, the FBMC/OQAM performance is considerably better at practical SNRs. At weak noise regimes, the inaccuracies of the assumed input-output model, which relies on the assumption of relatively low channel frequency selectivity, become more apparent, resulting in the well-known error floors in the FMBC/OQAM performance [33] (see Fig. 3.3(b)). Finally, one can see that the violation of the training conditions deteriorates the performance for both multicarrier systems.

3.4.2.2 Without the CC assumption

The simulation results when the CC assumption is not made, are depicted in Figs. 3.4(a) and 3.4(b), for the two channel models. As observed, the estimation performances of the FBMC cases are better than the CP-OFDM one for practical values of SNR. Moreover, in the case of low/mild frequency selectivity that leads to frequency flat subchannels, the use of the CC assumption provides better estimates because such an assumption entails the use of "pseudo-pilots" with the subsequent magnifying effect on the pilots' magnitude that attenuates the channel estimation error. This is also true in the severe frequency selectivity case at low SNR values, because there the noise power is more important and hence the boosted pseudo pilots improve the performance. However, at high SNR values, the model inconsistencies are more important than the noise power and the relaxation of the CC assumption yields a better performance (leading to a lower error floor) because it describes the system more accurately.

4. Widely linear filtering framework in the context of FB-MC

4.1 Widely linear processing in point-to-point MIMO FBMC/OQAM systems

Filter bank-based multicarrier modulation (FB-MC) is regarded as a promising alternative to orthogonal frequency division multiplexing with the cyclic prefix insertion (CP-OFDM). In contrast to CP-OFDM based systems, the insertion of a CP is not needed in FBMC/OQAM systems, leading to a higher spectral efficiency. Moreover, FB-MC reduces the sidelobes by using spectrally well-contained synthesis and analysis filter banks in the transmultiplexer configuration [43], [44]. Consequently it is able to avoid a high level of out-of-band radiation which CP-OFDM suffers from. These advantages of FB-MC give rise to great research attention on its use in different contexts, such as cognitive radio and professional mobile radio (PMR) networks, where an effective utilization of the available fragmented spectrum is required. In FBMC/OQAM systems, the real and imaginary parts of each complex-valued data symbol is staggered by half of the symbol period [43]. Therefore, the desired signal and the intrinsic interference are separated in the real domain and the pure imaginary domain, respectively.

However, the intrinsic interference in multiple-input multiple-output (MIMO) FBMC/OQAM systems is known as an obstacle of applying a variety of MIMO processing techniques often used when CP-OFDM is employed as the multi-carrier scheme. Widely linear processing is among one of them, while the use of OQAM gives rise to the potential of exploiting its benefits [45]. Widely linear filtering achieves a gain compared to conventional linear filtering in the case where either the correlation of the observation with its complex-conjugated version or the correlation of the observation with the complex-conjugated desired variable is non-zero [46]. The transmission of real-valued data symbols over a complex-valued channel is among such scenarios. Previous works, such as [47], have brought attention to the potential of employing widely linear processing in FBMC/OQAM systems. Nevertheless, it has not been explicitly established how to deal with the presence of the intrinsic interference such that the benefits of widely linear processing can be fully exploited. On the other hand, [48] points out that mitigating the intrinsic interference enables the application of maximum likelihood (ML) detection in MIMO transmissions with FBMC/OQAM.

Our emphasis here is on the use of widely linear processing in MIMO FBMC/OQAM systems. A two-step receiver is proposed where linear processing and widely linear processing are combined. In the first step, a linear MMSE receiver is applied. An estimate of the intrinsic interference term is obtained either by using the output of the linear MMSE receiver directly or via a reconstruction process by employing the already detected symbols. After the intrinsic interference term is canceled, a widely linear MMSE receiver is employed in the second step. It is derived taking into consideration the residual interference. Extensive simulations are performed to evaluate the performance of the proposed two-step receiver.

In the sequel, we first briefly introduce non-circular signals and the concept of widely linear processing followed by the data model of a point-to-point MIMO FBMC/OQAM system. Then the proposed two-step receiver is detailed. Numerical results are presented, before conclusions are drawn in the end.

4.1.1 Preliminaries

4.1.1.1 Non-circular signals and widely linear processing

Let us denote a complex-valued random vector by $\boldsymbol{v} = \boldsymbol{v}_{\mathrm{I}} + \jmath\boldsymbol{v}_{\mathrm{Q}} \in \mathbb{C}^M$, where $\boldsymbol{v}_{\mathrm{I}}, \boldsymbol{v}_{\mathrm{Q}} \in \mathbb{R}^M$ are zero-mean random vectors. The autocorrelation matrix and the pseudo-autocorrelation matrix of $\boldsymbol{v}$ are written as

$$\boldsymbol{\Phi}_{vv} = \mathbb{E}\{\boldsymbol{v}\boldsymbol{v}^{\mathrm{H}}\}$$

and

$$\boldsymbol{\Phi}_{vv^*} = \mathbb{E}\{\boldsymbol{v}\boldsymbol{v}^{\mathrm{T}}\},$$

respectively. The complex-valued random vector $\boldsymbol{v}$ is proper or second-order circular if $\boldsymbol{\Phi}_{vv^*}$ is an all-zero matrix. Otherwise, it is called improper or non-circular [49]. By employing some modulation formats, such as binary phase shift keying (BPSK), amplitude shift keying (ASK), or OQAM, the resulting data signals exhibit non-circularity which may be exploited by widely linear processing at the receiver. It is important to note that for an improper vector $\boldsymbol{v}$, its second-order statistics are described by both $\boldsymbol{\Phi}_{vv}$ and $\boldsymbol{\Phi}_{vv^*}$. By stacking $\boldsymbol{v}$ itself and its complex conjugate $\boldsymbol{v}^*$, a complex-valued augmented vector $\widetilde{\boldsymbol{v}}$ is obtained as

$$\widetilde{\boldsymbol{v}} = \left[\begin{array}{cc} \boldsymbol{v}^{\mathrm{T}}, & \boldsymbol{v}^{\mathrm{H}} \end{array} \right]^{\mathrm{T}} \in \mathbb{C}^{2M}. \tag{4.1}$$

Moreover, the autocorrelation matrix of $\widetilde{\boldsymbol{v}}$, also as an augmented version of the autocorrelation matrix of $\boldsymbol{v}$, is identified as

$$\boldsymbol{\Phi}_{\widetilde{vv}} = \left[\begin{array}{cc} \boldsymbol{\Phi}_{vv} & \boldsymbol{\Phi}_{vv^*} \\ \boldsymbol{\Phi}^*_{vv^*} & \boldsymbol{\Phi}^*_{vv} \end{array} \right] \in \mathbb{C}^{2M \times 2M}. \tag{4.2}$$

When $\boldsymbol{v}$ is non-circular, $\boldsymbol{\Phi}_{\widetilde{vv}}$ fully characterizes its second-order statistics. This also corresponds to the principle of widely linear filtering [46] where the filter outputs of the input signal and its complex conjugate are combined, leading to an improved performance.

4.1.1.2 System model

Consider a point-to-point MIMO FBMC/OQAM system with M_{T} transmit antennas and M_{R} receive antennas. The channel is assumed to be mildly frequency-selective, where each sub-channel can be treated as flat fading. The received vector on the k-th subcarrier and at the n-th time instant is then written as[1] [50], [48]

$$\boldsymbol{y} = \boldsymbol{H}\left(\boldsymbol{d} + \jmath\boldsymbol{u}\right) + \boldsymbol{n} \in \mathbb{C}^{M_{\mathrm{R}}}, \tag{4.3}$$

where $\boldsymbol{d} \in \mathbb{R}^{M_{\mathrm{T}}}$ is the desired signal on the k-th subcarrier and at the n-th time instant (alternatively written as $\boldsymbol{d}_k[n]$), $\boldsymbol{u} \in \mathbb{R}^{M_{\mathrm{T}}}$ and $\jmath\boldsymbol{u}$ is the pure imaginary intrinsic interference. Here $\boldsymbol{H} \in \mathbb{C}^{M_{\mathrm{R}} \times M_{\mathrm{T}}}$ contains the channel gains between each transmit antenna and each receive antenna, and $\boldsymbol{n}$ denotes the additive white Gaussian noise vector with variance σ_n^2. Note that when the PHYDYAS prototype filter [2] is used and the overlapping factor is chosen to be

[1] In this expression the index of the subcarrier and the index of the time instant are ignored for simplicity of notations. These indices only appear when explaining the intrinsic interference caused by adjacent subcarriers and time instants (see (4.4))

$K = 4$, the pure imaginary interference on the k-th subcarrier and at the n-th time instant is represented as [48]

$$\jmath \boldsymbol{u} = \sum_{i=n-3}^{n+3} \sum_{j=k-1}^{k+1} c_{ij} \cdot \boldsymbol{d}_j[i], \quad j \neq k \text{ and } i \neq n, \tag{4.4}$$

where the coefficients c_{ij} represent the system impulse response determined by the synthesis and analysis filters. Equivalently the imaginary units $\jmath$ in the OQAM modulated data symbols are shifted to their corresponding real-valued coefficients such that the transmit symbols can be regarded as all real-valued. The resulting coefficients are presented in Table 4-1. When a

Table 4-1: Coefficients determined by the system impulse of the synthesis and analysis filters

	$n-3$	$n-2$	$n-1$	n	$n+1$	$n+2$	$n+3$
$k-1$	$0.043\jmath$	$-0.125\jmath$	$-0.206\jmath$	$0.239\jmath$	$0.206\jmath$	$-0.125\jmath$	$-0.043\jmath$
k	$-0.067\jmath$	0	$0.564\jmath$	1	$0.564\jmath$	0	$-0.067\jmath$
$k+1$	$-0.043\jmath$	$-0.125\jmath$	$0.206\jmath$	$0.239\jmath$	$-0.206\jmath$	$-0.125\jmath$	$0.043\jmath$

linear MMSE receiver is employed, the desired symbols can be obtained as [48]

$$\hat{\boldsymbol{s}} = \boldsymbol{W}_{\text{MMSE}}^{\text{H}} \cdot \boldsymbol{y}, \tag{4.5}$$

$$\hat{\boldsymbol{d}} = \text{Re}\{\hat{\boldsymbol{s}}\}. \tag{4.6}$$

To apply widely linear processing, the obstacle is the pure imaginary intrinsic interference. In the sequel, we devise a two-step receiver to tackle this problem such that the benefits of widely linear processing can be exploited.

4.1.2 Proposed two-step receiver

We propose a two-step receiving procedure where linear processing and widely linear processing are combined. First, a linear MMSE receiver is applied to the received signal. The goal of the first step is to obtain an estimate of the intrinsic interference $\jmath\hat{\boldsymbol{u}}$. Assuming perfect channel state information at the receiver, the estimated interference component can be subtracted from the received signal as

$$\widetilde{\boldsymbol{y}} = \boldsymbol{H}\left(\boldsymbol{d} + \jmath\boldsymbol{u}\right) - \boldsymbol{H} \cdot \jmath\hat{\boldsymbol{u}} + \boldsymbol{n} = \boldsymbol{H}\left(\boldsymbol{d} + \jmath\boldsymbol{\epsilon}\right) + \boldsymbol{n}, \tag{4.7}$$

where $\jmath\boldsymbol{\epsilon}$ is the pure imaginary residual interference. We present two ways of obtaining an estimate of the interference. The first method is to directly take the imaginary part of the output of the linear MMSE receiver on the k-th subcarrier and at the n-th time instant as

$$\jmath\hat{\boldsymbol{u}} = \jmath \cdot \text{Im}\{\boldsymbol{W}_{\text{MMSE}}^{\text{H}} \cdot \boldsymbol{y}\}. \tag{4.8}$$

On the other hand, the idea of the second scheme is to construct an estimate of the interference by using the already detected data symbols shown as follows

$$\jmath\hat{\boldsymbol{u}} = \sum_{i=n-3}^{n+3} \sum_{j=k-1}^{k+1} c_{ij} \cdot \check{\boldsymbol{d}}_j[i], \quad j \neq k \text{ and } i \neq n, \tag{4.9}$$

where the $\check{\boldsymbol{d}}_j[i]$ are obtained by modulating the information bits detected from $\hat{\boldsymbol{d}}$ using OQAM.

In the second step, a widely linear MMSE receiver is employed on the resulting equivalent received signal $\widetilde{\boldsymbol{y}}$ and its complex conjugate. The detected desired signal is accordingly expressed as

$$\widetilde{\boldsymbol{d}} = \mathrm{Re}\left\{ \begin{bmatrix} \boldsymbol{W}_1^{\mathrm{H}} & \boldsymbol{W}_2^{\mathrm{H}} \end{bmatrix} \cdot \begin{bmatrix} \widetilde{\boldsymbol{y}} \\ \widetilde{\boldsymbol{y}}^* \end{bmatrix} \right\}, \tag{4.10}$$

where

$$\boldsymbol{W}_1 = \left(\boldsymbol{R}_{\widetilde{y}\widetilde{y}} - \boldsymbol{R}_{\widetilde{y}\widetilde{y}^*} \cdot \boldsymbol{R}_{\widetilde{y}\widetilde{y}}^{*\,-1} \cdot \boldsymbol{R}_{\widetilde{y}\widetilde{y}^*}^{*}\right)^{-1} \cdot \left(\boldsymbol{H} - \boldsymbol{R}_{\widetilde{y}\widetilde{y}^*} \cdot \boldsymbol{R}_{\widetilde{y}\widetilde{y}}^{*\,-1} \cdot \boldsymbol{H}^*\right)$$

and

$$\boldsymbol{W}_2 = \left(\boldsymbol{R}_{\widetilde{y}\widetilde{y}}^{*} - \boldsymbol{R}_{\widetilde{y}\widetilde{y}^*}^{*} \cdot \boldsymbol{R}_{\widetilde{y}\widetilde{y}}^{-1} \cdot \boldsymbol{R}_{\widetilde{y}\widetilde{y}^*}\right)^{-1} \cdot \left(\boldsymbol{H}^* - \boldsymbol{R}_{\widetilde{y}\widetilde{y}^*}^{*} \cdot \boldsymbol{R}_{\widetilde{y}\widetilde{y}}^{-1} \cdot \boldsymbol{H}\right).$$

Here $\boldsymbol{R}_{\widetilde{y}\widetilde{y}}$ and $\boldsymbol{R}_{\widetilde{y}\widetilde{y}^*}$ are the autocorrelation matrix of the equivalent received signal $\widetilde{\boldsymbol{y}}$ and its pseudo-autocorrelation matrix (the correlation matrix of $\widetilde{\boldsymbol{y}}$ and $\widetilde{\boldsymbol{y}}^*$), respectively.

Let P_{s} denote the power per symbol at each transmit antenna. The covariance matrix and the pseudo-covariance matrix of the desired signal $\boldsymbol{d} \in \mathbb{R}^{M_{\mathrm{T}}}$ are

$$\mathbb{E}\{\boldsymbol{d}\boldsymbol{d}^{\mathrm{H}}\} = \mathbb{E}\{\boldsymbol{d}\boldsymbol{d}^{\mathrm{T}}\} = \frac{P_{\mathrm{s}}}{2}\boldsymbol{I}_{M_{\mathrm{T}}}. \tag{4.11}$$

Assuming that the residual interference is uncorrelated with the desired signal and the noise as well, i.e.,

$$\mathbb{E}\{\boldsymbol{d} \cdot \boldsymbol{\epsilon}^{\mathrm{H}}\} = \mathbb{E}\{\boldsymbol{d} \cdot \boldsymbol{\epsilon}^{\mathrm{T}}\} = \boldsymbol{0}, \tag{4.12}$$

$$\mathbb{E}\{\boldsymbol{\epsilon} \cdot \boldsymbol{n}^{\mathrm{H}}\} = \boldsymbol{0}, \tag{4.13}$$

we obtain

$$\boldsymbol{R}_{\widetilde{y}\widetilde{y}} = \boldsymbol{H} \cdot \left(\frac{P_{\mathrm{s}}}{2}\boldsymbol{I}_{M_{\mathrm{T}}} + \boldsymbol{R}_{\epsilon\epsilon}\right) \cdot \boldsymbol{H}^{\mathrm{H}} + \sigma_n^2 \boldsymbol{I}_{M_{\mathrm{R}}}, \tag{4.14}$$

and

$$\boldsymbol{R}_{\widetilde{y}\widetilde{y}^*} = \boldsymbol{H} \cdot \left(\frac{P_{\mathrm{s}}}{2}\boldsymbol{I}_{M_{\mathrm{T}}} - \boldsymbol{R}_{\epsilon\epsilon}\right) \cdot \boldsymbol{H}^{\mathrm{T}}. \tag{4.15}$$

Here the covariance matrix of the residual interference related term $\boldsymbol{\epsilon}$ denoted by $\boldsymbol{R}_{\epsilon\epsilon}$ is calculated as

$$\boldsymbol{R}_{\epsilon\epsilon} \approx \frac{1}{N}\sum_{l=1}^{N}(\boldsymbol{u}_l - \hat{\boldsymbol{u}}_l) \cdot (\boldsymbol{u}_l - \hat{\boldsymbol{u}}_l)^{\mathrm{H}}. \tag{4.16}$$

A block diagram that illustrates the two-step receiver introduced above is shown in Fig. 4-1.

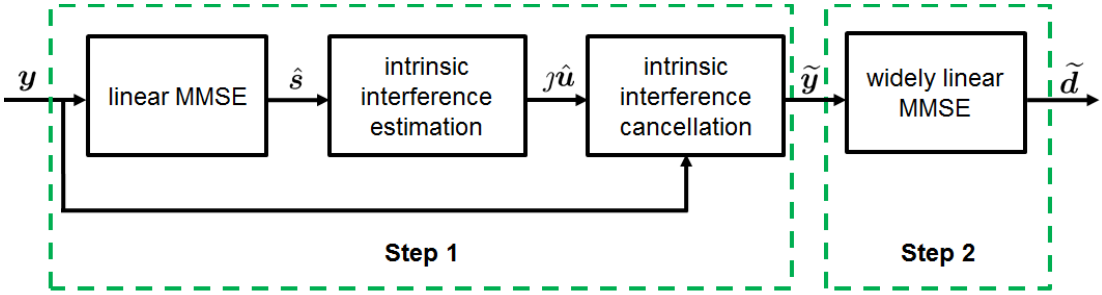

Figure 4-1: Block diagram of the proposed two-step receiver

Notice that to obtain an estimate of the intrinsic interference using (4.9) there is a delay since three future multi-carrier symbols have to be detected and used (cf. also Table 4-1). By making use of only two detected future symbols or even one, the delay is consequently smaller at the price of a performance degradation due to a larger residual interference term. This issue is further analyzed and discussed in Section 4.1.3 where the simulation results are shown.

4.1.3 Simulation results

In what follows, we evaluate the bit error rate (BER) performance of the proposed two-step receiver for MIMO FBMC/OQAM systems. The number of subcarriers is 512. Each subchannel is considered as Rayleigh flat fading. Perfect channel state information at the receiver is assumed. In addition, the PHYDYAS prototype filter with the overlapping factor $K = 4$ [2] is employed. First, a scenario where $M_{\mathrm{T}} = M_{\mathrm{R}} = 2$ is considered. Here SNR stands for the ratio of the total power at all transmit antennas and the noise variance. Fig. 4-2 presents a comparison between the BER performances of the linear MMSE receiver (as represented by (4.5) and (4.6)) and the proposed two-step receiver combining both linear processing and widely linear processing. Note that in the legend of the figure "MMSE + WL-MMSE 1" and "MMSE + WL-MMSE 2" correspond to the two versions of the two-step receiver where the estimated interference is obtained by using (4.8) and (4.9), respectively. We also illustrate in Fig. 4-2 an ideal case where the interference component is completely canceled, i.e., $\boldsymbol{\epsilon} = \mathbf{0}$ in (4.7), corresponding to the legend "WL-MMSE ideal". A performance improvement is observed by

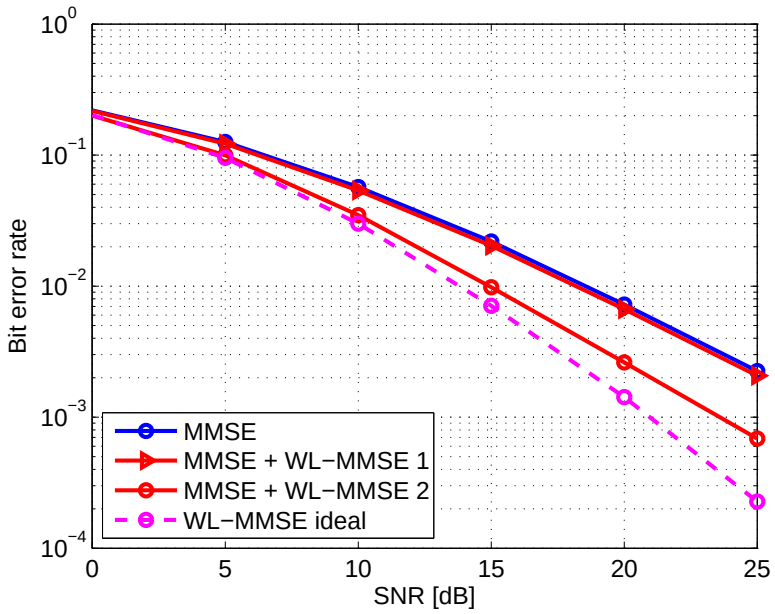

Figure 4-2: BER vs. SNR for the case where $M_{\mathrm{T}} = M_{\mathrm{R}} = 2$ ("MMSE + WL-MMSE 1" and "MMSE + WL-MMSE 2" correspond to the two versions of the two-step receiver where the estimated interference is obtained by using (4.8) and (4.9), respectively; "WL-MMSE ideal" corresponds to an ideal case where the interference component is completely canceled)

employing our proposed two-step receiver based on (4.7), (4.9) and (4.10) compared to the case where the linear MMSE receiver is used. It can also be seen that when the interference is estimated by using (4.8), the achieved gain over the linear MMSE receiver is negligible due to a relatively high level of the residual interference. In addition to the non-zero residual interference,

the violation of the assumptions (4.12) and (4.13) as well as the approximation of $\boldsymbol{R}_{\epsilon\epsilon}$ also contribute to the gap between the performance of the two-step receiver and the ideal case plotted for the purpose of comparison.

In the second example, we consider a $M_{\mathrm{T}} = M_{\mathrm{R}} = 4$ scenario and illustrate the corresponding results in Fig. 4-3. Similar observations as in the first experiment are obtained. Moreover, it is shown that by increasing the number of transmit and receive antennas, the gain achieved by the proposed two-step receiver over the linear MMSE receiver is even more significant when the estimated interference is obtained based on (4.9).

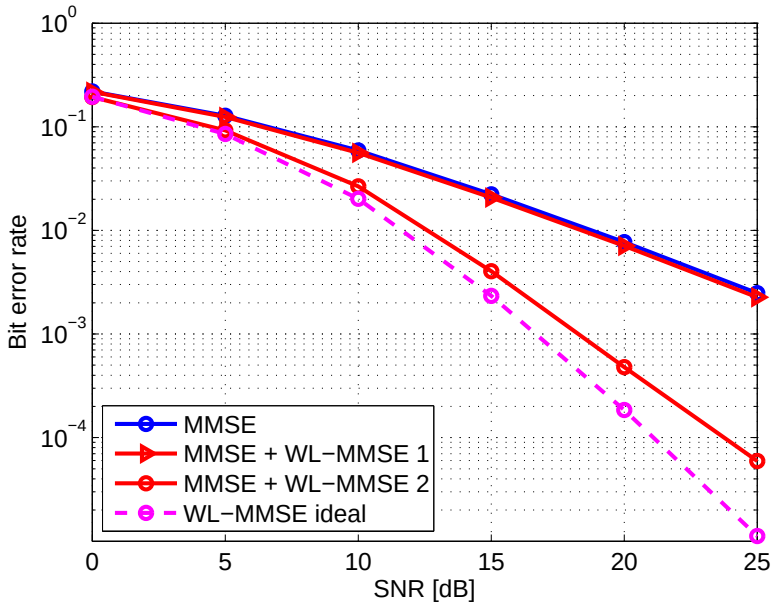

Figure 4-3: BER vs. SNR for the case where $M_{\mathrm{T}} = M_{\mathrm{R}} = 4$ ("MMSE + WL-MMSE 1" and "MMSE + WL-MMSE 2" correspond to the two versions of the two-step receiver where the estimated interference is obtained by using (4.8) and (4.9), respectively; "WL-MMSE ideal" corresponds to an ideal case where the interference component is completely canceled)

Now we concentrate on the two-step receiver where the intrinsic interference is estimated according to the second scheme as in (4.9). Its performance is evaluated when a smaller number of detected future multi-carrier symbols are used, and the intrinsic interference is thus only partially canceled. The simulation parameters are the same as in the first experiment. It can be observed in Fig. 4-4 that when two detected future symbols are used, the performance degradation compared to the case where all three future symbols contributing to the intrinsic interference are considered is quite small. As the delay is further reduced to one symbol, i.e., only one detected future symbol is used, the gap in the performance, which is around 2 dB, is still on an acceptable level. However, when no detected future symbols are utilized at all, the amount of the residual interference is large, and the performance degrades heavily. Still, it outperforms the version of the two-step receiver based on the first scheme of estimating the intrinsic interference as in (4.8).

Finally, we present a comparison between the proposed two-step receiver and the MMSE-ML scheme in [48]. In this technique, the intrinsic interference is also first mitigated by using the output of a linear MMSE receiver, and the ML detection is applied afterwards. In this example, the scenario is the same as for Fig. 4-3. For the purpose of comparison, the versions of the two-step receiver with less delay are also considered. The results are shown in Fig. 4-5. We can

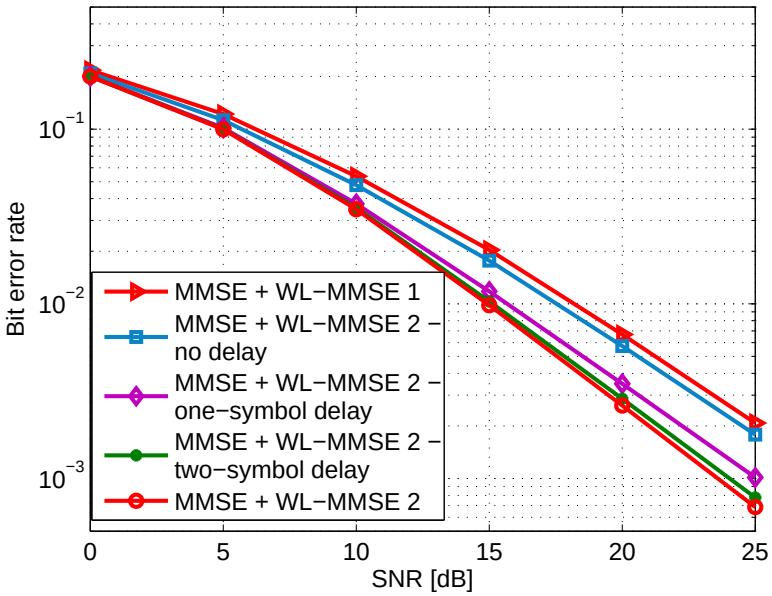

Figure 4-4: BER vs. SNR for the case where $M_{\mathrm{T}} = M_{\mathrm{R}} = 2$ ("MMSE + WL-MMSE 1" and "MMSE + WL-MMSE 2" correspond to the two versions of the two-step receiver where the estimated interference is obtained by using (4.8) and (4.9), respectively)

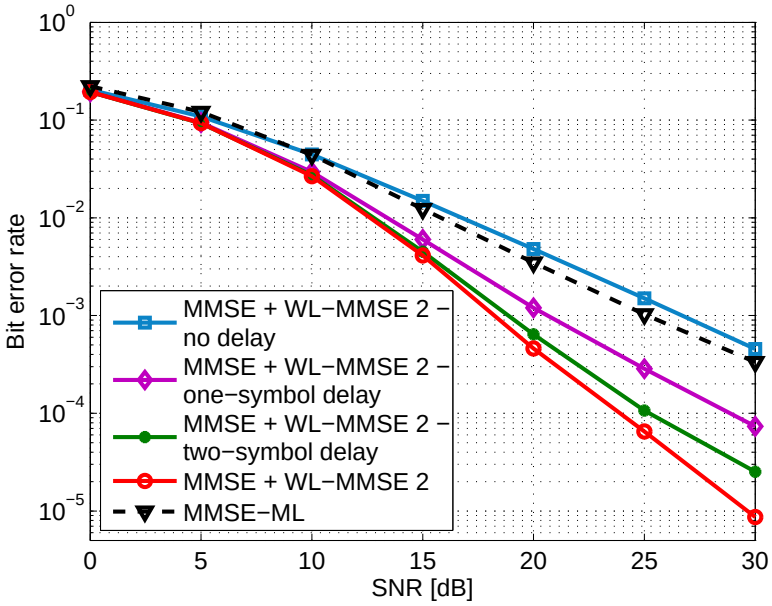

Figure 4-5: BER vs. SNR for the case where $M_{\mathrm{T}} = M_{\mathrm{R}} = 4$ ("MMSE + WL-MMSE 2" corresponds to the version of the two-step receiver where the estimated interference is obtained by using (4.9); "MMSE-ML" corresponds to the scheme combining MMSE and ML in [48])

observe that the proposed two-step receiver significantly outperforms the MMSE-ML scheme even when the intrinsic interference is only partially canceled and a smaller delay is incurred. Although the MMSE-ML technique provides a better performance compared to the version of the two-step receiver without taking advantage of any detected future symbols and thus

causing no delay, the ML detection in MMSE-ML leads to a higher computational complexity in contrast to the widely linear processing part of the two-step receiver.

4.1.4 Conclusion

To conclude, we develop a two-step receiver for a point-to-point MIMO FBMC/OQAM system. The intrinsic interference term is first estimated by using the output of a linear MMSE receiver and then subtracted from the received signal. A widely linear MMSE receiver is further applied on the resulting signal. Two schemes of estimating the intrinsic interference are presented and analyzed via simulations. In the first scheme, an estimate of the intrinsic interference is obtained by directly taking the imaginary part of the output of the linear MMSE receiver. It causes no delay in the processing but fails to provide a performance improvement compared to the case of a linear MMSE receiver. On the other hand, the second scheme uses the detected adjacent multi-carrier symbols. The two-step receiver with this scheme achieves a very promising performance. Since the knowledge of detected future symbols is required, some delay is incurred. We could cope with this issue by using a smaller number of detected future symbols with a slightly degraded performance.

In the future, the statistics of the residual interference will be analyzed. Some analytical performance evaluations will also be carried out. Moreover, the channel model will not be restricted to the flat fading case. Frequency selective channels will be considered, and the proposed scheme will be adapted to deal with the resulting inter-carrier interference and inter-symbol interference.

4.2 Possible extension to cooperative MIMO systems with FBMC/OQAM

With a focus on point-to-point MIMO FBMC/OQAM systems, we have shown that employing widely linear processing provides promising results. The way of dealing with the intrinsic interference that has been developed also inspires the design and use of the other widely linear processing-based techniques in more complicated communication scenarios. For instance, in uplink transmissions where cooperative MIMO is used, FBMC/OQAM is regarded as a promising alternative to CP-OFDM as the latter suffers from performance degradation due to the lack of synchronization in both the time and the frequency domain. The robustness of FBMC/OQAM in uplink transmissions in the presence of nodes with a single antenna or multiple antennas has been numerically shown in Chapter 2. It is thus interesting to investigate how widely linear processing can be incorporated into a cooperative MIMO FBMC/OQAM system. In such a case, relay nodes assist the transmissions from the source or sources to the destination such that the source signals arrive at the destination through a number of independent paths and are constructively combined. Unlike the point-to-point MIMO scenario where multiple antennas at the transmit and receive nodes provide spatial diversity, the relay nodes form a virtual antenna array which enhances the reliability of the transmissions without requiring multiple antennas at the nodes. To exploit the cooperative diversity of such a system, distributed beamforming is an effective technique. Compared to linear distributed beamforming algorithms, it is reported [51] that by applying widely linear processing a significant gain can be obtained. However, when FBMC/OQAM is used and amplify-and-forward (AF) is considered as the relaying scheme, the overall interference term observed at the destination that results from the intrinsic interference induced in all phases of the transmissions is a challenge. Hence, we propose that when designing a widely-linear distributed beamforming algorithm, decode-and-forward (DF) instead of AF should be considered. The intrinsic interference can then be mitigated at the relay nodes

based on the idea introduced in Section 4.1 such that the benefits due to the second-order non-circular property of the equivalently real-valued desired signals can be exploited.

5. Conclusions

In this report, we first present an extensive performance comparison study of CP-OFDM and FB-MC considering a variety of asynchronous scenarios with different configurations and settings. The robustness of FB-MC against time and frequency misalignments is shown via numerical results, which corroborate the theoretical analysis. In addition, some insights are provided to the application of a widely linear filtering framework and the use of multi-tap equalizers to combat the effects of the lack of synchronization. Moreover, the channel estimation issue in cooperative communications using FB-MC is addressed by proposing optimal designs of both sparse and full preambles, where the optimality is in the sense of the minimum Mean Square Error estimation subject to transmit energy constraints. Finally, we investigate the application of widely linear processing in the context of FB-MC and develop a two-step receiver for point-to-point MIMO FBMC/OQAM systems where both linear processing and widely linear processing are combined. It is also discussed how widely linear processing can be incorporated into a cooperative MIMO network.

6. References

[1] B. F-Boroujeny and C. H. Yuen. Cosine modulated and offset QAM filter bank multicarrier techniques: A continuous-time prospect. *EURASIP Journal on Advances in Signal Processing*, 2010(165654), December 2009.

[2] FP7-ICT Project PHYDYAS - Physical Layer for Dynamic Spectrum Access and Cognitive Radio. http://www.ict-phydyas.org.

[3] T. Pollet, M. van Bladel, and M. Moeneclaey. BER sensitivity of OFDM systems to carrier frequency offset and Wiener phase noise. *IEEE Transactions on Communications*, 43(2):191–193, May 1995.

[4] Yong S. Cho, Jaekwon Kim, Won Y. Yang, and Chung-Gu Kang.

[5] P. H. Moose. A technique for orthogonal frequency division multiplexing frequency offset correction. *IEEE Transactions on Communications*, 42:2908–2914, 1994.

[6] D. S. Waldhauser, L. G. Baltar, and J. A. Nossek. MMSE subcarrier equalization for filter bank based multicarrier systems. In *Proc. IEEE 9th Workshop Signal Processing Advances in Wireless Communications (SPAWC)*, July 2008.

[7] M. Olson et al. Single antenna interference rejection in GSM/EDGE networks. *VTC-Spring*, 2004.

[8] P. Nickel. Channel capacity evaluation of single antenna interference cancellation for single carrier transmission systems. *IWCMC*, 2008.

[9] M. Konrad and W. Gerstacker. Interference robust transmission for the downlink of an OFDM-based mobile communications systemt. *EURSIP Journal on Wireless Communications and Networking*, 2008.

[10] D.S. Waldhauser. Multicarrier systems based on filter banks. *Ph.D. Thesis, Technical University Munich*, 2009.

[11] D.S. Waldhauser at al. MMSE subcarrier equalization for filter bank based multicarrier systems. *ISCAS*, 2008.

[12] S. Nedic. An unified approach to equalization and echo cancellation in OQAM-based multi-carrier data transmission. *GLOBECOM*, 1997.

[13] M. Konrad and W. Gerstacker. OFDM transmission with single antenna interference cancellation. *Workshop on SPAWC*, 2008.

[14] P. Chevalier and F. Pipon. New insights into optimal widely linear array receivers for the demodulation of BPSK, MSK, and GMSK signals corrupted by noncircular interferences – application to SAIC. *IEEE Tr. on Signal Processing*, 54(3), March 2006.

[15] M.G. Bellanger. Specification and design of a prototype filter for filter bank based multicarrier transmission. In *Acoustics, Speech, and Signal Processing, 2001. Proceedings. (ICASSP '01). 2001 IEEE International Conference on*, volume 4, pages 2417 –2420 vol.4, 2001.

[16] Y. Mostofi and D.C. Cox. Mathematical analysis of the impact of timing synchronization errors on the performance of an ofdm system. *IEEE Trans. on Commun.*, 54(2):226 – 230, Feb. 2006.

[17] Andrea Goldsmith. *Wireless Communications*. Cambridge University Press, New York, NY, USA, 2005.

[18] David Tse and Pramod Viswanath. *Fundamentals of Wireless Communication*. Cambridge University Press, New York, NY, USA, 2005.

[19] P. Siohan, C. Siclet, and N. Lacaille. Analysis and Design of OFDM/OQAM Systems Based on Filter bank Theory,. *IEEE Trans. Signal Process.*, 50(5):1170–1183, May 2002.

[20] B. Le Floch, M. Alard, and C. Berrou. Coded Orthogonal Frequency Division Multiplex [TV broadcasting]. *Proceedings of the IEEE*, 83(6):982 –996, Jun. 1995.

[21] A. Vahlin and N. Holte. Optimal Finite Duration Pulses for OFDM. *Commun., IEEE Trans.*, 44(1):10 –14, Jan. 1996.

[22] L. Vandendorpe, L. Cuvelier, F. Deryck, J. Louveaux, and O. van de Wiel. Fractionally Spaced Linear and Decision-Feedback Detectors for Transmultiplexers. *Signal Processing, IEEE Trans.*, 46(4):996 –1011, Apr. 1998.

[23] S.D. Sandberg and M.A. Tzannes. Overlapped Discrete Multitone Modulation for High Speed Copper Wire Communications. *IEEE J. Select. Areas Commun.*, 13(9):1571 –1585, Dec. 1995.

[24] B. Hirosaki. An Analysis of Automatic Equalizers for Orthogonally Multiplexed QAM Systems. *Commun., IEEE Trans.*, 28(1):73 – 83, Jan. 1980.

[25] S. Nedic. An Unified Approach to Equalization and Echo Cancellation in OQAM-Based Multi-Carrier Data Transmission. In *Global Telecommunications Conference, IEEE*, volume 3, pages 1519 –1523, Nov. 1997.

[26] K. Van Acker, G. Leus, M. Moonen, O. van de Wiel, and T. Pollet. Per Tone Equalization for DMT-based Systems. *Commun., IEEE Trans.*, 49(1):109 –119, Jan. 2001.

[27] D.S. Waldhauser, L.G. Baltar, and J.A. Nossek. MMSE Subcarrier Equalization for Filter Bank based Multicarrier Systems. In *Signal Processing Advances in Wireless Communications, IEEE 9th Workshop on*, pages 525 –529, Jul. 2008.

[28] D.S. Waldhauser, L.G. Baltar, and J.A. Nossek. Adaptive Decision Feedback Equalization for Filter Bank based Multicarrier Systems. In *Circuits and Systems., IEEE International Symposium on*, pages 2794 –2797, May 2009.

[29] T. Ihalainen, T. Hidalgo Stitz, M. Rinne, and M. Renfors. Channel Equalization in Filter Bank Based Multicarrier Modulation for Wireless Communications. *EURASIP Journal on Advances in Signal Processing*, page 18, 2007.

[30] Y. Medjahdi, M. Terré, D. Le Ruyet, D. Roviras, and A. Dziri. Performance Analysis in the Downlink of Asynchronous OFDM/FBMC Based Multi-Cellular Networks. *Wireless Communications, IEEE Transactions on*, 10(8):2630 –2639, august 2011.

[31] Y. Medjahdi, M. Terré, D. Le Ruyet, D. Roviras, J.A. Nossek, and L. Baltar. Inter-cell interference analysis for OFDM/FBMC systems. In *Signal Processing Advances in Wireless Communications, 2009. SPAWC '09. IEEE 10th Workshop on*, pages 598 –602, june 2009.

[32] Y. Medjahdi, M. Terré, D. Le Ruyet, and D. Roviras. A new model for interference analysis in asynchronous multi-carrier transmission. *Available in ArXiv: 1006.4278v1 [cs.NI]*, abs/1006.4278, 2010.

[33] E. Kofidis, D. Katselis, A. A. Rontogiannis, and S. Theodoridis. Preamble-based Channel Etimation in OFDM/OQAM Systems: A Review. *Signal Processing*, July 2013.

[34] D. Katselis, E. Kofidis, A. A. Rontogiannis, and S. Theodoridis. Preamble-Based Channel Estimation for CP-OFDM and OFDM/OQAM Systems: A Comparative Study (see arXiv:0910.3928v1 [cs.IT] for an extended version). *IEEE Transactions on Signal Processing*, May 2010.

[35] D. Katselis, M. Bengtsson, C. Rojas, H. Hjalmarsson, and E. Kofidis. On preamble-based channel estimation in OFDM/OQAM systems. In *Proc. of EUSIPCO*, 2011.

[36] P. Siohan, C. Siclet, and N. Lacaille. Analysis and design of OFDM/OQAM systems based on filterbank theory. *IEEE Transactions on Signal Processing*, 50(5):1170–1183, May 2002.

[37] C. Lélé, J.-P. Javaudin, R. Legouable, A. Skrzypczak, and P. Siohan. Channel estimation methods for preamble-based OFDM-OQAM modulations. *European Transactions on Telecommunications*, 19:741–750, September 2008.

[38] J. Javaudin, D. Lacroix, and A. Rouxel. Pilot-aided channel estimation for OFDM/OQAM. In *Proc. of IEEE VTC*, 2003.

[39] C. Mavrokefalidis, E. Kofidis, A. A. Rontogiannis, and S. Theodoridis. Optimal training design for channel estimation in OFDM/OQAM cooperative systems. In *Proc. of IEEE SPAWC*, 2013.

[40] C. Mavrokefalidis, A. A. Rontogiannis, and K. Berberidis. Training design in single relay AF cooperative systems with correlated channels. In *Proc. of IEEE ICASSP*, 2011.

[41] C. Mavrokefalidis, E. Kofidis, A. A. Rontogiannis, and S. Theodoridis. Preamble design for channel estimation in OFDM/OQAM cooperative systems. In *Proc. of ISWCS*, 2013.

[42] M. G. Bellanger. Specification and design of a prototype filter for filter bank based multicarrier transmission. In *Proc. of IEEE ICASSP*, 2001.

[43] P. Siohan, C. Siclet, and N. Lacaille. Analysis and design of OFDM/OQAM systems based on filterbank theory. *IEEE Transactions on Signal Processing*, 50(5):1170–1183, May 2002.

[44] M. G. Bellanger. Specification and design of a prototype filter for filter bank based multicarrier transmission. In *Proc. IEEE Int. Conf Acoustics, Speech, and Signal Processing*, Salt Lake City, USA, May 2001.

[45] W. H. Gerstacker, R. Schober, and A. Lampe. Receivers with widely linear processing for frequency-selective channels. *IEEE Transactions on Communications*, 51(9):1512–1523, Sept. 2003.

[46] B. Picinbono and P. Chevalier. Widely linear estimation with complex data. *IEEE Transactions on Signal Processing*, 43:2030–2033, Aug. 1995.

[47] M. Caus and A. I. Perez-Neira. Multi-stream transmission in MIMO-FBMC systems. In *Proc. IEEE International Conference on Acoustics, Speech and Signal Processing (ICASSP 2013)*, May 2013.

[48] R. Zakaria, D. le Ruyet, and M. Bellanger. Maximum Likelihood Detection in spatial multiplexing with FBMC. In *Proc. 2010 European Wireless*, June 2010.

[49] F. D. Neeser and J. L. Massey. Proper complex random processes with applications to information theory. *IEEE Transactions on Information Theory*, 39(4):1293–1302, 1993.

[50] M. Bellanger. FBMC physical layer: A primer, Jun. 2010.

[51] Jens Steinwandt and Martin Haardt. Optimal widely-linear distributed beamforming for relay networks. In *Proc. IEEE Int. Conference on Acoustics, Speech, and Signal Processing (ICASSP)*, May 2013.

Glossary and Definitions

Acronym	Meaning
OFDM	Orthogonal Frequency Division Multiplexing
CP	Cyclic Prefix
OQAM	Offset Quadrature Amplitude Modulation
QAM	Quadrature Amplitude Modulation
SNR	Signal to Noise Ratio
NMSE	Normalized Mean Square Error
BER	Bit Error Rate
QPSK	Quadrature Phase Shift Keying
FB-MC	Filter Bank-based Multi-Carrier
FBMC/OQAM	Filter Bank-based Multi-Carrier with OQAM subcarrier modulation
PMR	Professional Mobile Radio
MIMO	Multiple-Input Multiple-Output
MMSE	Minimum Mean Square Error
BER	Bit Error Rate
AF	Amplify-and-Forward
DF	Decode-and-Forward
AP	Access Point
LTE	Long Term Evolution
FFT	Fast Fourier Transform
iFFT	inverse Fast Fourier Transform
TDL	Tapped Delay Line
ITU-R	International Telecommunication Union Radiocommunication sector
ISI	Inter-Symbol Interference
CFO	Carrier Frequency Offset